

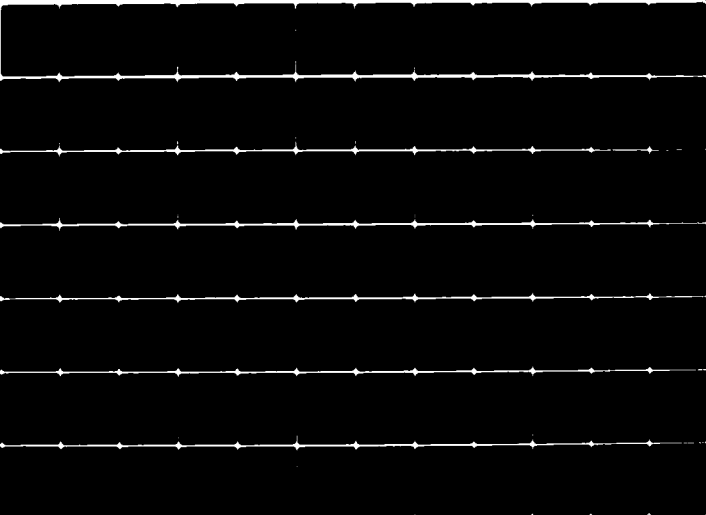
79-1884

RUTGERS - THE STATE UNIV NEW BRUNSWICK N J DEPT OF --ETC F/8 21/3  
CALCULATION OF HIGH SPEED INLET FLOWS USING THE NAVIER-STOKES E--ETC(U)  
FEB 80 D D KNIGHT F33615-78-C-3088

AFFDL-TR-79-3138-VOL-2 NL

UNCLASSIFIED

1 of 2  
80A  
084790



ADA 084790

AFFDL-TR-79-3138  
Volume II

②

111

APR 1979

# CALCULATION OF HIGH SPEED INLET FLOWS USING THE NAVIER-STOKES EQUATIONS

## Volume II: User's and Programmer's Guide

DOYLE D. KNIGHT

DEPARTMENT OF MECHANICAL, INDUSTRIAL AND  
AEROSPACE ENGINEERING

RUTGERS UNIVERSITY THE STATE UNIVERSITY OF NEW JERSEY  
NEW BRUNSWICK, NEW JERSEY 08903

FEBRUARY 1980

TECHNICAL REPORT AFFDL-TR-79-3138  
Final Report for period April 1978 - September 1979

DTIC

Approved for public release; distribution unlimited.

DDC FILE COPY.

AIR FORCE FLIGHT DYNAMICS LABORATORY  
AIR FORCE WRIGHT AERONAUTICAL LABORATORIES  
AIR FORCE SYSTEMS COMMAND  
WRIGHT-PATTERSON AIR FORCE BASE, OHIO 45433

80 5 27 077

NOTICE

When Government drawings, specifications, or other data are used for any purpose other than in connection with a definitely related Government procurement operation, the United States Government thereby incurs no responsibility nor any obligation whatsoever; and the fact that the government may have formulated, furnished, or in any way supplied the said drawings, specifications, or other data, is not to be regarded by implication or otherwise as in any manner licensing the holder or any other person or corporation, or conveying any rights or permission to manufacture, use, or sell any patented invention that may in any way be related thereto.

This report has been reviewed by the Information Office (OI) and is releasable to the National Technical Information Service (NTIS). At NTIS, it will be available to the general public, including foreign nations.

This technical report has been reviewed and is approved for publication.

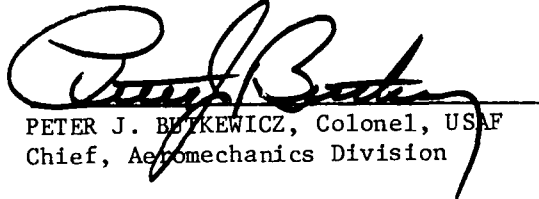


PROJECT ENGINEER



LOWELL C. KEEL, MAJOR, USAF  
Chief, Aerodynamics & Airframe Br.  
Aeromechanics Division

FOR THE COMMANDER



PETER J. BYTKEWICZ, Colonel, USAF  
Chief, Aeromechanics Division

"If your address has changed, if you wish to be removed from our mailing list, or if the addressee is no longer employed by your organization please notify AFWAL/FIMM, W-PAFB, OH 45433 to help us maintain a current mailing list".

Copies of this report should not be returned unless return is required by security considerations, contractual obligations, or notice on a specific document.





## FOREWORD

This report describes the principles and operation of a set of four computer programs that are used to compute the flowfield in two-dimensional mixed-compression high speed aircraft inlets. The programs are written in Fortran IV, and have been successfully operated on the CYBER 74 and CYBER 175 computers at the ASD Computing Center, Wright-Patterson AFB, Ohio, and the IBM 370/168 computer at Rutgers University. It is assumed that the prospective user is familiar with the operating system of the computer to be utilized and the use of permanent or magnetic tape files.

This report was prepared by Prof. Doyle D. Knight, Department of Mechanical Engineering, Rutgers University, New Brunswick, New Jersey, for the Air Force Flight Dynamics Laboratory, Air Force Systems Command, Wright-Patterson Air Force Base, Ohio. The study was performed under Air Force Contract F33615-78-C-3008, "Analytical Investigation of Inlet Internal Flow." The work was performed from April 1978 through September 1979, with Mr. Don Stava (AFFDL/FXM) of the Air Force Flight Dynamics Laboratory as Project Engineer. The report was submitted in September 1979.

## TABLE OF CONTENTS

SECTION	PAGE
I	GENERAL DESCRIPTION . . . . . 1
	A. Overview . . . . . 1
	B. Description of Physical Problem . . . . . 1
	C. Description of Mathematical Model . . . . . 2
	1. Coordinate Transformation . . . . . 2
	2. Navier-Stokes Equations . . . . . 4
	3. Computational Sublayer . . . . . 10
II	NUMERICAL ALGORITHMS . . . . . 12
	A. Coordinate Transformation . . . . . 12
	B. Navier-Stokes Equations . . . . . 19
	1. MacCormack's Method . . . . . 19
	2. Mesh Splitting. . . . . 23
	3. Mesh Overlapping. . . . . 25
	4. Boundary Conditions . . . . . 26
	5. Numerical Damping . . . . . 29
	6. Convergence of Flowfield to Steady State. . . . . 31
	7. Computational Sublayer. . . . . 31
	C. Overall Description of Programs . . . . . 33
III	GENERATION OF COORDINATE TRANSFORMATION . . . . . 36
	A. Preliminary Analysis . . . . . 36
	1. Streamwise Mesh Spacing . . . . . 36
	2. Boundary Layer Mesh Spacing . . . . . 37
	3. Example: Upstream Inlet Region for MCAIR Case 35. . . . . 41
	B. Determination of Mesh Spacing on Upstream and Downstream Boundaries Using Program BNDRY . . . . . 44
	1. Introduction . . . . . 44
	2. Description of Input Variables. . . . . 45
	3. Source Code Notation. . . . . 47
	4. Sample of Output: Upstream Inlet Region for MCAIR Case 35 . . . . . 47
	C. Generation of Coordinate Transformation Using Program COORD . . . . . 48
	1. Introduction . . . . . 48
	2. Description of Input Variables. . . . . 48

TABLE OF CONTENTS--CONTINUED

SECTION	PAGE
3. Flow Chart . . . . .	55
4. Source Code Notation. . . . .	57
5. File Structure . . . . .	61
6. Sample Calculation: Upstream Inlet Region for MCAIR Case 35 . . . . .	62
7. Sample Calculation: Downstream Inlet Region for MCAIR Case 35 . . . . .	65
8. Sample Output : Upstream Inlet Region for MCAIR Case 35 . . . . .	69
 IV      CALCULATION OF INLET FLOWFIELD	
A. Introduction . . . . .	70
B. Description of Input Variables. . . . .	71
C. Flow Charts . . . . .	76
1. Overall Program . . . . .	76
2. $L_z$ Operator . . . . .	79
3. $L_{\zeta}$ Operator for Regions 1 and 2 . . . . .	80
D. Source Code Notation. . . . .	82
E. File Structure. . . . .	90
F. Sample Calculation: Upstream Inlet Region for MCAIR Case 35 . . . . .	91
G. Sample Output: Upstream Inlet Region for MCAIR Case 35 . . . . .	94
H. Interpolating Flow Variables at Mesh Overlap Using Program UPSTRM . . . . .	96
1. Introduction. . . . .	96
2. Description of Input Variables. . . . .	98
3. Flow Chart: Program UPSTRM. . . . .	100
4. Source Code Notation. . . . .	101
5. File Structure. . . . .	103
6. Output. . . . .	103
 REFERENCES . . . . .	104

## LIST OF FIGURES

FIGURE		PAGE
1	Characteristics of Mixed Compression High Speed Inlet . . . . .	107
2	Coordinate Transformation . . . . .	108
3	Details of Mesh Distribution . . . . .	109
4	Mesh Splitting . . . . .	110
5	Mesh Overlapping . . . . .	111
6	Boundary Conditions . . . . .	112
7	Computational Sublayer Geometry . . . . .	113
8	Mesh Overlapping Employed for MCAIR Inlet . . . . .	114
9	Upstream Region of MCAIR Inlet--Case 35 . . . . .	115
10	Sample Output: Program BNDRY . . . . .	116
11a	Coordinate Transformation for MCAIR Inlet (Upstream)--Case 35	117
11b	Coordinate Transformation for MCAIR Inlet (Downstream)-- Case 35 . . . . .	118
12a	Sample Output: Program COORD . . . . .	119
12b	Sample Output: Program COORD . . . . .	120
12c	Sample Output: Program COORD . . . . .	121
12d	Sample Output: Program COORD . . . . .	122
12e	Sample Output: Program COORD . . . . .	123
13a	Sample Output: Program INLET . . . . .	124
13b	Sample Output: Program INLET . . . . .	125
13c	Sample Output: Program INLET . . . . .	126
13d	Sample Output: Program INLET . . . . .	127
13e	Sample Output: Program INLET . . . . .	128
13f	Sample Output: Program INLET . . . . .	129

LIST OF TABLES

TABLE		PAGE
1	Resources Required - Program BNDRY . . . . .	45
2	Input Data - Program BNDRY. . . . .	46
3	Resources Required - Program COORD . . . . .	48
4	Input Data - Program COORD . . . . .	50
5	Guidelines for Input Data - Program COORD . . . . .	54
6	Input Data - Coordinate System for MCAIR Case 35 (Upstream Region) . . . . .	63
7	Input Data - Coordinate System for MCAIR Case 35 (Downstream Region) . . . . .	66
8	Resources Required - Program INLET. . . . .	70
9	Input Data - Program INLET . . . . .	72
10	Guidelines for Input Data - Program INLET . . . . .	75
11	Input Data - Flowfield Calculation for MCAIR Case 35 (Upstream Region) . . . . .	92
12	Resources Required - Program UPSTRM . . . . .	97
13	Input Data - Program UPSTFM . . . . .	98

## SECTION I

### GENERAL DESCRIPTION

#### A. Overview

The purpose of this report is to document a series of four computer programs that are used to compute the flowfield within a two-dimensional mixed-compression high speed aircraft inlet. In Section I, a brief description is presented of the physical problem and the mathematical model. The numerical methods are discussed in Section II, and the limitations of the approach are indicated. A brief summary of the four programs is presented, together with the general sequence of application. In Section III, the coordinate system programs are discussed in detail, with emphasis on the pertinent criteria for successful implementation. In Section IV, the details of the Navier-Stokes code employed for solution of the inlet flowfield are presented. In addition, the details of a simple utility program used to interpolate flowfield data are discussed. In each section, examples of calculations performed on the CYBER 74 and 175 computers at WPAFB are presented to illustrate application of the numerical codes.

#### B. Description of Physical Problem

The basic problem is the computation of the steady flowfield within a two-dimensional high speed inlet. As indicated in Figure 1, the incoming supersonic flow is deflected by a pattern of oblique shock waves formed by the general curvilinear shape of the ramp and cowl surfaces. The boundary layers are turbulent over nearly the entire length of the inlet, owing to the typically high Reynolds numbers. Boundary layer bleed is distributed along the walls in order to prevent flow separation at the interaction of

the shock waves and the boundary layers on the ramp and cowl. A terminal shock may be positioned near the inlet throat.

The computer programs described herein determine the flowfield within the inlet, including both inviscid and viscous regions, by integration of the full mean compressible Navier-Stokes equations. Turbulence is represented by an algebraic turbulent eddy viscosity.

### C. Description of Mathematical Model

#### 1. Coordinate Transformation

In order to handle the general curvilinear inlet geometry, a numerical coordinate transformation is employed. The purpose of the transformation is to provide a set of curvilinear coordinates  $\zeta(x,y)$  and  $\eta(x,y)$  that are contoured to the inlet shape. As indicated schematically in Figure 2, the cowl and ramp surfaces are taken to be coincident with portions of the contours  $\eta(x,y) = 0$  and  $\eta(x,y) = 1$ , respectively. The upstream and downstream boundaries are defined by the lines  $\zeta(x,y) = 0$  and  $\zeta(x,y) = 1$ , respectively. The  $\eta$  coordinate increases in a general cross-stream direction across the inlet, while the  $\zeta$  coordinate increases basically in the streamwise direction. The clear advantages of a general coordinate transformation of this type are the simplicity of application of the fluid dynamical boundary conditions (e.g., adiabatic wall, no slip, mass bleed) for the ramp and cowl and the inherent accuracy of a surface-oriented coordinate system in the boundary layers. By construction, the coordinate transformation maps the desired domain of the inlet flowfield in the physical or x-y plane into the unit square in the transformed or  $\zeta$ - $\eta$  plane. For example, the portion of the  $\eta = 0$  line that corresponds to the cowl surface is mapped into a segment of the lower boundary of the

unit square in the transformed plane, where application of the appropriate boundary conditions is facilitated.

The coordinates  $\zeta(x,y)$  and  $\eta(x,y)$  are obtained using the basic approach of Thompson.<sup>1</sup> They are taken to satisfy the following equations:

$$\begin{aligned} \nabla^2 \zeta &= 0 \\ \nabla^2 \eta &= T(\zeta, \eta) \left[ \left( \frac{\partial \eta}{\partial x} \right)^2 + \left( \frac{\partial \eta}{\partial y} \right)^2 \right] \end{aligned} \quad (1)$$

where  $\nabla^2$  is the Laplacean operator  $\partial^2/\partial x^2 + \partial^2/\partial y^2$ . The coordinates  $\zeta(x,y)$  and  $\eta(x,y)$  are subject to Dirichlet boundary conditions as illustrated in Figure 2 (e.g.,  $\zeta = 0$  on the upstream boundary). The coordinate transformation is generally non-orthogonal. The source terms on the right-hand side of (2) are employed to control the mesh spacing in the  $\eta$ -direction in order to provide accurate resolution within the boundary layers on the ramp and cowl. The expression employed for  $T(\zeta, \eta)$  is

$$T(\zeta, \eta) = \begin{cases} -C_1/\eta_1 & 0 \leq \eta < \eta_1 \\ 0 & \eta_1 \leq \eta \leq \eta_2 \\ +C_2/(1 - \eta_2) & \eta_2 \leq \eta < 1 \end{cases} \quad (2)$$

where  $C_1$ ,  $C_2$ ,  $\eta_1$  and  $\eta_2$  are slowly varying functions of the streamwise variable  $\zeta$ . As discussed later in Section III, these quantities are determined by the requirements of accurate resolution of the boundary layers and controllable mesh spacing near the walls. The particularly simple form of the source term in (2) provides for substantial automation of the coordinate generation process. A different formulation for the

source terms has been employed by Thompson<sup>1</sup> utilizing a series of exponential functions. Although possessing greater generality than the present technique, its operation typically requires a trial-and-error procedure in order to generate a suitable coordinate system. In contrast, the present technique permits direct generation of a suitable coordinate transformation satisfying the necessary requirements of accurate resolution and controllable mesh spacing within the boundary layers.

The governing fluid dynamic equations are solved in the transformed  $\zeta$ - $\eta$  plane. From knowledge of the inverse transformation  $x(\zeta, \eta)$  and  $y(\zeta, \eta)$ , the flowfield within the inlet in the physical plane is obtained.

## 2. Navier-Stokes Equations

The governing equations are the full mean compressible Navier-Stokes equations utilizing mass-averaged variables<sup>2</sup> for two-dimensional turbulent flow. Written in strong conservation form utilizing the transformed coordinates  $\zeta(x, y)$  and  $\eta(x, y)$ , the equations are<sup>3,4</sup>

$$\frac{\partial U}{\partial t} + \frac{\partial F}{\partial \zeta} + \frac{\partial G}{\partial \eta} = 0 \quad (3)$$

where

$$U = \frac{1}{J} \begin{pmatrix} \rho \\ \rho u \\ \rho v \\ \rho e \end{pmatrix} \quad (4)$$

$$F = \frac{1}{J} \begin{pmatrix} \rho U \\ \rho u U + \zeta_x (p - \tau_{xx}) - \zeta_y \tau_{xy} \\ \rho v U + \zeta_y (p - \tau_{yy}) - \zeta_x \tau_{xy} \\ (\rho e + p)U + \zeta_x \beta_x + \zeta_y \beta_y \end{pmatrix} \quad (5)$$

$$G = \frac{1}{J} \begin{pmatrix} \rho V \\ \rho uV + \eta_x(p - \tau_{xx}) - \eta_y \tau_{xy} \\ \rho vV + \eta_y(p - \tau_{yy}) - \eta_x \tau_{xy} \\ (\rho e + p)V + \eta_x \beta_x + \eta_y \beta_y \end{pmatrix} \quad (6)$$

where  $\zeta_x$  denotes  $\partial\zeta/\partial x$ , etc. The cartesian x- and y-velocity components are denoted by  $u$  and  $v$ , respectively. The density is indicated by  $\rho$  and the pressure by  $p$ . The gas is assumed to be calorically and thermally perfect with the equation of state  $p = \rho RT$ , where  $T$  is the absolute temperature and  $R$  is the gas constant. The total energy per unit mass  $e$  is given by  $e = e_i + (1/2)(u^2 + v^2)$ , where  $e_i$  is the internal energy per unit mass and is equal to  $c_v T$ , with  $c_v$  denoting the specific heat at constant volume. The fluid is assumed to be air, with  $c_v = 4290 \text{ ft}^2/\text{sec}^2\text{-}^\circ\text{R}$  and  $R = 1716 \text{ ft}^2/\text{sec}^2\text{-}^\circ\text{R}$ , where  $^\circ\text{R}$  denotes degrees Rankine. The contravariant velocity components  $U, V$  and Jacobian  $J$  are

$$\begin{aligned} U &= \zeta_x u + \zeta_y v \\ V &= \eta_x u + \eta_y v \\ J &= \zeta_x \eta_y - \zeta_y \eta_x \end{aligned} \quad (7)$$

The components of the cartesian stress tensor are

$$\begin{aligned} \tau_{xx} &= \lambda_T \text{div } \vec{v} + 2(\mu + \epsilon) \frac{\partial u}{\partial x} \\ \tau_{xy} &= (\mu + \epsilon) \left( \frac{\partial u}{\partial y} + \frac{\partial v}{\partial x} \right) \\ \tau_{yy} &= \lambda_T \text{div } \vec{v} + 2(\mu + \epsilon) \frac{\partial v}{\partial y} \end{aligned} \quad (8)$$

where  $\mu$  is the molecular dynamic viscosity given by Sutherland's relation,

$\epsilon$  is the turbulent eddy viscosity,  $\lambda_T = - (2/3)(\mu + \epsilon)$  and  $\text{div } \vec{v} = \partial u/\partial x + \partial v/\partial y$ .

The partial derivatives in (8) are replaced by derivatives with respect to

the transformed variables  $\zeta$  and  $\eta$  by means of the chain rule (e.g.,

$\partial u/\partial x = \zeta_x(\partial u/\partial \zeta) + \eta_x(\partial u/\partial \eta)$ ). The quantities  $\beta_x$  and  $\beta_y$  in (5) and (6)

are

$$\beta_x = Q_x - u\tau_{xx} - v\tau_{xy} \quad (9)$$

$$\beta_y = Q_y - u\tau_{xy} - v\tau_{yy}$$

where  $Q_x, Q_y$  are components of the heat flux given by

$$Q_x = -\gamma \left( \frac{\mu}{Pr} + \frac{\epsilon}{Pr_t} \right) \frac{\partial e_i}{\partial x} \quad (10)$$

$$Q_y = -\gamma \left( \frac{\mu}{Pr} + \frac{\epsilon}{Pr_t} \right) \frac{\partial e_i}{\partial y}$$

where  $\gamma = c_p/c_v$  is the ratio of specific heats (taken to be 1.4) and  $Pr$  and  $Pr_t$  are the molecular and turbulent Prandtl numbers, respectively, with values of 0.72 and 0.90. Although  $Pr_t$  is, in general, a function of position within the boundary layer, numerical computations of high speed turbulent boundary layers have shown only a weak dependence on  $Pr_t$  variations.<sup>5</sup>

The turbulent eddy viscosity  $\epsilon$  is given by the two-layer equilibrium eddy viscosity model of Cebeci-Smith<sup>6-8</sup> (except as noted later) with the transition model of Dhawan and Narasimha.<sup>9</sup> Within the inner region, the equilibrium eddy viscosity  $\epsilon_{eq_i}$  is given by

$$\epsilon_{eq_i} = \rho(\kappa n D)^2 \left| \frac{\partial u}{\partial \eta} \right| \Gamma(s) \quad (11)$$

while in the outer region

$$\epsilon_{eq_0} = \rho k_2 U_{ref} \delta_i^* \Gamma(s) \quad (12)$$

where  $n$  = distance normal to surface

$s$  = distance along surface from leading edge

$\kappa = 0.40$  (von Karman's constant)

$k_2 = 0.0168$

$\Gamma(s)$  = transition factor

$U_{ref}$  = mean velocity outside boundary layer

$u$  = component of velocity parallel to the surface

$$\delta_i^* = \int_0^\delta (1 - u/U_{ref}) dn$$

$\delta$  = local boundary layer thickness

and  $D$  is the modified Van Driest damping factor given by

$$D = 1 - \exp\left(-\frac{n \sqrt{|\tau_w| \rho_w}}{26 \mu_w} N\right) \quad (13)$$

where  $N$  is a modification due to mass bleed:

$$N = \exp\left[5.9 \frac{\mu_w \dot{m}}{\mu \sqrt{|\tau_w| \rho_w}}\right] \quad (14)$$

In the above, the subscript  $w$  implies evaluation at the wall, with  $\tau_w$  denoting the wall shear stress, and  $\dot{m}$  is the normal mass flux at the surface (i.e.,  $\dot{m} = \rho \vec{v} \cdot \hat{n}$ , where  $\hat{n}$  is the outward normal at the wall, pointing into the fluid). The above expression for the Van Driest damping factor  $D$  differs from that of Cebeci-Smith<sup>8</sup> in two respects. First, the density and dynamic viscosity in the Van Driest damping factor

D in (13) are evaluated at the wall, rather than locally, in agreement with most studies of strong shock-boundary layer interaction.<sup>10-13</sup> Second, the pressure gradient correction<sup>8</sup> to N has been omitted. Previous investigations of flows with strong shock-boundary layer interaction have been performed both with<sup>13</sup> and without<sup>10-12</sup> a pressure gradient correction. The present code, however, employs the eddy viscosity relaxation model of Shang and Hankey<sup>10</sup> (discussed below), which has been developed without inclusion of a pressure gradient correction, and for this reason the pressure gradient correction has been omitted.

The transition from the inner equilibrium eddy viscosity  $\epsilon_{eq_i}$  to the outer eddy viscosity  $\epsilon_{eq_o}$  occurs at a distance  $n_m$  at which  $\epsilon_{eq_i} = \epsilon_{eq_o}$ . Thus, the full form of the equilibrium eddy viscosity is

$$\epsilon_{eq} = \begin{cases} \epsilon_{eq_i} & n \leq n_m \\ \epsilon_{eq_o} & n > n_m \end{cases} \quad (15)$$

The transition factor  $\Gamma(s)$ , employed to allow a smooth development of the eddy viscosity in the region of transition from laminar to turbulent flow, is given by

$$\Gamma(s) = 1 - \exp(-0.412\bar{s}^2) \quad (16)$$

$$\bar{s} = (s - s_i)/\Lambda, \quad s_i \leq s \leq s_f$$

where  $s_i$  and  $s_f$  denote initial and final locations of the transition zone with

$$\Lambda = s|_{\Gamma=3/4} - s|_{\Gamma=1/4}$$

As applied in the numerical code, the transition model requires only the specification of  $s_i$  and  $s_f$ . These values may be obtained by the method of Deem and Murphy<sup>14</sup> and the generally accepted criterion that the Reynolds number based on the distance from the leading edge approximately doubles across the transition region.<sup>9</sup>

In the vicinity of the interaction of a shock wave with a turbulent boundary layer, a modification of the eddy viscosity is required in order to incorporate the experimental observation that the turbulent shear stress does not immediately react to an abrupt change in the flow.<sup>15</sup> This effect is modeled by the approach of Shang and Hankey,<sup>10,16</sup> which employs the following relaxation model for the eddy viscosity:

$$\epsilon(s,n) = \epsilon_{eq}(s_0,n) + [\epsilon_{eq}(s,n) - \epsilon_{eq}(s_0,n)][1 - \exp(-(s - s_0)/\lambda)] \quad (17)$$

where  $s_0$  is a location approximately seven boundary layer thicknesses upstream of the intersection of the shock wave and the wall,  $\epsilon_{eq}$  is the equilibrium eddy viscosity given by (11) to (15) and  $\lambda$  is typically twenty times the boundary layer thickness  $\delta_0$  at  $s_0$ . In the above,  $s$  is the distance along the surface from the leading edge, and  $n$  is the distance normal to the surface. The above expression is employed for  $s > s_0$ , and provides for a relaxation of  $\epsilon$  across the shock-boundary layer interaction region, ultimately approaching the equilibrium expression given by (11) to (15) for  $s - s_0$  much greater than  $20 \delta_0$ .

The relaxation model is important at shock-boundary layer interactions when flow separation occurs.<sup>10,16</sup> The model has not been thoroughly investigated for boundary layers subject to repeated shock impingement (particularly for those cases where the distance between shock impingement

is less than the relaxation length  $\lambda$ ), and has therefore been incorporated in the numerical code for use at one shock-boundary layer interaction each on the ramp and cowl.

### 3. Computational Sublayer

A major factor governing the efficiency of the numerical algorithm employed in the code to solve the Navier-Stokes equations is the requirement of resolving all pertinent scales within the turbulent boundary layers on the ramp and cowl. The exceedingly fine mesh spacing required to resolve the viscous sublayer portion of the turbulent boundary layers would ordinarily severely impair the efficiency of the numerical code. In order to alleviate this difficulty, a separate and efficient treatment of the region\* containing the viscous sublayer and transition portion of the boundary layer is employed. Within this region, an approximate form of the full equations of motion is utilized in agreement with previous studies of turbulent boundary layers.<sup>7,17</sup> The governing equations are

$$\dot{m} \frac{\partial u'}{\partial y'} = - \frac{\partial p}{\partial x'} + \frac{\partial \tau_{x'y'}}{\partial y'} \quad (18)$$

$$\frac{\partial}{\partial y'} \left[ \dot{m} \left( c_p T + \frac{1}{2} u'^2 \right) - c_p \left( \frac{\mu}{Pr} + \frac{\epsilon}{Pr_t} \right) \frac{\partial T}{\partial y'} - u' \tau_{x'y'} \right] = 0 \quad (19)$$

$$\tau_{x'y'} = (\mu + \epsilon) \frac{\partial u'}{\partial y'} \quad (20)$$

where, in this case,  $x'$  and  $y'$  are local cartesian coordinates parallel and normal to the surface, respectively;  $\tau_{x'y'}$  is the shear stress parallel to

---

\* This region is defined by  $0 \leq n \leq 50 v_w / u_*$ , where  $v_w = \mu_w / \rho_w$  and  $u_* = \sqrt{\tau_w / \rho_w}$ . In this context, the expression "transition region" refers to the approximate domain  $10 v_w / u_* \leq n \leq 50 v_w / u_*$  and is not to be confused with the "transition zone" discussed in reference to (16).

the wall; and  $u'$  is the velocity component parallel to the wall. The equations are applied within a narrow region  $0 \leq y' \leq y'_m$  adjacent to the walls denoted as the "computational sublayer." The applicability of the above expressions (18) and (19) imposes an upper limit on the value of  $y'_m$ , which has been found to be roughly  $60v_w/u_*$ .<sup>18</sup> The achievement of maximum code efficiency implies that the value of  $y'_m$  should be as large as possible within the above limit. In practice, the value of  $y'_m$  is determined by the mesh obtained from the coordinate transformation program and the nature of the flowfield (e.g.,  $v_w$ ,  $\tau_w$ ), as discussed in a later section. Precise control of  $y'_m$  at every location is not afforded by the numerical codes. However, proper operation can limit the typical range of  $y'_m$  from approximately  $20v_w/u_*$  to  $60v_w/u_*$ , thereby achieving an efficient and accurate solution of the flow.

SECTION II  
NUMERICAL ALGORITHMS

A. Coordinate Transformation

The function of the coordinate transformation program is to provide a distributed mesh of points that can be used to accurately resolve all pertinent features of the flow. The basic concept is indicated in Figure 3. The unit square in the transformed plane is covered by a uniform mesh of points  $(\zeta_i, \eta_j)$  where

$$\begin{aligned}\zeta_i &= (i - 1) \Delta\zeta, & i &= 1, \dots, IL \\ \eta_j &= (j - 1) \Delta\eta, & j &= 1, \dots, JL\end{aligned}\tag{21}$$

where IL and JL are the number of points in the  $\zeta$ - and  $\eta$ -directions, respectively. By definition,  $\Delta\zeta = 1/(IL - 1)$  and  $\Delta\eta = 1/(JL - 1)$ . The values of  $\Delta\zeta$  and  $\Delta\eta$  are constant, although not necessarily equal. The image of the points  $(\zeta_i, \eta_j)$  in the physical plane, obtained from equations (1) and (2), is a general curvilinear mesh of points with corresponding cartesian components  $(x_{i,j}, y_{i,j})$ . The distribution of points  $(x_{i,j}, y_{i,j})$  is highly non-uniform in order to accurately resolve the features of the flow. The governing fluid dynamic equations are solved in the transformed plane, and the flowfield within the inlet is obtained directly from the knowledge of the coordinate transformation.

In order to facilitate determination of the coordinate transformation, the governing equations (1) and (2) are inverted.<sup>1</sup> The resultant equations are

$$\alpha \frac{\partial^2 x}{\partial \zeta^2} - 2\beta \frac{\partial^2 x}{\partial \zeta \partial \eta} + \gamma \frac{\partial^2 x}{\partial \eta^2} + \delta \frac{\partial x}{\partial \eta} = 0$$

$$\alpha \frac{\partial^2 y}{\partial \zeta^2} - 2\beta \frac{\partial^2 y}{\partial \zeta \partial \eta} + \gamma \frac{\partial^2 y}{\partial \eta^2} + \delta \frac{\partial y}{\partial \eta} = 0$$
(22)

where

$$\alpha = \left( \frac{\partial x}{\partial \eta} \right)^2 + \left( \frac{\partial y}{\partial \eta} \right)^2$$

$$\beta = \frac{\partial x}{\partial \zeta} \frac{\partial x}{\partial \eta} + \frac{\partial y}{\partial \zeta} \frac{\partial y}{\partial \eta}$$

$$\gamma = \left( \frac{\partial x}{\partial \zeta} \right)^2 + \left( \frac{\partial y}{\partial \zeta} \right)^2$$

$$\delta = T(\zeta, \eta) \gamma$$
(23)

where  $T(\zeta, \eta)$  is given in (2).<sup>\*</sup> Equations (22) and (23) are solved in the unit square in the transformed plane. The coordinates  $x(\zeta, \eta)$  and  $y(\zeta, \eta)$  are subject to Dirichlet boundary conditions on the boundaries of the unit square, i.e.,

$$\left. \begin{array}{l} x = f_1(\zeta) \\ y = g_1(\zeta) \end{array} \right\} \text{ on } \eta = 0$$

$$\left. \begin{array}{l} x = f_2(\zeta) \\ y = g_2(\zeta) \end{array} \right\} \text{ on } \eta = 1$$

$$\left. \begin{array}{l} x = f_3(\eta) \\ y = g_3(\eta) \end{array} \right\} \text{ on } \zeta = 0$$

---

<sup>\*</sup>The symbols  $\alpha$ ,  $\beta$ ,  $\gamma$  and  $\delta$  in (23) are used to represent different quantities in sections other than the present (II.A).

$$\left. \begin{aligned} x &= f_4(\eta) \\ y &= g_4(\eta) \end{aligned} \right\} \text{ on } \zeta = 1$$

The above boundary conditions can be clearly interpreted as specifying the location of the mesh points on the entire boundary of the computational domain in the physical plane (e.g., the ramp, cowl, upstream and downstream boundaries). As shall be discussed later, the specification of the boundary mesh point distribution requires careful consideration of the nature of the flowfield to be computed.

Equations (22) are solved numerically using an Accelerated Gauss-Seidel Method.<sup>19</sup> Beginning with an initial estimate  $(x_{i,j}^1, y_{i,j}^1)$ , an iterative sequence of values  $(x_{i,j}^n, y_{i,j}^n)$ ,  $n = 2, 3, \dots$  is obtained from

$$\begin{aligned} x_{i,j}^{n+1} &= x_{i,j}^n + \omega_{i,j}(\tilde{x}_{i,j} - x_{i,j}^n) \\ y_{i,j}^{n+1} &= y_{i,j}^n + \omega_{i,j}(\tilde{y}_{i,j} - y_{i,j}^n) \end{aligned} \quad n = 1, 2, 3, \dots \quad (24)$$

where

$$\begin{aligned} \tilde{x}_{i,j} &= x_{i,j}^n + \alpha_{i,j}(x_{i+1,j}^n + x_{i-1,j}^{n+1} - 2x_{i,j}^n)/\Delta\zeta^2 \\ &\quad - 2\beta_{i,j}(x_{i+1,j+1}^n - x_{i-1,j+1}^n - x_{i+1,j-1}^{n+1} + x_{i-1,j-1}^{n+1})/4\Delta\zeta\Delta\eta \\ &\quad + \gamma_{i,j}(x_{i,j+1}^n + x_{i,j-1}^{n+1} - 2x_{i,j}^n)/\Delta\eta^2 \\ &\quad + \delta_{i,j}(x_{i,j+1}^n - x_{i,j-1}^{n+1})/2\Delta\eta \end{aligned} \quad (25)$$

and a similar expression is employed for  $\tilde{y}_{i,j}$ .

The coefficients  $\alpha_{i,j}$ ,  $\beta_{i,j}$ ,  $\gamma_{i,j}$  and  $\delta_{i,j}$  are obtained by straightforward second-order accurate finite-difference expressions for the terms in (23),

e.g.,

$$\alpha_{i,j} = [(x_{i,j+1}^n - x_{i,j-1}^{n+1})^2 + (y_{i,j+1}^n - y_{i,j-1}^{n+1})^2] / 4 \Delta \eta^2$$

The algorithm (24) is used to update the coordinates along lines of constant  $\eta$  (i.e., constant  $j$ ) in the direction of increasing  $\zeta$  (i.e., increasing  $i$ ).

Thus, in forming  $\tilde{x}_{i,j}$  and  $\tilde{y}_{i,j}$ , the most recent values of  $x$  and  $y$  on the  $j - 1$  line (e.g.,  $x_{i,j-1}^{n+1}$ ,  $y_{i,j-1}^{n+1}$ ) are employed to facilitate convergence and reduce computer storage requirements.

The acceleration parameter  $\omega_{i,j}$  is employed to speed convergence of the iteration sequence. Since equations (22) are non-linear, an optimum value for  $\omega$  at each point cannot be found. A linearized stability analysis of the highest-order terms yields the following criterion for stability of the algorithm:

$$0 < \omega_{i,j} < \frac{\Delta \zeta^2 \Delta \eta^2}{\Delta \eta^2 \alpha_{i,j} + \Delta \zeta^2 \gamma_{i,j}}$$

Based on experience with the code, the following criterion is employed:

$$\omega_{i,j} = 0.95 \frac{\Delta \zeta^2 \Delta \eta^2}{\Delta \eta^2 \alpha_{i,j} + \Delta \zeta^2 \gamma_{i,j}} \quad (26)$$

The convergence of sequence (24) is monitored by computing the following ratios at all interior points at selected values of  $n$ :

$$r_{x_{i,j}} = |x_{i,j}^{n+1} - x_{i,j}^n| / (1 + |x_{i,j}^{n+1}|)$$

$$r_{y_{i,j}} = |y_{i,j}^{n+1} - y_{i,j}^n| / (1 + |y_{i,j}^{n+1}|)$$
(27)

These quantities essentially represent the absolute relative change in the values of  $(x_{i,j}, y_{i,j})$  during the previous iteration, with an additional additive unitary term in the denominator to prevent an undefined operation when  $x_{i,j}$  or  $y_{i,j}$  is zero. Iteration sequence (24) is considered to have converged when

$$\max_{i,j} r_{x_{i,j}} + \max_{i,j} r_{y_{i,j}} < \text{CONVER}$$
(28)

where, for example,  $\max_{i,j} r_{x_{i,j}}$  is the maximum value of  $r_{x_{i,j}}$  over all interior points and CONVER is a small quantity, typically  $10^{-6}$  or smaller. Further guidelines for the choice of CONVER are given in Section III.C. (Table 5).

The function of the source term  $T(\zeta, \eta)$  in (1) is to provide stretching of the mesh in the  $\eta$ -direction within the boundary layers on the ramp and cowl and approximately uniform spacing in between the boundary layers. The effect of this term can be seen by considering an arbitrary streamwise location given by  $\zeta = \zeta_i$  within the inlet. For typical inlet configurations, the second equation in (22) may be approximated to lowest order by

$$\frac{\partial^2 y}{\partial \eta^2} + T(\zeta, \eta) \frac{\partial y}{\partial \eta} = 0$$
(29)

The solution to this equation can be written in the following form, noting that  $\eta_j = (j - 1)/(JL - 1)$ :

$$y_{i,j} = \begin{cases} y_{i,1} + a_1[\exp(C_1 \eta_j / \eta_1) - 1], & 0 \leq \eta_j \leq \eta_1 & (30) \\ y_{i,1} + a_1[\exp(C_1) - 1] + a_2(\eta - \eta_1), & \eta_1 \leq \eta \leq \eta_2 & (31) \\ y_{i,JL} - a_3[\exp(a_4(1 - \eta_j)) - 1], & \eta_2 < \eta_j \leq 1 & (32) \end{cases}$$

where

$$\begin{aligned} a_0 &= \frac{y_{i,JL} - y_{i,1}}{\eta_1[\exp(C_1) - 1]/C_1 + \exp(C_1)[\eta_2 - \eta_1 + (1 - \eta_2)(1 - \exp(-C_2))]/C_2} \\ a_1 &= a_0 \eta_1 / C_1 \\ a_2 &= a_0 \exp(C_1) \\ a_3 &= a_0 (\exp(C_1 - C_2))(1 - \eta_2) / C_2 \\ a_4 &= C_2 / (1 - \eta_2) \end{aligned} \quad (33)$$

Noting that the expressions  $a_0$ ,  $a_1$ ,  $a_2$ ,  $a_3$ ,  $a_4$  and terms  $C_1$ ,  $C_2$ ,  $\eta_1$  and  $\eta_2$  are not functions of  $\eta$ , it is evident that the above approximate solution for  $y_{i,j}$  is characterized by an exponentially stretched mesh between  $\eta = 0$  and  $\eta = \eta_1$ , a uniformly distributed mesh between  $\eta = \eta_1$  and  $\eta = \eta_2$ , and an exponentially stretched mesh between  $\eta = 1$  and  $\eta = \eta_2 < 1$ .

The application of the source term  $T(\zeta, \eta)$  requires specification of the quantities  $C_1$ ,  $C_2$ ,  $\eta_1$  and  $\eta_2$  at each value of  $\zeta_i$ ,  $i = 1, 2, \dots, IL$ . In practice, this is accomplished in the following fashion. First, values for  $\eta_1$  and  $\eta_2$  are chosen that reflect the desired number of points to be stretched in the vicinity of the upper and lower surfaces. By definition,  $\eta_1 = (j_0 - 1)/(JL - 1)$ , where  $j_0$  is the number of exponentially stretched points near the lower boundary (including the point on the boundary), and  $\eta_2 = (j_1 - 1)/(JL - 1)$ , where the number of exponentially stretched points

near the upper boundary is  $JL - j_1 + 1$ . In conjunction with a separate program (called BNDRY), which is discussed in a subsequent section, the values of  $j_0$  and  $j_1$  are chosen in order to provide a sufficient number of points within the boundary layers on the ramp and cowl. Although the coordinate transformation program permits  $j_0$  and  $j_1$  to vary with  $\zeta$ , satisfactory results have been obtained with judiciously chosen constant values for  $j_0$  and  $j_1$ .

Secondly, the values of  $C_1(\zeta)$  and  $C_2(\zeta)$  are determined by the requirement that the height above the wall of the first row of points adjacent to the upper and lower surfaces (i.e.,  $\eta = \Delta\eta$  and  $\eta = 1 - \Delta\eta$ , which correspond to  $j = 2$  and  $j = JL - 1$ , respectively) remains within the limits indicated by the computational sublayer model (see Section III.A) at all streamwise locations  $\zeta$ . This is accomplished automatically by the coordinate transformation code, using information specified by the user that relates the approximate desired height of the rows  $\eta = \Delta\eta$  and  $\eta = 1 - \Delta\eta$  from the lower and upper surfaces, respectively, as a function of streamwise position  $\zeta$  (see Section III). From (30) the approximate height of the first row of points above the lower surface is the following:

$$y_{i,2} - y_{i,1} = a_1 [\exp(C_1 \Delta\eta / \eta_1) - 1] \quad (34)$$

while the height of the row of points adjacent to the upper boundary is

$$y_{i,JL} - y_{i,J2} = a_3 [\exp(a_4 \Delta\eta) - 1] \quad (35)$$

The above expressions are non-linear equations for  $C_1$  and  $C_2$ , and are solved by Newton's method.<sup>19</sup>

In solving the governing fluid dynamic equations (3) to (6), the coordinate transformation derivatives  $\zeta_x$ ,  $\zeta_y$ ,  $\eta_x$ ,  $\eta_y$  are required. They may be expressed as

$$\begin{aligned}\frac{\partial \zeta}{\partial x} &= \frac{1}{J'} \frac{\partial y}{\partial \eta} \\ \frac{\partial \zeta}{\partial y} &= - \frac{1}{J'} \frac{\partial x}{\partial \eta} \\ \frac{\partial \eta}{\partial x} &= - \frac{1}{J'} \frac{\partial y}{\partial \zeta} \\ \frac{\partial \eta}{\partial y} &= \frac{1}{J'} \frac{\partial x}{\partial \zeta}\end{aligned}\tag{36}$$

where  $J' = (\partial x / \partial \zeta)(\partial y / \partial \eta) - (\partial x / \partial \eta)(\partial y / \partial \zeta)$ . At all interior points, the derivatives on the right-hand side of (36) are obtained using second-order central differences, while on the boundaries of the domain second-order one-sided differences are employed as required. In addition, the coordinate transformation code permits the recognition of a finite number of discontinuities in the slope of the upper and lower surfaces between  $\zeta = 0$  and  $\zeta = 1$ , introducing additional second-order one-sided differences to account for them.

## B. Navier-Stokes Code

### 1. MacCormack's Method

The inlet flowfield is obtained by numerical integration of the Navier-Stokes equations (3) in time from an assumed initial condition until a steady-state solution is obtained. The numerical algorithm employed is MacCormack's method,<sup>20,21</sup> which is an alternating-direction explicit technique of Lax-Wendroff type. It has been applied to the solution of a wide variety of problems in high speed flow involving strong viscous-inviscid

interactions. A representative sample of applications is indicated in References 10, 16 and 20 through 30.

The numerical algorithm is applied on the finite-difference mesh in the  $(\zeta, \eta)$  transformed plane indicated in Figure 3. Denoting a sequence of time levels  $t^n = n \Delta t$ ,  $n = 1, 2, 3, \dots$ , where  $\Delta t$  is the time step, the vector of dependent variables  $u_{i,j}^n$  at position  $(\zeta_i, \eta_j)$  and time  $t^n$  is updated to time  $t^{n+1}$  by the following expression:

$$u_{i,j}^{n+1} = L(\Delta t)u_{i,j}^n \quad (37)$$

where  $L(\Delta t)$  is a symmetric sequence (discussed below) of time-split one-dimensional difference operators  $L_\zeta(\Delta t_\zeta)$  and  $L_\eta(\Delta t_\eta)$ . The operator  $L_\zeta(\Delta t_\zeta)$  is a second-order accurate finite-difference algorithm for the one-dimensional equation

$$\frac{\partial u}{\partial t} + \frac{\partial F}{\partial \zeta} = 0$$

Using the dummy time indices  $*$  and  $**$  with

$$u_{i,j}^{**} \equiv L_\zeta(\Delta t_\zeta)u_{i,j}^* \quad (38)$$

the  $L_\zeta$  operator is given by the following two-step predictor-corrector method:

$$\text{Predictor Step: } \overline{u}_{i,j}^{**} = u_{i,j}^* - \frac{\Delta t}{\Delta \zeta} \zeta (F_{i,j}^* - F_{i-1,j}^*)$$

$$\text{Corrector Step: } u_{i,j}^{**} = \frac{1}{2} \left[ u_{i,j}^* + \overline{u}_{i,j}^{**} - \frac{\Delta t}{\Delta \zeta} \zeta (F_{i+1,j}^{**} - F_{i,j}^{**}) \right]$$

where  $F_{i,j}^*$  implies that the flux terms are evaluated using  $u_{i,j}^*$  and so forth. Further information regarding the differencing of the stress terms

in  $F$  is given in References 21 and 25. The operator  $L_\eta(\Delta t_\eta)$  is a second-order finite-difference algorithm for the one-dimensional equation

$$\frac{\partial u}{\partial t} + \frac{\partial G}{\partial \eta} = 0$$

Using a similar dummy index notation as in (38), the  $L_\eta$  operator is given by the following two-step predictor-corrector method:

$$\text{Predictor Step: } u_{i,j}^{\overline{**}} = u_{i,j}^* - \frac{\Delta t_\eta}{\Delta \eta} (G_{i,j}^* - G_{i,j-1}^*)$$

$$\text{Corrector Step: } u_{i,j}^{**} = \frac{1}{2} \left[ u_{i,j}^* + u_{i,j}^{\overline{**}} - \frac{\Delta t_\eta}{\Delta \eta} (G_{i,j+1}^{\overline{**}} - G_{i,j}^{\overline{**}}) \right]$$

where, for example,  $G_{i,j}^{\overline{**}}$  implies that the flux term is evaluated using  $u_{i,j}^{\overline{**}}$ , etc.

The operator  $L(\Delta t)$  in (37) is constructed from a symmetric sequence of the operators  $L_\zeta(\Delta t_\zeta)$  and  $L_\eta(\Delta t_\eta)$ . In the numerical code, two particular forms are employed, specifically

$$L(\Delta t) = L_\eta(\Delta t/2) L_\zeta(\Delta t) L_\eta(\Delta t/2) \quad (40)$$

and

$$L(\Delta t) = L_\zeta(\Delta t/2) L_\eta(\Delta t) L_\zeta(\Delta t/2) \quad (41)$$

where the operators on the right-hand side are applied to  $u_{i,j}$  sequentially from right to left. Both sequences (40) and (41) provide a spatially and temporally second-order accurate integration of the full Navier-Stokes equations (3). The time step size indicated by the argument of each operator  $L_\zeta$  and  $L_\eta$  must not exceed the maximum allowed for that operator. An approximate linearized stability analysis yields the following:

$$\Delta t_{\zeta} = \min_{i,j} \Delta t_{1,i,j} \quad (42)$$

$$\Delta t_{\eta} = \min_{i,j} \Delta t_{2,i,j} \quad (43)$$

where

$$\Delta t_{1,i,j} = \frac{\Delta s_{\zeta}}{\left[ |u_{\zeta}| + c + \left[ \frac{2\theta_1}{\Delta s_{\zeta}} + \frac{\theta_2}{\Delta s_{\eta}} \right] / \rho \right]} \quad (44)$$

$$\Delta t_{2,i,j} = \frac{\Delta s_{\eta}}{\left[ |u_{\eta}| + c + \left[ \frac{2\theta_1}{\Delta s_{\eta}} + \frac{\theta_2}{\Delta s_{\zeta}} \right] / \rho \right]} \quad (45)$$

where min denotes the minimum value of the right-hand side evaluated at all points  $(\zeta_i, \eta_j)$  within a given region of the flow, and

$$\begin{aligned} \Delta s_{\zeta} &= \Delta \zeta / \sqrt{\zeta_x^2 + \zeta_y^2} \\ \Delta s_{\eta} &= \Delta \eta / \sqrt{\eta_x^2 + \eta_y^2} \end{aligned} \quad (46)$$

$$u_{\zeta} = (u\zeta_x + v\zeta_y) / \sqrt{\zeta_x^2 + \zeta_y^2}$$

$$u_{\eta} = (u\eta_x + v\eta_y) / \sqrt{\eta_x^2 + \eta_y^2}$$

$$c = \sqrt{\gamma RT}, \quad R = c_p - c_v = \text{gas constant}$$

$$\theta_1 = \max \left[ \left| 2(\mu + \epsilon) + \lambda_T \right|, \quad \gamma \left( \frac{\mu}{Pr} + \frac{\epsilon}{Pr_t} \right) \right]$$

$$\theta_2 = \sqrt{(\mu + \epsilon)\lambda_T}$$

In practice, the quantities (44), (45) are multiplied by a factor (denoted as CFL) that is slightly less than one.

## 2. Mesh Splitting

Due to the non-uniformity of the mesh spacing in the physical plane, the values of  $\Delta t_{1,i,j}$  and  $\Delta t_{2,i,j}$  vary substantially within the flow. Specifically, the small mesh spacing in the  $\eta$ -direction within the boundary layers (which implies large values of  $\eta_y$  and consequently small values of  $\Delta s_\eta$ ) results in particularly small values of  $\Delta t_{2,i,j}$ . On the other hand, the larger values of  $\Delta s_\eta$  occurring outside the boundary layer imply larger values of  $\Delta t_{2,i,j}$ . If the min in (43) were taken over all points in the flow, the value of  $\Delta t_\eta$  would be controlled by the values of  $\Delta t_{2,i,j}$  in the boundary layer, and hence for a large number of points outside the boundary layers the  $L_\eta$  operator in (40) or (41) would be applied using a value of  $\Delta t_\eta$  that is smaller than the maximum allowed locally by (45). This implies that the algorithm is not being optimally applied.

A substantial improvement is realized by incorporation of the split mesh technique.<sup>21</sup> As utilized in the numerical code, the computational domain is divided in the  $\eta$ -direction into five regions (see Figure 4) given by

<u>Region</u>	<u>Extent</u>
1	$1 \leq j \leq JI1$
2	$JI1 + 1 \leq j \leq JI2$
3	$JI2 + 1 \leq j \leq JI3$
4	$JI3 + 1 \leq j \leq JI4$
5	$JI4 + 1 \leq j \leq JL$

where  $1 < JI1 < JI2 < JI3 < JI4 < JL$ . Within each region the operator sequence is

Regions 1, 2, 4 and 5:  $L(\Delta t) = [L_{\eta}(\Delta t/2m_{\ell})L_{\zeta}(\Delta t/m_{\ell})L_{\eta}(\Delta t/2m_{\ell})]^{m_{\ell}}$ ,  $\ell = 1, 2, 4, 5$  (47)

Region 3:  $L(\Delta t) = L_{\zeta}(\Delta t/2)L_{\eta}(\Delta t)L_{\zeta}(\Delta t/2)$  (48)

where  $m_{\ell}$ ,  $\ell = 1, 2, 4, 5$  are integers, and the exponent  $m_{\ell}$  implies that the operator sequence within the brackets is applied  $m_{\ell}$  times. The application of the stability requirements (42) to (45) within each region yields the following:

Regions 1, 2, 4, 5:  $\Delta t/m_{\ell} \leq \min_{\ell}(\Delta t_{1,i,j}, 2\Delta t_{2,i,j})$  (49)

Region 3:  $\Delta t \leq \min_3(2\Delta t_{1,i,j}, \Delta t_{2,i,j})$  (50)

where  $\min_{\ell}(\Delta t_{1,i,j}, 2\Delta t_{2,i,j})$  implies the minimum value of  $\Delta t_{1,i,j}$  and  $2\Delta t_{2,i,j}$  within the  $\ell^{\text{th}}$  region. A further requirement is that the ratios  $m_1/m_2$  and  $m_5/m_4$  be integers, in order that adjacent regions may be updated in time in a near-simultaneous fashion.

An automatic optimization algorithm is utilized in order to determine the most efficient splitting of the five regions. At each time step, the following ratio is computed for every set of values of JI1, JI2, JI3 and JI4:

$$\frac{\Delta t}{\sum_{\ell=1}^5 P_{\ell} m_{\ell}} \quad (51)$$

where  $P_{\ell}$  is the number of rows in region  $\ell$  (e.g.,  $P_2 = JI2 - JI1$ ) and  $m_{\ell}$  is defined in (47) with  $m_3 = 1$ . This quantity is essentially

proportional to the ratio of the time step  $\Delta t$  to the computer time required to update the flowfield by the amount  $\Delta t$ , and hence is a direct measure of the relative efficiency of a particular mesh splitting. The set of values of  $J_{I1}$ ,  $J_{I2}$ ,  $J_{I3}$  and  $J_{I4}$  that yields the largest value of the ratio (51) while having integer values for  $m_1/m_2$  and  $m_5/m_4$  is then employed in updating the solution by the amount  $\Delta t$ . The process is continually repeated, thereby achieving maximum code efficiency at all times. To the author's knowledge, this represents the first incorporation of a completely automatic mesh-splitting algorithm with MacCormack's method.

Special consideration is required at the intermesh boundaries between the five regions in order to conserve mass, momentum and energy. Details of the intermesh conservation relations are given in Reference 21.

### 3. Mesh Overlapping

Due to limitations in computer core memory, it is often not feasible to compute the entire flowfield of a high speed inlet using a single mesh. In such cases, the technique of mesh overlapping is useful. The basic concept is illustrated in Figure 5. The entire inlet flowfield is divided into two or more overlapping regions denoted by A, B, etc. A steady-state solution is obtained first in region A (defined by the boundary abcd). The values of the flowfield variables at station a'd' are then used as the upstream profile for region B (defined by the boundary a'b'c'd'). The equations of motion are then integrated in time in region B until a steady-state solution is achieved. Further downstream regions can be computed in the same fashion.

The application of the mesh overlapping technique requires that two conditions be satisfied. First, within each overlapping zone (e.g.,

a'b c d'), the flowfield outside the boundary layers must be supersonic in order that there be no downstream influence on the flow in this area. Secondly, within the vicinity of the restart station (curve a'd'), the boundary layers on the ramp and cowl must be developing smoothly. In particular, the restart station must not coincide with any strong viscous-inviscid interaction (e.g., shock-boundary layer interaction) or abrupt change in conditions in the boundary layer (e.g., an abrupt change in the bleed mass flux). This condition implies that the behavior of the flow in the boundary layer in the vicinity of the restart station is essentially governed by the boundary layer equations with no strong viscous-inviscid coupling, and hence mathematically there is no downstream influence on the flow in the boundary layers near the restart station.

The technique of overlapping mesh regions has been widely used in high speed flow calculations, including inlet flows.<sup>10,16,21,25,26</sup> It has been tested and proven in the present numerical code.

#### 4. Boundary Conditions

The boundary conditions for the Navier-Stokes equations can be categorized into four major types (see Figure 6a)--upstream, downstream, wall and no reflection. On the upstream boundary, the flow variables are held fixed at the appropriate freestream values. In the case of mesh overlap, the variables at the restart station (a'd' in Figure 5) are held fixed at their steady-state values. At the downstream boundary, the conventional zero-gradient boundary condition is applied, i.e.,

$$\frac{\partial u}{\partial \xi} = 0 \quad (52)$$

On the ramp and inlet surfaces, the following boundary conditions are used:

$$\begin{aligned}
\vec{v} \cdot \vec{s} &= 0 \quad (\text{Zero tangential velocity}) \\
\vec{v} \cdot \vec{n} &= v_w \quad (\text{Boundary layer bleed}) \\
\frac{\partial T}{\partial n} &= 0 \quad (\text{Adiabatic wall}) \\
\frac{\partial p}{\partial n} &= 0 \quad (\text{Approximate derived boundary condition for pressure})
\end{aligned}
\tag{53}$$

where  $\vec{s}$  and  $\vec{n}$  are tangential and normal unit vectors, respectively, at the wall that can be expressed in terms of  $\eta_x$  and  $\eta_y$ . Also,  $v_w$  is the normal velocity at the wall, obtained from the specified mass flux along the boundaries. The approximate derived boundary condition for the pressure has been successfully employed in a variety of flows exhibiting strong viscous-inviscid interaction.<sup>23,28,31</sup> The fourth category of boundary conditions refers to curves AB and DE of Figure 6a. As the name suggests, these contours are assumed to be no-reflection boundaries. The boundary conditions are<sup>30</sup>

$$\begin{aligned}
\frac{\partial u}{\partial \xi} &= 0 \\
\frac{\partial v}{\partial \xi} &= 0 \\
\frac{\partial T}{\partial \xi} &= 0 \\
\frac{\partial p}{\partial \xi} &= 0
\end{aligned}
\tag{54a}$$

where the derivative  $\partial/\partial \xi$  is taken along the outwards running characteristic at the boundary, which is oriented at the Mach angle  $\mu = \sin^{-1}(1/M)$  with respect to the velocity vector  $\vec{v}$  as illustrated in Figure 6b. The velocity  $\vec{v}$  may, in general, be pointing in or out of the computational domain at either

boundary. The utilization of the no-reflection boundary condition requires that the following conditions be satisfied:

a) The local Mach number  $M = |\vec{v}|/c$ , where  $c$  is the local speed of sound, must be greater than one.

b) The local normal Mach number  $|\vec{v} \cdot \vec{n}|/c$  must be less than one.

The first requirement implies that the characteristics exist (i.e., the flow is locally supersonic), and the second requirement insures that there is a single outwards running characteristic. The no-reflection boundary condition permits the angle of attack of the inlet to be varied by constructing the contours AB and DE to be parallel to the incoming flow, with the cartesian x-axis aligned with AB and DE. In those instances where the shock wave emanating from the ramp leading edge E intersects the lower surface upstream of the cowl leading edge B, the contour between the intersection point and B may have to be roughly aligned with the local flow direction in order to satisfy condition b) above. If either condition a) or b) is not satisfied locally, the numerical code assigns freestream values to the flow variables according to

$$\begin{aligned} u &= U_{\infty} \\ \vec{v} \cdot \vec{n} &= 0 \\ p &= p_{\infty} \\ T &= T_{\infty} \end{aligned} \tag{54b}$$

and prints a warning message. Since the boundary conditions (54b) may not be physically realistic under such circumstances, the user must take appropriate steps to remedy the situation if the warning messages persist throughout the calculation. If condition a) is being violated (e.g., a

terminal shock is located upstream of the cowl lip, as occurs in fully external compression inlets), it should be recognized that the boundary conditions (54) are inappropriate and the flowfield cannot be computed unless proper modifications are made to the boundary condition subroutine. If condition b) is not satisfied (e.g., the ramp shock intersects the curve AB upstream of the cowl leading edge, and the normal Mach number on the segment between the intersection point and cowl leading edge is greater than one), the user can realign the appropriate segment of the boundary as discussed previously.

The boundary conditions are implemented in the numerical code using second-order accurate finite-difference approximations in general. The zero normal derivative boundary condition on the pressure in (53) is incorporated using first-order accurate differencing.

#### 5. Numerical Damping

The algorithm of MacCormack is a "shock-capturing" type in which shock waves are effectively broadened or "smeared" over several mesh points, rather than appearing as sharp discontinuities in the flow. In the vicinity of strong shock waves, the numerical truncation error associated with the shock broadening can lead to numerical instability. Although this difficulty can, in principle, be avoided by refining the mesh sufficiently in the vicinity of the shock to resolve its physical structure (i.e., by employing mesh spacing normal to the shock of the order of the mean free path of the gas), the cost would be prohibitive. Alternately, a fourth-order "pressure damping" term is employed,<sup>21</sup> which is of significance only in the vicinity of pressure oscillations where the solution has been adversely affected by truncation error anyway. In the  $L_{\zeta}$  operator in (40) and (41), the following

expression is added to the flux  $F_{i,j}^*$  in the predictor step:

$$-\alpha(|U_{i,j}| + |\vec{v}_\zeta| c_{i,j}) \frac{|p_{i+1,j} - 2p_{i,j} + p_{i-1,j}|}{(p_{i+1,j} + 2p_{i,j} + p_{i-1,j})} (u_{i+1,j} - u_{i,j}) \quad (55)$$

where the expression is evaluated using  $*$  level quantities,  $\alpha$  is a damping constant (typical values range from 0.5 to 5.0 depending on the flow),

$|\vec{v}_\zeta| = \sqrt{\zeta_x^2 + \zeta_y^2}$ , and  $c$  is the speed of sound. Similarly, the following term is added to the flux  $F_{i,j}$ :

$$-\alpha(|U_{i,j}| + |\vec{v}_\zeta| c_{i,j}) \frac{|p_{i+1,j} - 2p_{i,j} + p_{i-1,j}|}{(p_{i+1,j} + 2p_{i,j} + p_{i-1,j})} (u_{i,j} - u_{i-1,j}) \quad (56)$$

where the expression is evaluated using  $**$  level quantities. Corresponding expressions are used for the  $L_\eta$  operator. The numerical code permits the user to omit the pressure damping terms for the purpose of increased efficiency when computing flows with no shock waves.

An additional form of damping is incorporated into the numerical code in order to control any destabilizing oscillations that may result from initial flow transients.<sup>32</sup> The technique consists of multiplying the viscosity  $\lambda_T = -(2/3)(\mu + \epsilon)$  by a large negative constant  $\beta$  during the early stages of the calculation, resetting  $\lambda_T$  to  $-(2/3)(\mu + \epsilon)$  (i.e.,  $\beta = +1$ ) and then converging the flow. In all calculations with the numerical code, it was not found necessary to utilize this damping.

Finally, the convective damping technique of MacCormack<sup>16,20</sup> is incorporated into the  $L_\zeta$  operator in order to prevent occurrence of a non-linear instability in regions of separated flow.

## 6. Convergence of Flowfield to Steady State

Since the steady-state flowfield is obtained by integration in time from an assumed initial condition, a criterion for convergence must be stipulated. Appealing to the physics of the flow, it is evident that the physical time (referring to the time  $t$  in equation (3)) necessary for achievement of a steady-state solution is a multiple of the characteristic time  $t_c$  required for a fluid particle to travel from the upstream to the downstream boundaries of the computational domain. Denoting an approximate value of the velocity in the inviscid region by  $U_e$  and the length of a given region by  $L$ ,

$$t_c = L/U_e \quad (57)$$

Experience has shown that a total physical time of approximately  $3t_c$  is sufficient to guarantee achievement of a steady-state solution provided there is no flow separation.<sup>26</sup> For cases with flow separation, a somewhat larger physical time of  $5t_c$  to  $6t_c$  is required. The above criteria are general guidelines. In application, a prudent strategy is to check the change in the flow variables (e.g., surface pressure, skin friction) between two physical time levels that are separated by approximately  $1t_c$  (e.g.,  $t \approx 2t_c$  and  $t \approx 3t_c$ ). Provided that the changes are typically one to two percent or less, the flowfield may be considered converged.

## 7. Computational Sublayer

The geometry associated with the computational sublayer calculation is illustrated in Figure 7 for the  $n = 0$  and  $n = 1$  surfaces. The "ordinary mesh" obtained from the coordinate generation program is indicated by the open symbols. The algorithm of MacCormack is employed on the ordinary

mesh. The region between the wall and the first row of adjacent ordinary mesh points is denoted as the "computational sublayer." Within this region, a locally orthogonal coordinate system  $(x',y')$  is employed. The approximate governing equations (18) to (20) are solved on a finite-difference mesh, indicated by the closed symbols.

As indicated previously, the achievement of maximum code efficiency implies that the distance  $y'_m$  of the first row of ordinary points should be as large as possible within the upper limit of roughly  $60 \nu_w/u_*$ . Since this height is substantially greater than the viscous sublayer, accurate values for the stress components and heat transfer vector cannot be obtained at the matching points by ordinary finite differences involving the velocity components at the wall and the matching points. The purpose of the computational sublayer technique is to provide values of the stress components and heat transfer vector at the wall and at the matching points for use in application of MacCormack's method at the matching points. The cartesian stress components  $\tau_{xx}$ ,  $\tau_{xy}$ ,  $\tau_{yy}$  are obtained from the sublayer solution by a simple coordinate transformation, under the reasonable assumption that the normal stresses in the  $x'-y'$  coordinate system (i.e.,  $\tau_{x'x'}$ ,  $\tau_{y'y'}$ ) are negligible compared to  $\tau_{x'y'}$ . Similarly, the heat transfer components  $Q_x$ ,  $Q_y$  are obtained by coordinate transformation from the sublayer solution under the reasonable assumption that  $Q_x \ll Q_y$  in the sublayer.

The computational sublayer region is solved after each updating of the adjacent region of the ordinary mesh. Denoting  $\tau_{x'y'}$  as  $\tau$ , with subscripts  $w$  and  $m$  implying the wall and matching point, respectively, the sequence of solution is as follows. First, the shear stress components

are found from

$$\tau_w = \frac{\left[ u_m - \frac{\partial p}{\partial x'}, \int_0^{y'_m} \frac{f(y') y' dy'}{(\mu + \epsilon)} \right]}{\int_0^{y'_m} \frac{f(y') dy'}{(\mu + \epsilon)}} \quad (58)$$

$$\tau_m = \tau_w + \frac{\partial p}{\partial x'} y'_m + \dot{m} u_m$$

where  $u_m$  is the component of the velocity at the matching point parallel to the surface and

$$f(y') = \exp \int_{y'}^{y'_m} \frac{\dot{m} dy'}{(\mu + \epsilon)} \quad (59)$$

Expression (58) is obtained by integrating (18) twice. The velocity in the sublayer is then obtained by integrating

$$\frac{\partial u'}{\partial y'} - \frac{\dot{m}}{(\mu + \epsilon)} u' = \frac{(\tau_w + \frac{\partial p}{\partial x'} y')}{(\mu + \epsilon)} \quad (60)$$

The temperature field is then determined by (19), and the heat transfer vectors computed. Further details are given in Reference 18.

### C. Overall Description of Programs

There are, in general, a total of four separate computer programs that are employed to compute the flowfield in a high speed inlet. The purposes of the programs are as follows:

#### a) Coordinate Generation Program (COORD)

This program is employed to generate the sequence of overlapping mesh systems that are utilized by the Navier-Stokes code.

b) Upstream/Downstream Boundary Mesh Distribution Program (BNDRY)

The purpose of this code is to determine the appropriate distribution of mesh points in general for the upstream and downstream boundaries of each mesh system. It is utilized in conjunction with the coordinate generation program.

c) Navier-Stokes Program (INLET)

This program solves for the steady-state flowfield within each mesh system.

d) Upstream Boundary Interpolation Program (UPSTRM)

The purpose of this short program is to permit interpolation of flow data at the restart station of two overlapped meshes where the height of the two mesh systems is not identical. This procedure is employed in the calculation of the simulated high speed inlets developed by McDonnell Aircraft Company (MCAIR)<sup>33</sup> and is illustrated in Figure 8.

For the MCAIR inlet configuration, the calculation proceeds in two basic stages. In the first stage, the boundary layer development on the ramp (i.e., the lower surface in Figure 8) is computed. This procedure is accomplished in the following steps.

- a) Using program BNDRY, the desired mesh spacing on the upstream and downstream boundaries of mesh A is determined.
- b) Using the information from a) above, the coordinate system of mesh A is computed using program COORD.
- c) Using the coordinate transformation computed in b), the steady-state flow in region A is computed using program INLET.

In the event that the entire ramp boundary layer development upstream of the inlet entrance cannot be computed with a single mesh system, a second overlapping mesh system is generated using COORD and the flowfield is determined using INLET. This procedure is repeated until the ramp boundary layer has been computed up to the vicinity of the inlet entrance.

In the second stage, the flowfield within the inlet is computed.

This procedure requires the following steps:

- a) Using program BNDRY, the desired mesh spacing on the upstream and downstream boundaries of mesh B is determined. See also step c) immediately below.
- b) Using this information, the coordinate system of mesh B is determined using program COORD.
- c) Because the vertical distributions of points in meshes A and B at the restart station are not identical, the program UPSTRM is used to interpolate the flow variables onto the upstream boundary of mesh B. There are certain restrictions on the use of program UPSTRM (see Section IV.H.1) that must be satisfied in determining the mesh distribution on the upstream boundary of mesh B.
- d) The steady-state flowfield is obtained using program INLET.

For all subsequent regions, the following steps are taken:

- a) The program BNDRY is used to determine the desired mesh spacing on the downstream boundary on the next mesh region.
- b) The coordinate transformation is obtained using COORD.
- c) The steady-state flowfield is obtained using INLET.

In those cases where a variety of inlet configurations are to be tested at the same entrance conditions, the first stage need only be accomplished once.

## SECTION III

### GENERATION OF COORDINATE TRANSFORMATION

#### A. Preliminary Analysis

The basic requirement for a finite-difference mesh is to provide accurate resolution of all pertinent features in the flow. The mesh point distribution, therefore, is dependent on the particular flowfield to be computed, and requires preliminary analysis in two major areas, as discussed below.

##### 1. Streamwise Mesh Spacing

In general, the controlling influence on streamwise mesh spacing for high speed inlet calculations is the necessity of accurately resolving the boundary layer development. Unfortunately, there does not exist precise criteria for the determination of the appropriate streamwise mesh spacing, except an exhaustive (and usually infeasible) truncation error study in each case. An oft-quoted guideline in computational fluid mechanics is that a streamwise mesh spacing with cell Reynolds number less than two is sufficient to resolve all characteristic streamwise features within the boundary layer.<sup>34</sup> However, this criterion is based on a truncation error analysis for the particular case in which first-order upwind differencing is employed for the convective terms of the governing equations, and does not specifically apply to MacCormack's method. Furthermore, experience in strong viscous-inviscid interacting boundary layer flows has shown this criterion to be unnecessarily severe.<sup>21,35</sup>

A generally successful guideline for determining streamwise mesh spacing is based on the ratio  $\Delta x/\delta$ , where  $\Delta x$  is the streamwise mesh spacing (typically evaluated on the upper and lower boundaries) and  $\delta$  is a reference boundary layer thickness. In those regions in which the boundary is

approximately in equilibrium (e.g., mesh A of Figure 8), a mesh spacing of  $\Delta x/\delta_0 \approx 1$  to 2 is satisfactory, where  $\delta_0$  is the boundary layer thickness at, say, the downstream boundary of the mesh region. For regions of strong viscous-inviscid interaction, such as occur within the inlet, the value of  $\Delta x/\delta_0$  (where  $\delta_0$  is the boundary layer thickness immediately upstream of the shock-boundary layer interaction) is generally taken to be less than one. Typical values of  $\Delta x/\delta_0$  for shock-turbulent boundary layer interactions are 0.17 in Reference 16, 0.45 in Reference 10 and 1.0 in Reference 36. The presence of flow separation has an important influence on  $\Delta x/\delta_0$ , requiring it to be less than 0.5 in general. Experience with the numerical code<sup>18</sup> in computing inlet flows that do not exhibit flow separation has shown that the criterion  $\Delta x/\delta_0 \approx 1$  is generally sufficient.

The coordinate transformation program can be used with either uniform or arbitrary mesh spacing in the x-direction. For uniform mesh spacing, the procedure is to estimate the values of  $\delta_0$  as discussed above, using either experimental data or approximate techniques, and to choose a value of  $\Delta x$  that insures that the criterion on  $\Delta x/\delta_0$  is met at all streamwise locations.

## 2. Boundary Layer Mesh Spacing

The mesh spacing in the boundary layer or  $\eta$ -direction is influenced by three major factors. First, there must be sufficient resolution of the boundary layer by the computational sublayer mesh and ordinary mesh combined. Typically, a total of 10 to 15 ordinary mesh points should be within each boundary layer on the ramp and cowl at all streamwise locations. Of course, since the entire flowfield is not known a priori, this achievement of this criterion can only be determined a posteriori. The practical impact of

this criterion for the purpose of preliminary analysis is to assist in determining the appropriate distribution of mesh points on the upstream and downstream boundaries, using program BNDRY. Past results in calculation of high speed inlet flows<sup>18</sup> have shown that the satisfaction of the requirement of 10 to 15 ordinary mesh points within each boundary layer at the upstream and downstream boundary generally insures achievement of the requirement at all streamwise locations. Insofar as the computational sublayer mesh is concerned, a sufficient number of points are required in order that the viscous sublayer be adequately resolved. This implies<sup>36,37</sup> that  $\Delta y_{SL}^+ \leq 5$  at all streamwise locations, where  $\Delta y_{SL}^+ = \Delta y_{SL} u_* N / \nu_w$ , with  $\Delta y_{SL}$  = mesh spacing in computational sublayer,  $u_* = \sqrt{\tau_w / \rho_w}$  and  $\nu_w = \mu_w / \rho_w$ , and N is defined by (14). Naturally, the quantities  $\tau_w$ ,  $\rho_w$  and  $\mu_w$  are not known a priori, and in practice an engineering estimate is used (see below) to insure satisfaction of the requirement at a selected number of streamwise locations.

The second factor influencing mesh spacing in the boundary layer direction is the requirements of efficiency and accuracy imposed by the use of the computational sublayer technique. As discussed in Section I.C.3, this implies (see Figure 7)

$$20 \frac{\nu_w}{u_*} \leq y_m' \leq 60 \frac{\nu_w}{u_*} \quad (61)$$

Assuming  $\partial p / \partial n \approx 0$  in the boundary layer, the length scale  $\nu_w / u_*$  is given by

$$\frac{\nu_w}{u_*} = \frac{\mu_w}{\rho_w} \frac{RT_w}{U_e} \sqrt{\frac{2}{c_f} \frac{T_e}{T_w}} \quad (62)$$

where  $c_f = \tau_w / [(1/2) (\rho_e U_e^2)]$  and the subscript e refers to conditions at the edge of the boundary layer. The utilization of this expression requires

estimates for  $M_e$  (the Mach number at the boundary layer edge) and the wall pressure  $p_w$ , obtained either from experimental data or a simplified inviscid analysis. The value of  $T_w$  (and hence  $\mu_w$ ) can then be estimated (for adiabatic walls) from

$$T_w = \left(1 + \frac{\gamma - 1}{2} \text{Pr}_t M_e^2\right) T_e \quad (63)$$

where  $T_e$  is approximated by

$$T_e = T_{t_\infty} / \left[1 + \frac{\gamma - 1}{2} M_e^2\right] \quad (64)$$

where  $T_{t_\infty}$  is the freestream stagnation temperature. The value of  $U_e$  may be obtained from  $U_e = M_e \sqrt{\gamma R T_e}$ . The value of  $c_f$  may be estimated by a variety of engineering techniques.<sup>38</sup> It is important to note that  $c_f$  can be increased substantially by boundary bleed. Experience in computing high speed inlets<sup>18</sup> indicates that typical values of  $c_f$  in bleed regions can be as large as 0.01 depending on the bleed mass flux.

In practice, it is generally only necessary to estimate an appropriate value of  $y'_m$  from (61) at a few points. These points are typically taken to be upstream and downstream of each shock-boundary layer interaction, since the value of  $v_w/u_{*}$  varies inversely with the wall pressure. The above expression (62) can also be used to determine the number of points required in the sublayer in order to satisfy the requirement  $\Delta y_{SL}^+ \leq 5$  discussed above.

The third factor influencing mesh spacing in the boundary layer direction is given by the requirement of numerical stability in the computational sublayer in the presence of bleed. The condition is that the bleed cell Reynolds number  $Re_m$  defined by

$$Re_m^* = \frac{|\dot{m}| \Delta y_{SL}}{2(\mu + \epsilon)} \quad (65)$$

be everywhere less than approximately 0.25 within the computational sublayer. Noting that the maximum value of  $Re_m^*$  generally occurs on the wall, this condition can be approximated by

$$\frac{|\dot{m}| \Delta y_{SL}}{2u_w} \leq 0.25 \quad (66)$$

at all streamwise locations. Since the values of  $\dot{m}$  are known, and  $u_w$  is a function of  $T_w \approx T_{t\infty}$  for adiabatic walls, this condition can be directly evaluated at all locations.

In some instances, there is a boundary layer on the lower surface only (e.g., mesh A in Figure 8). The upper boundary  $n = 1$  must therefore be placed at a sufficiently large distance from the lower surface in order that the freestream boundary conditions are applicable. This distance is typically taken to be approximately  $5\delta$ , where  $\delta$  is the boundary layer thickness at the downstream end of the mesh.<sup>16</sup> The use of equations (30) to (32) will cause a decrease in mesh spacing near the upper boundary. This decrease will not seriously affect code performance, and has surprisingly yielded an improved solution for a flat plate turbulent boundary layer.\*

---

\* In particular, calculations for a fully turbulent flat plate boundary layer have been performed using a rectangular computational domain whose spacing in  $y$  is symmetrical about the line midway between the lower and upper boundaries. This type of coordinate system can easily be obtained by choosing  $JL$  to be odd,  $DY\phi = DY1$  and  $n_1 = n_2 = 0.5$  (i.e.,  $J\phi\phi = J\phi 1 = J1\phi = J11 = (JL+1)/2$ ; see Sections 11.B and 11.C). It has been found that with this type of coordinate system, there is no characteristic "hump" in  $\delta_1^*$  immediately downstream of the leading edge. This hump had been observed with the code for fully turbulent flat plate boundary layer calculations with mesh spacing in  $y$  consisting of a uniform stretching within the boundary layer followed by a constant mesh spacing.

### 3. Example: Upstream Inlet Region for MCAIR Case 35

In Figure 9, a portion of the flowfield of a simulated high speed inlet is illustrated. The configuration corresponds to the upstream inlet portion of Case 35 of the MCAIR study.<sup>33</sup> The freestream Mach number  $M_\infty$  is 3.51, and the freestream total temperature  $T_{t_\infty}$  and total pressure  $p_{t_\infty}$  are  $576^\circ\text{R}$  and  $7,099 \text{ lbf/ft}^2$ , respectively. The freestream static pressure and temperature are  $91.8 \text{ lbf/ft}^2$  and  $166^\circ\text{R}$ . A fully developed turbulent boundary on the ramp enters a converging duct formed by two plates. The shock wave formed by the cowl surface deflection intersects the ramp at  $x = 20 \text{ in.}$  The values of the boundary layer bleed mass flux on the ramp and cowl are indicated.

First, the appropriate streamwise mesh spacing  $\Delta x$  is determined. Due to the presence of substantial boundary layer bleed on the ramp in the vicinity of the shock-boundary layer interaction, it is unlikely that flow separation will occur, and hence the criterion  $\Delta x/\delta_o \approx 1$  is satisfactory on the ramp. The experimental values of  $\delta$  on the ramp vary from  $0.25 \text{ in.}$  at  $x = 19.2 \text{ in.}$  to  $0.20 \text{ in.}$  at  $x = 24 \text{ in.}$  as indicated in Figure 9, and thus a value  $\Delta x = 0.25 \text{ in.}$  is sufficient. Since the maximum allowable value of IL is 40, this places the downstream boundary at  $x = 23.63 \text{ in.}$  upstream of the reflected shock intersection on the cowl. Thus the cowl boundary layer is not subject to any strong viscous-inviscid interaction within this computational domain. Based on the experimental value of  $\delta = 0.10 \text{ in.}$  at  $x = 25 \text{ in.}$ , this yields  $\Delta x/\delta = 2.5$  on the cowl, which is satisfactory for this region.

Secondly, the requirement of resolution of the boundary layers is considered. Based on the experimental values of the boundary layer

thickness on the ramp and cowl, the following criteria are established.

<u>Boundary</u>	<u>Surface</u>	<u>Criterion</u> <sup>*</sup>
Upstream	Ramp	10 to 15 points below $y = 0.25$ in.
	Cowl	10 to 15 points above $y = 2.09$ in.
Downstream	Ramp	10 to 15 points below $y = 0.20$ in.
	Cowl	10 to 15 points above $y = 0.88$ in.

\* Ordinary mesh points.

These criteria are directly utilized in determining the boundary mesh distribution using program BNDRY.

Next, the computational sublayer requirement (61) is considered. Considering the ramp, it is evident that the major changes to the boundary layer arise due to the shock-boundary layer interaction and mass bleed. It is sufficient, then, to consider the ramp at two locations, e.g.,  $x = 13.88$  in. (upstream boundary) and  $x = 21.8$  in. At the first location,  $T_e = 166^\circ\text{R}$  and  $T_w = 534^\circ\text{R}$  from (63). Using an estimate of  $c_f = 1.7 \times 10^{-3}$  (typical for  $M = 3.5$  adiabatic flat plate boundary layer at these Reynolds numbers), and noting that  $p_w \approx p_\infty$ , the estimated value of  $v_w/u_x$  is  $3.3 \times 10^{-5}$  ft. From (61), the desired range of  $y'_m$  at  $x = 13.88$  in. is approximately  $6.5 \times 10^{-4}$  to  $2.0 \times 10^{-3}$  ft. At the second location, the experimental Mach number  $M_e$  is 2.5 (this could also be estimated from a simple inviscid analysis, knowing the cowl surface deflection) and the wall pressure  $p_w = 5 p_\infty$ . From (63) and (64),  $T_e = 256^\circ\text{R}$  and  $T_w = 544^\circ\text{R}$ . Since boundary layer bleed is present at  $x = 21.8$  in., an estimate of  $8 \times 10^{-3}$  is used for  $c_f$  (based on experience), yielding  $v_w/u_x = 4.4 \times 10^{-6}$  ft, indicating a desired range of  $8.7 \times 10^{-5}$  ft to  $2.6 \times 10^{-4}$  ft for  $y'_m$  at  $x = 21.8$  in.

On the basis of this information, it was decided to use  $y_m' = 5 \times 10^{-4}$  from  $x = 13.875$  in. to approximately  $x = 19$  in., decreasing to  $y_m' = 2.5 \times 10^{-4}$  at  $x = 20$  in. and constant thereafter. Although the upstream value of  $y_m'$  is slightly below the range indicated, it nonetheless does not impact the code efficiency because of the smaller values of  $y_m'$  for  $x > 20$  in. The values of  $y_m^{'+}$  are thus expected to vary from 15 at  $x = 13.88$  in. to 57 at  $x = 23.63$  in.

The number of mesh points in the computational sublayer on the ramp is determined by the requirement that  $\Delta y_{SL}^+ \leq 5$  everywhere. Since the sublayer solution is extremely rapid, the maximum allowable number of points (approximately 20) may be employed. For 20 points in the sublayer, it is evident that  $\Delta y_{SL}^+$  varies from 0.79 to 3.0 on the ramp, which is entirely satisfactory.

Finally, it is necessary to check that the condition (66) is satisfied everywhere in the ramp boundary layer. In bleed zone 1,  $\dot{m} = -3.85 \times 10^{-7}$  slugs/ft<sup>2</sup>-sec and the maximum value of  $\Delta y_{SL}$  is  $5.0 \times 10^{-4}$  ft/10 or  $2.6 \times 10^{-5}$  ft, yielding a value  $|\dot{m}| \Delta y_{SL} / 2 \rho_w = 0.13$ . In bleed zone 2, the maximum value of  $\Delta y_{SL}$  is  $1.3 \times 10^{-5}$  ft, and  $|\dot{m}| \Delta y_{SL} / 2 \rho_w = 0.14$ . Both values are within the limit indicated by (66).

An analysis similar to the above is also required for the lower ramp. The results indicate that  $y_{i,JL} - y_{i,JL-1}$  should behave similar to  $y_{i,2} - y_{i,1}$ .

B. Determination of Mesh Spacing on Upstream and Downstream Boundaries Using Program BNDRY

1. Introduction

The program BNDRY is employed to determine the distribution of mesh points in general on the upstream and downstream boundaries. These boundaries are assumed to be vertical lines, with a mesh point distribution given by equations (30) to (32). The purpose of the program is to determine the values of the parameters  $C_1$ ,  $C_2$ ,  $\eta_1$  and  $\eta_2$  that yield the desired mesh distribution on the boundaries. This information is then utilized by the coordinate generation program in determining the entire mesh.

As discussed in Section III.A, the following information is required for each boundary: (1) the desired height of the first ordinary mesh point above the lower and upper boundaries, i.e.,  $y_{i,2} - y_{i,1}$  and  $y_{i,JL} - y_{i,JL-1}$ , respectively (where  $i = 1$  or  $IL$ ), (2) the boundary layer thickness on the lower and upper boundaries, (3) the height of the boundary  $y_{i,JL} - y_{i,1}$ . All dimensions in the program are in feet. The user chooses a range of values of  $\eta_1$  and  $\eta_2$  to be investigated. For each value of  $\eta_1$  and  $\eta_2$ , the program computes by Newton's method the values of  $C_1$  and  $C_2$  from (34) and (35) that yield the specified values of  $y_{i,2} - y_{i,1}$  and  $y_{i,JL} - y_{i,JL-1}$  and prints the entire mesh distribution on the boundary  $y_{i,j}$ ,  $j = 1, \dots, JL$  (where  $i = 1$  or  $IL$ ). The user then chooses the particular set of values for  $\eta_1$  and  $\eta_2$  that yield the desired number of ordinary mesh points in each boundary layer (e.g., 10 to 15).

The following table provides information on the resources required to execute program BNDRY on the CYBER 175.

TABLE 1. RESOURCES REQUIRED FOR EXECUTION OF PROGRAM BNDRY

<u>Resource</u>	<u>Details</u>
Computer time	< 5 seconds (typical)
Input/Output time	< 2 seconds (typical)
Core Memory	< 60,000 words (octal)
Files required	INPUT, OUTPUT

## 2. Description of Input Variables

The input to program BNDRY consists of two cards (card "images" or lines in the case of batch input from a terminal). The definition and format of the input data is indicated in Table 2. For all source code variable names, the symbol  $\emptyset$  implies zero, and the symbol O implies the letter O.

If the estimates for  $C_1$  and  $C_2$  are too far off, the program may converge to  $C_1 = C_2 = 0$  (and possibly display an error message indicating an underflow and/or overflow has occurred). Since  $C_1$  and  $C_2$  must be positive, the program should then be rerun with alternate choices for  $C_1$  and  $C_2$ . With some experience, this difficulty will be avoided.

TABLE 2. INPUT DATA FOR PROGRAM BNDRY

Line 1: DYØ, DY1, RH, YØ, CEST1, CEST2

(Format 6F10.4)

<u>Fortran</u>	<u>Definition</u>	<u>Range or Value</u>
DYØ	$y_{i,2} - y_{i,1}$	Units: feet
DY1	$y_{i,JL} - y_{i,JL-1}$	Units: feet
RH	$y_{i,JL} - y_{i,1}$	Units: feet
YØ	$y_{i,1}$	Units: feet
CEST1	Rough estimate for C1	Typically between 1 and 10
CEST2	Rough estimate for C2	Typically between 1 and 10

Line 2: JL, JØSTAR, JØEND, J1STAR, J1END

(Format 5I5)

<u>Fortran</u>	<u>Definition</u>	<u>Range or Value</u>
JL	Number of points in $\eta$ -direction	$\leq 48$
JØSTAR, JØEND	Define smallest and largest values of $\eta_1$ to be investigated, i.e., $(JØSTAR-1)/(JL-1) \leq \eta_1 \leq (JØEND-1)/(JL-1)$	$2 \cdot JØSTAR$ $JØSTAR \cdot JØEND$ $JØEND \cdot JL - 2$
J1STAR, J1END	Same as above but for $\eta_2$	Similar to above

### 3. Source Code Notation

The definition of the pertinent source code variables is given below. For any array, the index J is equivalent to the subscript j (e.g., ETA(J) is equivalent to  $\eta_j$ ).

<u>Fortran</u>	<u>Definition</u>	<u>Range or Value</u>
DETA	$\Delta\eta = 1/(JL-1)$	
DY	$DY(J) = y_{i,j} - y_{i,j-1}$ (i = 1 or IL)	Units: feet
ETA1	$\eta_1$	
ETA2	$\eta_2$	
YY	$YY(J) = y_{i,j}$ (i = 1 or IL)	Units: feet

### 4. Sample of Output: Upstream Inlet Region for MCAIR Case 35

A portion of the sample output of program EMDM for the case of the upstream inlet region of the MCAIR inlet discussed in Section 11.1 is indicated in Figure 10. This calculation was performed using the parameters presented in the example in the previous section. As indicated earlier, the requirements for the upstream boundary of the upstream inlet region are the following:

<u>Requirement</u>	<u>Criterion</u>
Resolution of ramp boundary layer	a. 10 to 15 ordinary points $y = 0.25$ in. b. $y_{1,2} - y_{1,1} = 5.0 \times 10^{-7}$
Resolution of cowl boundary layer	a. 10 to 15 ordinary points $y = 2.00$ in. b. $y_{1,46} - y_{1,45} = 5.0 \times 10^{-7}$

It is evident from Figure 10 that values of  $\eta_1 = (JL-1)/(JL-1) = 1.0$  and  $\eta_2 = (J1-1)/(JL-1) = 27/47$  are satisfactory. The corresponding values of  $C_1$  and  $C_2$  are 2.98068 and 2.87725, respectively. The four parameters  $J1, C_1, C_2$  are utilized in the coordinate generation program.

## C. Generation of Coordinate Transformation Using Program COORD

### 1. Introduction

The program COORD is employed to calculate the coordinate transformation. Prior to the execution of this program the desired streamwise and boundary layer mesh spacing must be determined by a preliminary analysis as discussed in Section III.A.

In the present form, the COORD program incorporates the general category of inlet shapes employed by the MCAIR study,<sup>33</sup> including, of course, the flat plate portion of the ramp upstream of the inlet entrance, using uniform streamwise mesh spacing. The program can be simply modified to handle arbitrary inlet geometries, as detailed in subroutine INIT of the program.

The following table provides information on the resources required to execute program COORD on the CYBER 175. Care must be taken to insure that sufficient computer time is requested in order to complete the number of iterations specified. The program permits restarting and continuation of the calculation if convergence is not achieved within the requested number of iterations.

TABLE 3. RESOURCES REQUIRED FOR EXECUTION  
OF PROGRAM COORD

<u>Resource</u>	<u>Details</u>
Computer time	<60 seconds (typical)
Input/Output time	<10 seconds (typical)
Core Memory	150,000 words (octal)
Files Required	INPUT, OUTPUT, XY, OVRLAP, RSTART (See Section III.C.5)

### 2. Description of Input Variables

The input to program COORD consists of a variable number of cards. The definition and format of the input data is indicated in the required

order in Table 4. In those cases where the definition of an input variable is lengthy, the reader is referred to Section III.C.4. Line numbers are not assigned since the total number of input lines is variable. Additional information is given in Section III.C.4. Useful guidelines for the selection of certain input parameters are provided in Table 5.

TABLE 4. INPUT DATA FOR PROGRAM COORD

Line: M, N, MAXITR, IRDZET, IOVLP, IRETRY

(Format 6I5)

<u>Fortran</u>	<u>Definition</u>	<u>Range or Value</u>
M	Number of points in $\zeta$ -direction (i.e., IL)	$\leq 40$
N	Number of points in $\eta$ -direction (i.e., JL)	$\leq 48$
MAXITR	Maximum number of iterations of equation (24)	$\geq 1$
IRDZET	See Section III.C.4	0 or 1
IOVLP	See Section III.C.4	$1 < IOVLP < M$
IRETRY	See Section III.C.4	0 or 1

Line: J00, J01, J10, J11, IREF1, IREF2

(Format 6I5)

<u>Fortran</u>	<u>Definition</u>	<u>Range or Value</u>
J00	Defines $\eta_1$ at $\zeta = 0$	$2 < J00 < J10$
J01	Defines $\eta_1$ at $\zeta = 1$	$2 < J01 < J11$
J10	Defines $\eta_2$ at $\zeta = 0$	$J00 < J10 < JL$
J11	Defines $\eta_2$ at $\zeta = 1$	$J01 < J11 < JL$
IREF1	See Section III.C.4	$1 < IREF1 < N$
IREF2	See Section III.C.4	$1 < IREF2 < N$

TABLE 4. CONT'D

<div style="border: 1px solid black; padding: 2px; display: inline-block;">Line: JREF, IDSCNT</div>		
(Format 2I5)		
<u>Fortran</u>	<u>Definition</u>	<u>Range or Value</u>
JREF	See Section III.C.4	1<JREF<N
IDSCNT	See Section III.C.4	0<IDSCNT<20
<p>* <div style="border: 1px solid black; padding: 2px; display: inline-block;">Line: ID(1), ID(2), ..., ID(16)</div></p>		
(Format 16I5)		
<p>* <div style="border: 1px solid black; padding: 2px; display: inline-block;">Line: ID(17), ..., ID(20)</div></p>		
(Format 4I5)		
} as required		
<u>Fortran</u>	<u>Definition</u>	<u>Range or Value</u>
ID(K),	See Section III.C.4	1<ID(K)<M
K=1, ..., 20		K=1, ..., 20
<p>* <div style="border: 1px solid black; padding: 2px; display: inline-block;">Line: JD(1), JD(2), ..., JD(16)</div></p>		
(Format 16I5)		
<p>* <div style="border: 1px solid black; padding: 2px; display: inline-block;">Line: JD(17), ..., JD(20)</div></p>		
(Format 4I5)		
} as required		
<u>Fortran</u>	<u>Definition</u>	<u>Range or Value</u>
JD(K)	See Section III.C.4	JD(K) = 1 or N
K=1, ..., 20		K=1, ..., 20

\* If IDSCNT = 0, these lines are omitted

TABLE 4. CONT'D

Line: DY00, DY01, DY10, DY11

(Format 4F10.4)

<u>Fortran</u>	<u>Definition</u>	<u>Range or Value</u>
DY00	$y_{1,2} - y_{1,1}$	Units: feet
DY01	$y_{IL,2} - y_{IL,1}$	Units: feet
DY10	$y_{1,JL} - y_{1,JL-1}$	Units: feet
DY11	$y_{IL,JL} - y_{IL,JL-1}$	Units: feet

Line: CC1(1), CC2(1), CC1(M), CC2(M)

(Format 4F10.4)

<u>Fortran</u>	<u>Definition</u>	<u>Range or Value</u>
CC1(1)	Value of C1 at $\zeta = 0$	} From Program BNDRY
CC2(1)	Value of C2 at $\zeta = 0$	
CC1(M)	Value of C1 at $\zeta = 1$	
CC2(M)	Value of C2 at $\zeta = 1$	

Line: SCALE1, SCALE2, SCALE3, SCALE4

(Format 4F10.4)

<u>Fortran</u>	<u>Definition</u>	<u>Range or Value</u>
SCALE1	Provides smooth transition for $T(\zeta, \eta)$ between three regions in equation (2).	0.375
SCALE2	Same as above	0.375
SCALE3	See Section III.C.4	
SCALE4	See Section III.C.4	

TABLE 4. CONT'D

Line: SØ(1), S1(1), CONVER

(Format 3F10.4)

<u>Fortran</u>	<u>Definition</u>	<u>Range or Value</u>
SØ(1)	See Section III.C.4	Units: feet
S1(1)	See Section III.C.4	Units: feet
CONVER	Convergence Criteria (See (28))	See Table 5

\*\* Line: XØ, DX, XH1, DELTAC

(Format: 4F10.4)

<u>Fortran</u>	<u>Definition</u>	<u>Range or Value</u>
XØ	Value of X at upstream boundary of mesh region	Units: feet
DX	Mesh spacing in X-direction	Units: feet
XH1	Height of inlet throat	Units: feet
DELTAC	Cowl angle	Units: Degrees

\*\*This applies to MCAIR inlet (Reference 33)

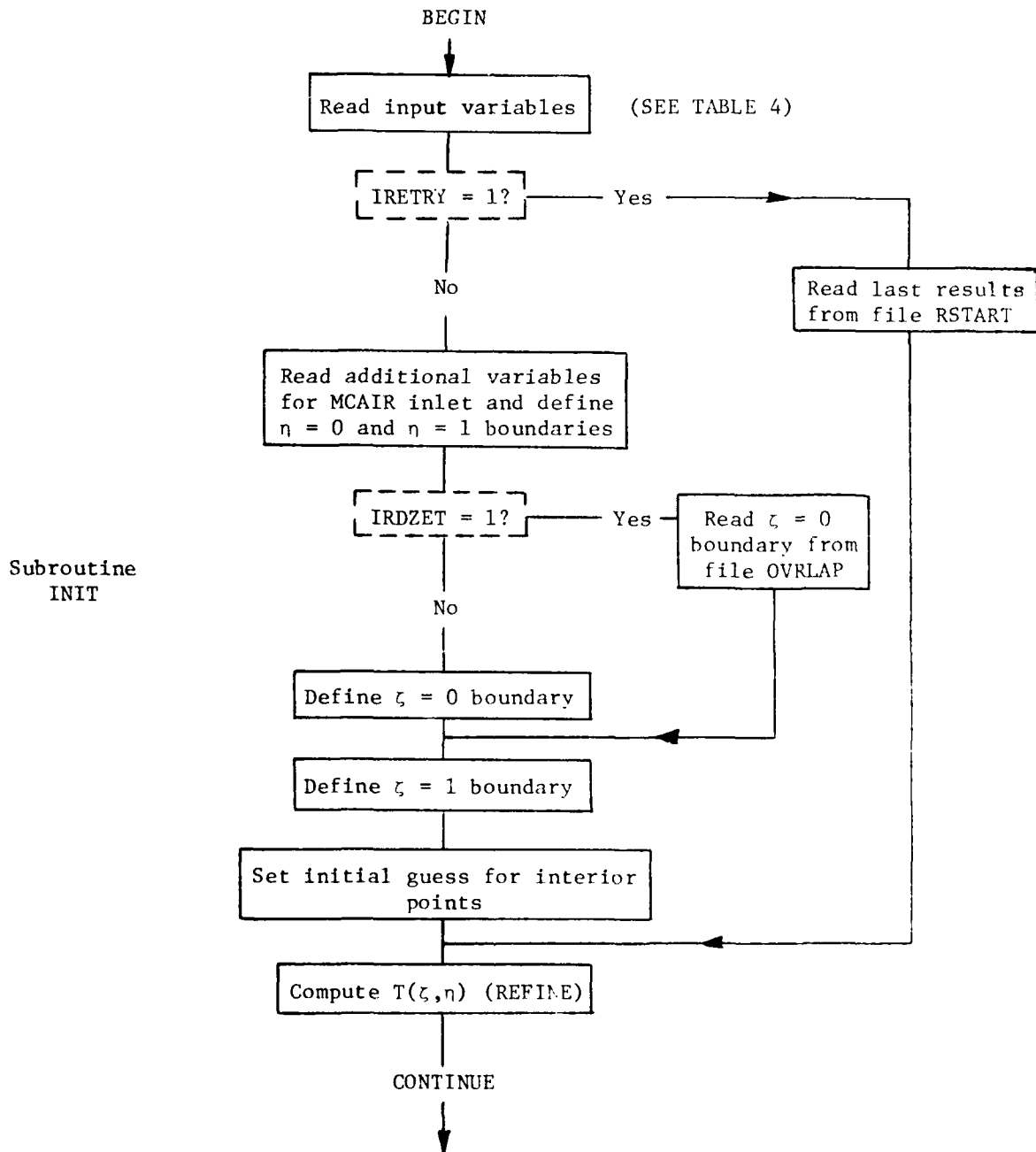
Note that X = 0 at the ramp leading edge for  
the MCAIR inlet.

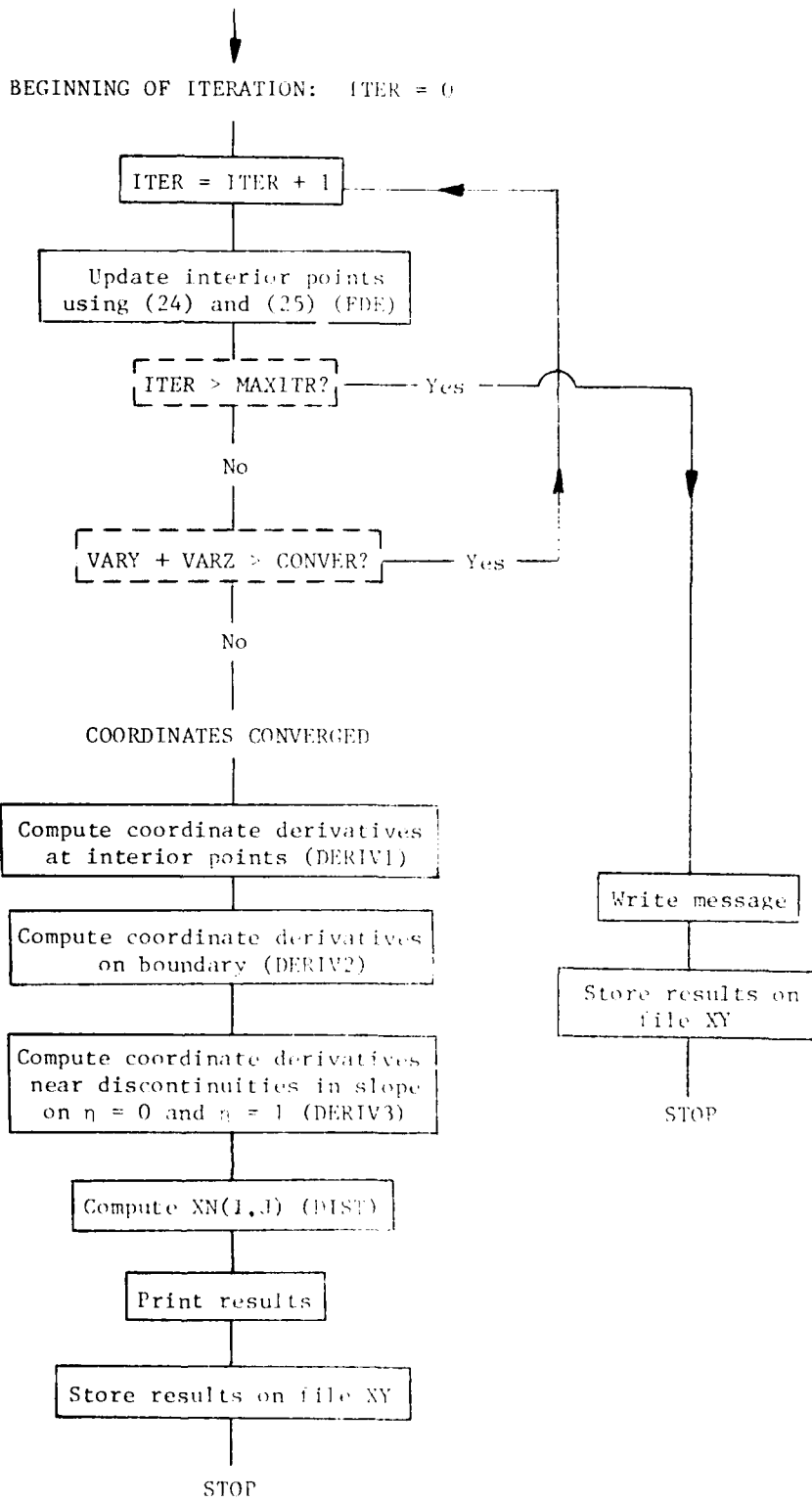
TABLE 5. GUIDELINES FOR INPUT DATA FOR PROGRAM COORD

<u>Parameter(s)</u>	<u>Guideline</u>
J00, J01	Use same value for both, in general, for all overlapping mesh regions (e.g., meshes B and C in Fig. 8)
J10, J11	Same as above
IREF1	Care must be taken that $\xi_{IREF}$ corresponds to same <u>physical</u> location when overlapping mesh regions
IREF2	Same as above
JREF	Same value required for all overlapping mesh regions
IDSCNT, ID(K), JD(K)	Care must be taken to insure that each surface slope discontinuity is always referred to its proper <u>physical</u> location when overlapping mesh regions
DY00, DY10	When overlapping mesh regions, the values of DY00 and DY11 can be obtained from the coordinates of the upstream mesh at the restart station
DY01, DY11	These values are always obtained from program BNDRY
CC1(1), CC2(1)	When overlapping mesh regions, these values can be obtained from the output of the upstream mesh at the restart station
S0(1), S1(1)	These values represent the <u>arc</u> distance along the lower and upper surfaces from the leading edges on the respective surfaces, even though the leading edge does not lie in that particular mesh region.
CONVER	Usual values are $10^{-5}$ or less. Typically, CONVER is 100 to 1000 times smaller than the smallest mesh spacing in feet in either $\xi$ or $\eta$ direction.

### 3. Flow Chart

The flow chart for program COORD is indicated below. The names of the subroutines called are shown by capital letters in parentheses.





#### 4. Source Code Notation

The definition of the pertinent source code variables is given below. For any array, the index I is equivalent to the subscript i (e.g., the Fortran variable ZETA(I) is equivalent to  $\zeta_i$  in that ZETA(1) =  $\zeta_1$ , ZETA(2) =  $\zeta_2$ , etc.) and the index J refers to the subscript j.

<u>Fortran</u>	<u>Definition</u>
CC1(I)	Value of $C_1$ at $\zeta_i$ (see (2) and Note 1*)
CC2(I)	Value of $C_2$ at $\zeta_i$ (see (2) and Note 1)
CONVER	Convergence criteria (see (28))
DELTA C	Cowl angle for MCAIR inlet (in degrees)
DX	Mesh spacing in x-direction (in feet)
DY00	Value of $y_{1,2} - y_{1,1}$ (in feet)
DY01	Value of $y_{IL,2} - y_{IL,1}$ (in feet)
DY10	Value of $y_{1,JL} - y_{1,JL-1}$ (in feet)
DY11	Value of $y_{IL,JL} - y_{IL,JL-1}$ (in feet)
EDA(J)	$\eta_j$
H	$\Delta \zeta$
HH	$(\Delta \zeta)^2$
ID(K), JD(K)	Denote locations on the lower and upper boundaries where surface slope is discontinuous. Denoting ID(K) by $\ell$ and JD(K) by $m$ , the $K^{\text{th}}$ discontinuity lies <u>between</u> $\zeta_\ell$ and $\zeta_{\ell+1}$ on the line $\eta_m$ . A maximum of 20 discontinuities is allowed. The discontinuities may be listed in any order. See Note 2.
IDSCNT	Total number of discontinuities in surface slope on lower and upper boundaries (maximum: 20). Corners are not included. If there are no discontinuities, set IDSCNT = 0.

IOVLP Used in generating overlapping mesh regions, such as regions B and C in Figure 8. The curve  $\zeta = \zeta_{IOVLP}$  of the upstream mesh is taken to represent the  $\zeta = 0$  boundary of the downstream mesh.

IREF1 In conjunction with the quantity SCALE3, this term defines the streamwise extent over which the height of the first row of ordinary mesh points above the lower surface (i.e.,  $y_{i,2} - y_{i,1}$ ) changes from DY00 to DY01. See Note 3.

IREF2 In conjunction with the quantity SCALE4, this term defines the streamwise extent over which the distance of the first row of ordinary mesh points below the upper surface (i.e.,  $y_{i,JL} - y_{i,JL-1}$ ) changes from DY10 to DY11. See Note 3.

IRDZET Used in generating overlapping mesh regions. If IRDZET equals 1, the upstream mesh is read in order to define the  $\zeta = 0$  boundary of the downstream mesh. If mesh overlapping is not to be performed, set IRDZET equal to 0.

IRETRY Used to continue iterating a mesh that did not converge in the previously specified number of iterations. If IRETRY equals 1, the last results are read and the iteration continued. If this restart feature is not desired, set IRETRY equal to 0.

ITER Denotes iteration number during the course of the calculation.

JREF Used in defining array XN(I,J) (see below). For  $J \leq JREF$ , the quantity XN(I,J) is the normal distance of the point  $(x_{i,j}, y_{i,j})$  above  $\eta = 0$ . For  $J > JREF$ , the quantity XN(I,J) is the normal distance of  $(x_{i,j}, y_{i,j})$  from  $\eta = 1$ .  
 Note: In utilizing program INLET, it is imperative that the following be observed:  
 $JREF0 = JREF$   
 $JREF1 = JREF$   
 where JREF0 and JREF1 are variables defined in program INLET.

J00 Defines value of  $\eta_1$  at  $\zeta = 0$  (see (2)) through  $\eta_1 = (J00-1)/(JL-1)$

J01 Defines  $\eta_1$  at  $\zeta = 1$

J10 Defines  $\eta_2$  at  $\zeta = 0$  through  $\eta_2 = (J10-1)/(JL-1)$

J11 Defines  $\eta_2$  at  $\zeta = 1$

K	$\Delta\eta$
KK	$(\Delta\eta)^2$
M	Number of points in $\zeta$ -direction (i.e., IL). Maximum: 40
MI	M - 1
MAXITR	Maximum number of iterations of algorithm (24). See IRETRY.
N	Number of points in $\eta$ -direction (i.e., JL). Maximum: 48
NI	N - 1
SØ(I)	Distance of $i^{\text{th}}$ point on $\eta = 0$ from leading edge of lower surface (in feet). Negative values imply points ahead of leading edge. The distance is measured along the $\eta = 0$ curve (not necessarily the x-direction). Note that the value of SØ(I) is positive if the $\zeta = 0$ boundary of a particular mesh region lies downstream of the leading edge of the lower surface.
S1(I)	Same as above, except refers to the upper surface.
SCALE1,SCALE2	Provides smooth transition for T( $\zeta,\eta$ ) between the three regions in equation (2). Typical value is 0.374 for each.
SCALE3,SCALE4	See IREF1, IREF2 and Note 2
T(I,J)	T( $\zeta_i,\eta_j$ ) (see (2))
TRAN(I,J,1)	$\zeta_{x_{i,j}}$ (ZETAX(I,J); units: $\text{ft}^{-1}$ )
TRAN(I,J,2)	$\zeta_{y_{i,j}}$ (ZETAY(I,J); units: $\text{ft}^{-1}$ )
TRAN(I,J,3)	$\eta_{x_{i,j}}$ (ETAX(I,J); units: $\text{ft}^{-1}$ )
TRAN(I,J,4)	$\eta_{y_{i,j}}$ (ETAY(I,J); units: $\text{ft}^{-1}$ )
VARY	Maximum value of $r_{x_{i,j}}$ (see (27))
VARZ	Maximum value of $r_{y_{i,j}}$ (see (27))
X(I,J)	$x_{i,j}$ (in feet)



## 5. File Structure

The program employs, in general, three files in addition to the conventional files INPUT and OUTPUT. The descriptions are indicated below.

<u>File</u>	<u>Description</u>	<u>Data Structure</u>
XY	Output file for coordinate transformation results	a) Convergence achieved: X, Y, ZETAX, ZETAY, ETAX, ETAY, XN, S0, S1 b) Convergence not achieved: X, Y
OVRLAP	Input file for coordinate transformation for upstream region. Used in generating overlapping meshes	Same as a) above
RSTART	Input file for non-converged results	X, Y

The data are written unformatted in the sequence indicated, with all variables except S0 and S1 having array size 40 by 48. The arrays S0 and S1 are each of size 40. The data sequence for file XY is thus X(1,1), X(2,1), ..., X(40,1), X(1,2), X(2,2), ..., X(40,2), ..., Y(1,1), Y(1,2), ..., etc. The utilization of the files is as follows:

<u>File</u>	<u>Type</u>	<u>Utilized</u>
XY	Output	Required for every code execution
OVRLAP	Input	Required only if IRDZET = 1
RSTART	Input	Required only if IRETRY = 1

## 6. Sample Calculation: Upstream Inlet Region for MCAIR Case 35

In Figure 11a, the coordinate system for the upstream inlet region of MCAIR Case 35 is shown (only odd-numbered  $\eta$ -lines are shown). The configuration is also indicated in Figure 9. The input data is indicated in Table 6 and the input variables are explained in Table 4 and Section III.C.4.

It is instructive to note how the preliminary analysis for the upstream inlet region is used in the input to program COORD, recalling the discussion of Section III.A. The two major areas of the preliminary analysis are discussed below:

### a) Streamwise mesh spacing

The chosen value of  $\Delta x = 0.25$  in. = .0208 ft, and appears as DX in line 10.

### b) Boundary Layer mesh spacing

The results of the analysis and program BNDRY indicate  $J1 = 28$ ,  $J11 = 28$ ,  $C1 = 2.89068$  and  $C2 = 2.87725$  on the upstream boundary. These values are input as  $J00$ ,  $J10$ ,  $CC1(1)$  and  $CC(1)$ , respectively. A second analysis (not detailed in this report) yielded  $J11 = 28$ ,  $J11 = 28$ ,  $CC1(M) = 2.75649$  and  $CC2(M) = 2.74370$ . These values appear on lines 2 and 7.

The preliminary analysis also indicates that  $y'_m = 5 \times 10^{-4}$  ft at the upstream boundary on the ramp and cowl (i.e.,  $DY00 = DY10 = .0005$ ) and  $y'_m = 2.5 \times 10^{-4}$  ft at the downstream boundary on the ramp and cowl (i.e.,  $DY10 = DY11 = .00025$ ). This appears on line 6.

As discussed in note 3 of Section III.C.4, a value of 1.51 for SCALE3 and SCALE4 is typical (line 8). As indicated in Section III.A.3, it is desired for  $y'_m$  to decrease from  $5.0 \times 10^{-4}$  to  $2.5 \times 10^{-4}$  ft in the vicinity of  $X = 19.5$  inch on both the ramp and cowl.

TABLE 6. INPUT DATA FOR COORDINATE SYSTEM OF  
UPSTREAM INLET REGION (MCAIR CASE 35)

Line 1 (Format 6I5)	M	N	MAXITR	IRDZET	IOVLP	IRETRY
	40	48	1000	0	0	0
Line 2 (Format 6I5)	J00	J01	J10	J11	IREF1	IREF2
	18	18	28	28	23	23
Line 3 (Format 2I5)	JREF		IDSCNT			
	28		1			
Line 4 (Format 16I5)	ID(1)					
	5					
Line 5 (Format 16I5)	JD(1)					
	48					
Line 6 (Format 4F10.4)		DY00	DY01	DY10		DY11
		.0005	.00025	.0005		.00025
Line 7 (Format 4F10.4)		CC1(1)	CC2(1)	CC1(M)		CC2(M)
		2.89068	2.87725	2.75649		2.74370
Line 8 (Format 4F10.4)		SCALE1	SCALE2	SCALE3		SCALE4
		0.374	0.374	1.5		1.5
Line 9 (Format 3F10.4)		S0(1)	S1(1)	CONVER		
		1.156	-.093	.000001		
Line 10 (Format 4F10.4)		X0	DX	XH1		DELTAC
		1.156	.020833	.06650		7.79

Noting that the upstream boundary is at  $x = 13.88$  inch (Figure 9) and the streamwise mesh spacing is 0.25 inch, we conclude that the station  $x = 19.5$  inch is midway between the stations  $I = 23$  and  $I = 24$ . Thus, we take  $IREF1 = IREF2 = 23$  (line 2).

In the following, each of the data input lines in Table 6 is described.

a) Line 1

A mesh of 40 points by 48 points ( $M = 40$ ,  $N = 48$ ) is chosen. The maximum number of iterations permitted is  $MAXITR = 1000$ . The upstream boundary is at the inlet entrance, and thus there is no need to read a prior coordinate system ( $IRDZET = 0$ ,  $IOVLP = 0$ ). This job represents the initial attempt to solve equations (22), and thus  $IRETRY = 0$  (the equations (24) will converge in this case is less than 1000 iterations).

b) Line 2

The choice of the values for the variables in this line were discussed previously.

c) Line 3

The value of  $JREF$  is chosen to insure that  $v_{i,JREF}$  ( $i = 1, \dots, M$ ) always lies between the ramp and cowl boundary layers. Based on Figures 9 and 10, we choose  $JREF = 28$ . We also note from Figure 11a that there is only one discontinuity on the lower and upper boundary, namely at the cowl leading edge; thus  $1DSCNT = 1$ .

d) Lines 4 and 5

From Figure 9 and the chosen value of  $\Delta x = 0.25$  inch, we note that the cowl leading edge discontinuity lies on the upper surface ( $j = N = 48$ ) between the fifth and sixth vertical coordinate line (i.e., between  $i = 5$  and  $i = 6$ ). Therefore, we choose  $ID(1) = 5$  and  $JD(1) = 48$ .

e) Lines 6, 7 and 8

The choice of the values for the variables in these lines were discussed previously.

f) Line 9

As indicated in Figure 9, the mesh point  $(i,j) = (1,1)$  is located at 13.88 inch (1.156 ft) from ramp leading edge; thus  $S0(1) = 1.156$ . Similarly, the cowl leading edge is 1.12 inch (.093 ft) downstream of the mesh point  $(i,j) = (1,48)$  and thus  $S1(1) = -.093$ . As indicated in equation (28) and Table 5, we choose  $CONVER = .000001$ .

g) Line 10

As indicated in Figure 9,  $X0$  is 1.156 ft. Furthermore,  $\Delta x = .25$  inch (.020833 ft), thus  $DX = .020833$ . The throat height of the inlet is .798 inch (.0665 ft), thus  $XH1 = .0665$ . The cowl angle  $\delta_c$  is 7.97 degrees, thus  $DELTA C = 7.97$ .

#### 7. Sample Calculation: Downstream Inlet Region for MCAIR Case 35

In Figure 11b, the coordinate system for the downstream inlet region of MCAIR Case 35 is shown (only odd-numbered  $\eta$ -lines are shown). The upstream boundary of this region corresponds to the  $i = 31$  station of Figure 11a. The input data is indicated in Table 7, and is explained below:

a) Line 1

A mesh of 40 points by 48 points ( $M = 40$ ,  $N = 48$ ) is chosen. The maximum number of iterations permitted is  $MAXITR = 1000$ . Since the downstream region overlaps the upstream region (with  $i = 1$  in the downstream region chosen to be coincident with  $i = 31$  of the upstream region, i.e.,  $IOVLP = 31$ ), the upstream coordinate transformation data must be read from file `OVRLAP` and thus  $IRDZET = 1$ . This

TABLE 7. INPUT DATA FOR COORDINATE SYSTEM OF  
DOWNSTREAM INLET REGION (MCAIR CASE 35)

Line 1	M	N	MAXITR	IRDZET	IOVLP	IRETRY
(Format 6I5)	40	48	1000	1	31	0
Line 2	J00	J01	J10	J11	IREF1	IREF2
(Format 6I5)	18	18	28	28	20	20
Line 3	JREF	IDS CNT				
(Format 2I5)	28	3				
Line 4	ID(1)	ID(2)	ID(3)			
(Format 16I5)	36	15	33			
Line 5	JD(1)	JD(2)	JD(3)			
(Format 16I5)	1	48	48			
Line 6	DY00	DY01	DY10	DY11		
(Format 4F10.4)	.0002476	.00025	.0002532	.00025		
Line 7	CC1(1)	CC2(1)	CC1(M)	CC2(M)		
(Format 4F10.4)	3.101	3.984	2.83529	2.82212		
Line 8	SCALE1	SCALE2	SCALE3	SCALE4		
(Format 4F10.4)	.374	.374	1.5	1.5		
Line 9	S0(1)	S1(1)	CONVER			
(Format 3F10.4)	1.78125	.5705	.000001			
Line 10	X0	DX	XH1	DELTAC		
(Format 4F10.4)	1.78125	.020833	.06650	7.97		

job is the initial attempt to solve equations (22) in the downstream region, and thus IRETRY = 0 (the equations (24) will converge in this case in less than 1000 iteration).

b) Line 2

The values of  $J\emptyset\emptyset$  and  $J1\emptyset$  (defining  $\eta_1$  and  $\eta_2$  at  $i = 1$ ) are chosen identical to the values used in the upstream region ( $J\emptyset\emptyset = 18$ ,  $J1\emptyset = 28$ ). A preliminary analysis (not contained in this report), similar to that described in Section III.A.3, together with program BNDRY indicates that  $J1\emptyset = 18$  and  $J11 = 28$ . Furthermore, this analysis indicates  $DY\emptyset1 = DY11 = .00025$  ft, which implies that  $y'_m$  is essentially unchanged on the ramp and cowl (see line 6). Thus, the values of IREF1 and IREF2 are irrelevant. They are arbitrarily chosen to be equal to 20.

c) Line 3

The value JREF = 28 is again found to be satisfactory. There are three discontinuities (see Figure 11b), and thus IDSCNT = 3.

d) Lines 4, 5

The discontinuities are located immediately downstream of the following points:  $(i,j) = (36,1)$ ,  $(i,j) = (15,48)$ , and  $(i,j) = (33,48)$ . Thus,  $ID(1) = 36$ ,  $JD(1) = 1$ ,  $ID(2) = 15$ ,  $JD(2) = 48$ ,  $ID(3) = 33$  and  $JD(3) = 48$ .

e) Line 6

The value of  $DY\emptyset\emptyset$  is equal to  $Y_{31,2} - Y_{31,1}$  in the upstream region. From the output from the upstream region (see Figure 12b), we note that  $Y_{31,2} - Y_{31,1} = .0002478$ . Similarly,  $DY\emptyset1$  is equal to  $Y_{31,48} - Y_{31,47}$  which from the output is equal to .00025. A

preliminary analysis (not contained in this report) indicates

$y'_m = 2.5 \times 10^{-4}$  ft. is satisfactory at  $i = 40$ , and thus  $DY10 = DY11 = .00025$ .

f) Line 7

The values of  $CC1(1)$  and  $CC2(1)$  correspond to the values of  $C1$  and  $C2$  at  $i = 31$  in the upstream region. From the output (see Figure 12a),  $CC1(1) = 3.101$  and  $CC2(1) = 3.084$ . An analysis of the downstream boundary using  $BNDRY$  (not contained in this report) indicates  $CC1(M) = 2.83529$  and  $CC2(M) = 2.82212$ .

g) Line 8

The values of  $SCALE1$  and  $SCALE2$  are chosen as before. Since  $y'_m$  is essentially uncharged on the ramp and cowl,  $SCALE3$  and  $SCALE4$  are irrelevant and are arbitrarily taken to be equal to 1.5.

h) Line 9

The upstream boundary (coincident with  $i = 31$  of the upstream region) is located at  $x = 21.38$  inch = 1.78125 ft., thus  $S0(1) = 1.78125$ . At the upstream boundary on the ramp, the mesh point  $(i,j) = (1,48)$  is a distance of 6.44 inch = .53705 ft. along the cowl from the cowl leading edge and thus  $S1(1) = .53705$ . The value of  $CONVER$  is same as previously used.

i) Line 10

The upstream boundary is located at 21.38 inch = 1.78125 ft. from the ramp leading edge, thus  $X0 = 1.78125$ . The remaining variables are identical to their previous values. A preliminary analysis indicates  $\Delta x = .25$  inch = .020833 ft. is satisfactory, and thus  $DX = .020833$ .

8. Sample Output: Upstream Inlet Region for MCAIR Case 35

The output from the program is illustrated in Figures 12a through 12e, where sample of each major section of output for the upstream inlet region of MCAIR Case 35 are given. In Figure 12a, the values of the input data are printed, together with the computed values of  $CC1(I)$ ,  $I = 1, \dots, M$  and  $CC2(I)$ ,  $I = 1, \dots, M$ , where the index  $I$  increases from left to right along each row of output. In Figure 12b, a portion of the computed values of the coordinates  $x_{ij}$ ,  $y_{i,j}$  are shown. The values of the coordinate pair  $(x_{i,j}, y_{i,j})$  in feet are given at each value of  $\eta$  (i.e., at each value of  $j$ ) in a sequential manner. For each value of  $\eta$ , the index  $i$  increases from left to right along each row of output. The coordinate transformation derivatives appear next, as illustrated in Figure 12c, where the results for  $\zeta_{x_{i,j}}$  are shown. Again, for each value of  $\eta$ , the quantity  $\zeta_{x_{i,j}}$  is listed, with the index  $i$  increasing from left to right along each row of output. Similarly, the results for  $\zeta_y$ ,  $\eta_x$  and  $\eta_y$  are printed. In Figure 12d, the results for  $XN(I,J)$  are shown for  $J \leq JREF$  in the same manner. These are followed by  $XN(I,J)$  for  $J > JREF$  (not shown). Finally, the distance along the lower and upper boundaries (i.e.,  $S0$  and  $S1$ ) are displayed as in Figure 12e.

In calculations involving overlapping, the message "RM ERROR 0142 on line OVERLAP" will appear in the dayfile. This message is of no significance, and may be ignored.

SECTION IV  
CALCULATION OF INLET FLOWFIELD

A. Introduction

The program INLET is employed to compute the inlet flowfield. Prior to execution of this program, the coordinate transformation must be calculated as discussed in Section III.

The following table provides information on the resources required to execute program INLET on the CYBER 175.

TABLE 8. RESOURCES REQUIRED FOR EXECUTION  
OF PROGRAM INLET

<u>Resource</u>	<u>Details</u>
Computer time	See discussion below
Input/Output time	< 60 seconds (typical)
Core Memory	225,000 words (octal)
Files required	INPUT, OUTPUT, RSTART, STORE, XY (See Section IV.F)

Because the total execution time required to obtain a converged solution within a given mesh region is typically tens of minutes to an hour, the most efficient approach is to submit a sequence of computer jobs. Each job reads in the most recent results for the flow variables, integrates the equations of motion for a number of time steps (see ITER) and then stores the results on file. This procedure is repeated until a converged solution is obtained. Due to the nature of the code, the computer time per time step may vary considerably for a given mesh during the course of a calculation. Typical values are 10 to 20 seconds per time step on the CYBER 175 for a high speed inlet with a 40 by 48 grid. The code incorporates a timer, which automatically determines at each time step whether the remaining computer time is sufficient for continued execution. If sufficient time does not remain, the integration

is terminated and the results written on file for continued execution by the next job. Thus, no job can run out of computer time.

#### B. Description of Input Variables

The input to program INLET consists of a variable number of cards. The definition and format of the input data is indicated in the required order in Table 9. Additional information is provided in Section IV.D. Useful guidelines for the selection of certain input parameters are provided in Table 10.

TABLE 9. INPUT DATA FOR PROGRAM INLET

Line 1: UINF, PINF, XMINF, CFL, ALPHA, BETA, TMAX

(Format 7F10.8)

<u>Fortran</u>	<u>Definition</u>	<u>Range or Value</u>
UNIF	$U_{\infty}$	Units: ft/sec
PINF	$P_{\infty}$	Units: lbf/ft <sup>2</sup>
XMINF	$M_{\infty}$	
CFL	Courant-Freidrichs-Lewy number	$0 < CFL < 1$
ALPHA	$\alpha$	$0 \leq \alpha \leq 5$
BETA	$\beta$	See Section IV.D
TMAX	CP time requested on job card	Units: seconds

Line 2: XLMBDA(1), XLMBDA(2), PDOWN, SREF(1), SREF(2)

(Format: 5F10.8)

<u>Fortran</u>	<u>Definition</u>	<u>Range or Value</u>
XLMBDA(1)	$\lambda$ on $\eta = 0$	Units: feet
XLMBDA(2)	$\lambda$ on $\eta = 1$	Units: feet
PDOWN	static pressure at $\zeta = 1$	Units: lbf/ft <sup>2</sup>
SREF(1)	$s_o$ for $\eta = 0$ boundary layer (see (17))	Units: feet
SREF(2)	$s_o$ for $\eta = 1$ boundary layer (see (17))	Units: feet

TABLE 9. CONT'D

Line 3:	IL, JL, ITER, ILE(1), ILE(2), JSL0, JSL1
---------	--

(Format 7I5)

<u>Fortran</u>	<u>Definition</u>	<u>Range or Value</u>
IL	Number of points in $\zeta$ -direction	$\leq 40$
JL	Number of points in $\eta$ -direction	$\leq 48$
ITER	Number of time steps	$\geq 0$
ILE(1)	Value of $i$ at leading edge on $\eta = 0$	$1 \leq \text{ILE}(1) \leq \text{IL}$
ILE(2)	Same as above for $\eta = 1$	Same as above
JSL0	Number of points in CSL on $\eta = 0$	$3 \leq \text{JSL0} \leq 20$
JSL1	Same as above for $\eta = 1$	$3 \leq \text{JSL1} \leq 20$

Line 4:	JREF0, JREF1, IDAMP1, IDAMP2, ISTART, IPRINT
---------	--

(Format 6I5)

<u>Fortran</u>	<u>Definition</u>	<u>Range or Value</u>
JREF0	See Section IV.D	
JREF1	See Section IV.D	
IDAMP1	See Section IV.D	0 or 1
IDAMP2	See Section IV.D	0 or 1
ISTART	See Section IV.D	0, 1 or 2
IPRINT	Flow data printed every IPRINT steps	$\geq 1$

TABLE 9. CONT'D

Line 5: ITNS(1), ITNS(2), ITNE(1), ITNE(2), IOVLP, IPDOWN

(Format 61.)

<u>Fortran</u>	<u>Definition</u>	<u>Range or Value</u>
ITNS(1)	Value of $i$ at start of transition on $\eta = 0$	$1 \leq \text{ITNS}(1) \leq \text{IL}$
ITNS(2)	Same as above for $\eta = 1$	Same as above
ITNE(1)	Value of $i$ at end of transition on $\eta = 0$	Same as above
ITNE(2)	Same as above for $\eta = 1$	Same as above
IOVLP	See Section IV.D	
IPDOWN	See Section IV.D	0 or 1

Lines: XMDOT(1,1), ..., XMDOT(7,1)  
 ... (as required)  
 (Format 7F10.8)

Lines: XMDOT(1,2), ..., XMDOT(7,2)  
 ... (as required)  
 (Format 7F10.8)

<u>Fortran</u>	<u>Definition</u>	<u>Range or Value</u>
XMDOT(I,1), I = 1, ..., IL	$\dot{m}$ on $\eta = 0$	Units: slugs/ft <sup>2</sup> -sec
XMDOT(I,2), I = 1, ..., IL	$\dot{m}$ on $\eta = 1$	Same as above

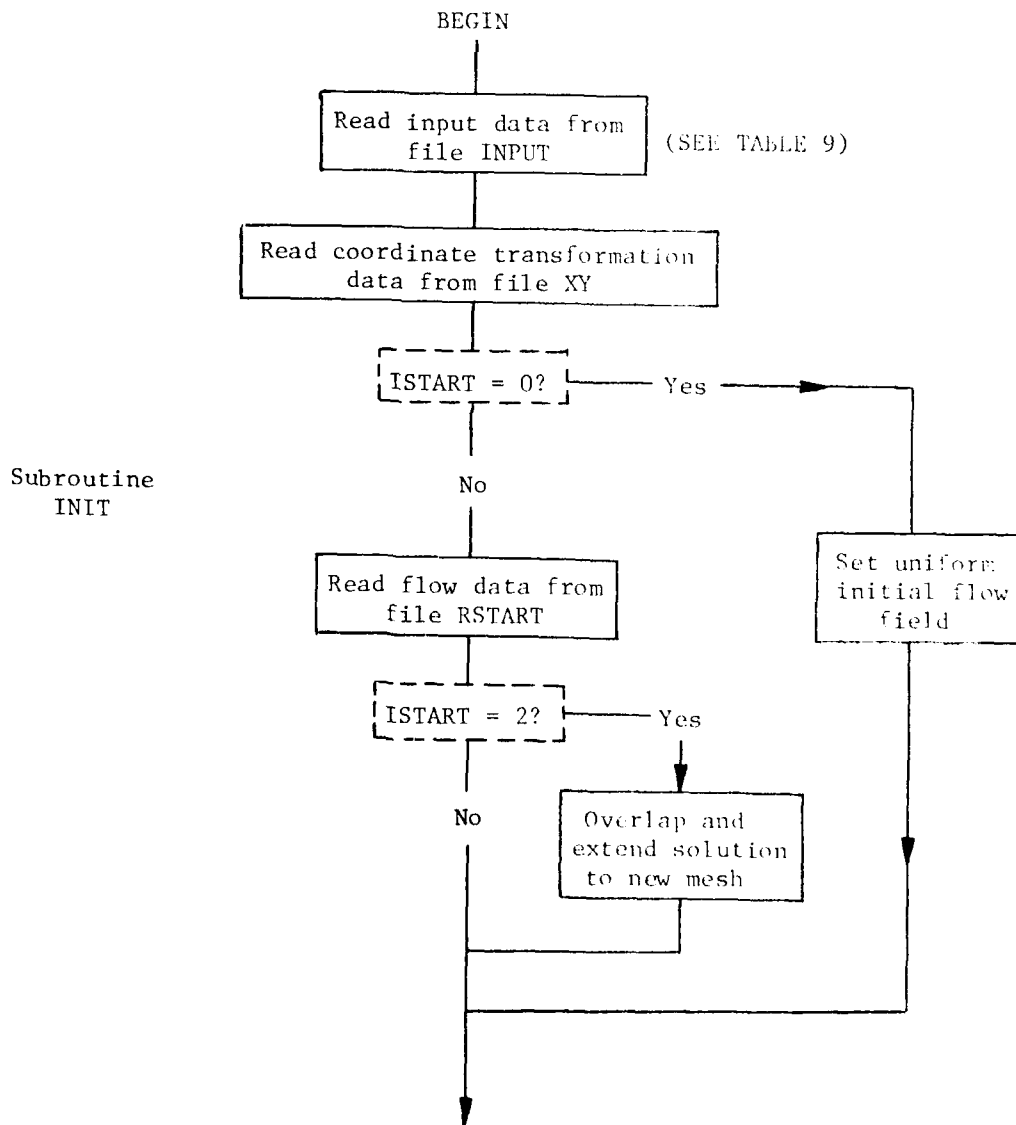
TABLE 10. GUIDELINES FOR INPUT DATA FOR PROGRAM INLET

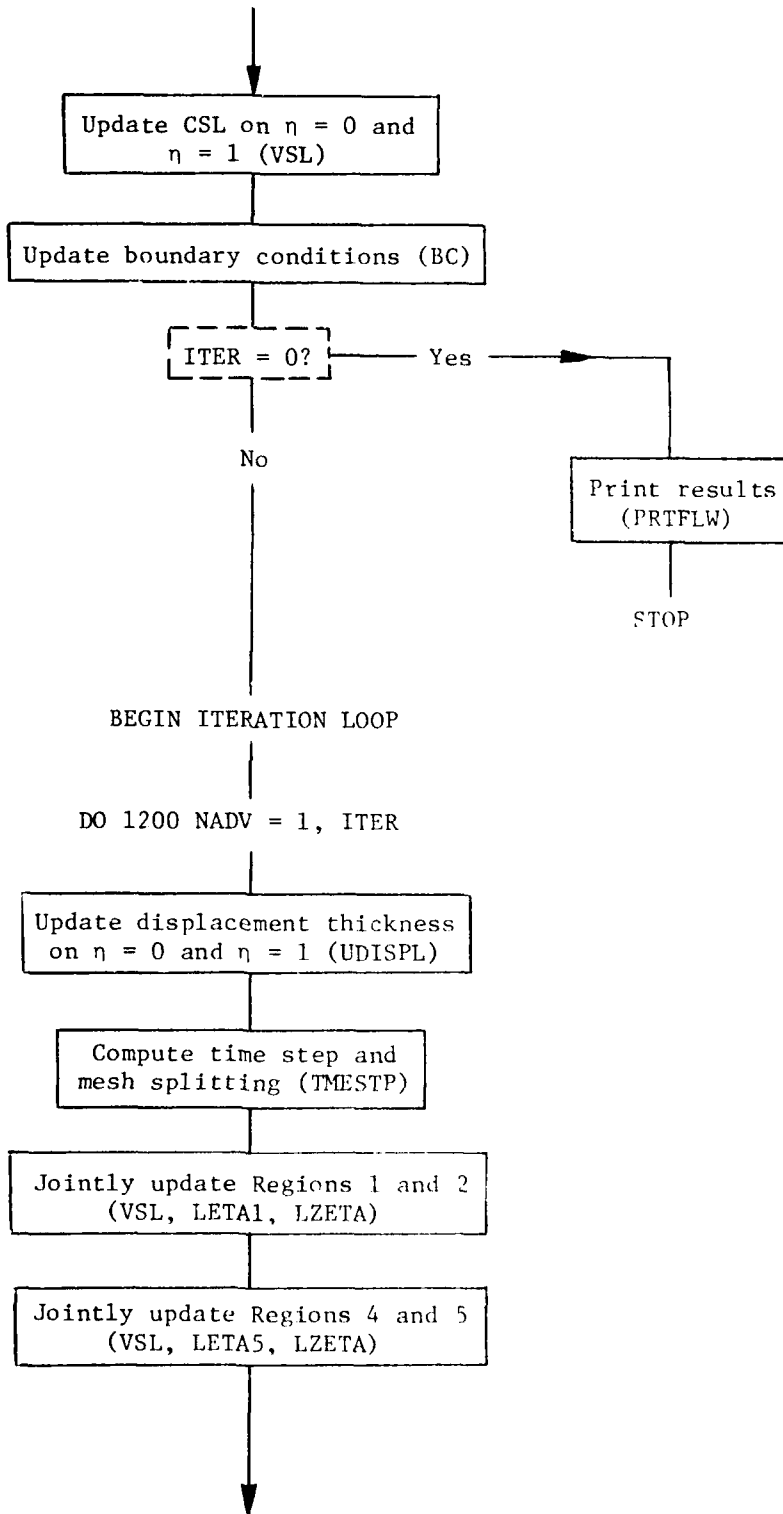
<u>Parameter(s)</u>	<u>Guideline</u>
UINF, PINF, XMINF	These quantities are the freestream values ahead of the inlet entrance.
CFL	Typically, a value of 0.9 is satisfactory. Occurrence of numerical instability (manifested by arithmetic overflow error messages) can often be cured by restarting the calculation and using a smaller value of CFL, although code efficiency is thereby decreased.
ALPHA	The pressure-damping term (55), (56) prevents numerical instability in the presence of shock waves and eliminates unphysical "wiggles" in the pressure therein. A value of $\alpha = 5.0$ is typical. Too high a value of $\alpha$ can cause numerical instability.
BETA	Must be used only to control transients if necessary. Over at least several $t_c$ (see (57)), $\beta$ must equal 1.
XLMBDA(1), XLMBDA(2)	When experimental values for $\delta_0$ in (17) are not available, the calculation can be run awhile with no relaxation until a good estimate for $\delta_0$ is obtained. If relaxation is not used, set both parameters equal to 1.
PDOWN	See Note 5 in Section IV.D. If IPDOWN = 0, set PDOWN = 0.
SREF(1), SREF(2)	For no relaxation, set SREF(1) and SREF(2) equal to anything greater than S(IL,1) and S(IL,2), respectively (e.g., 999). For relaxation, set SREF equal to <u>arc distance</u> at which relaxation begins.
ILE(K)	See Note 1 in Section IV.D.
JSL $\emptyset$ , JSL1	See Note 4 in Section IV.D.
JREF $\emptyset$ , JREF1	See Note 3 in Section IV.D.
ITNS(K), ITNE(K)	See Note 2 in Section IV.D.
IOVLP	If not overlapping, set IOVLP = 0.
IPDOWN	See Note 5 in Section IV.D.
XMDOT(I,K)	See Note 7 in Section IV.D.

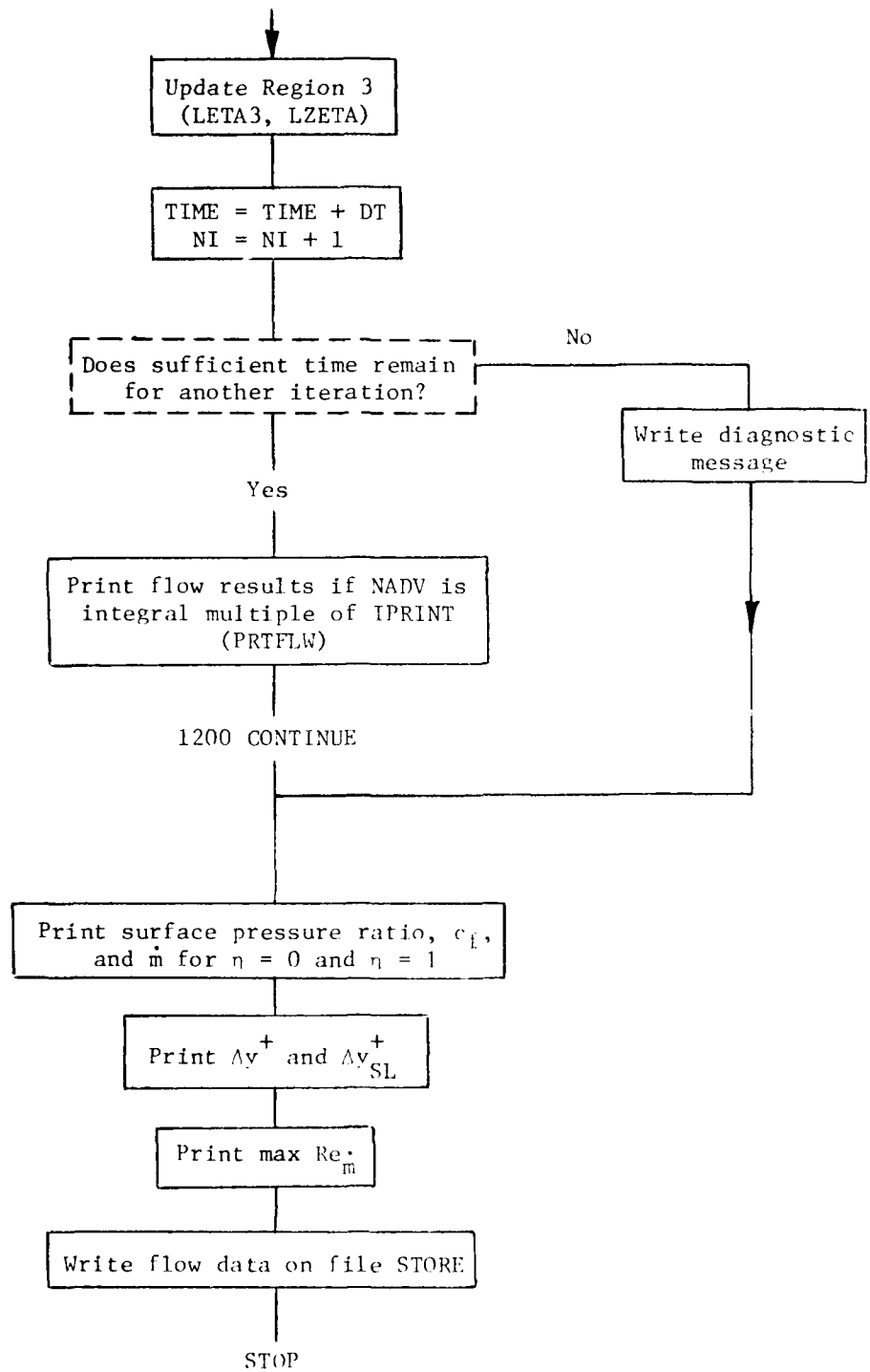
C. Flow Charts

1. Overall Program

The pertinent features of the overall program INLET are indicated below. The names of the subroutines called are indicated in capital letters in parentheses. CSL refers to computational sublayer.

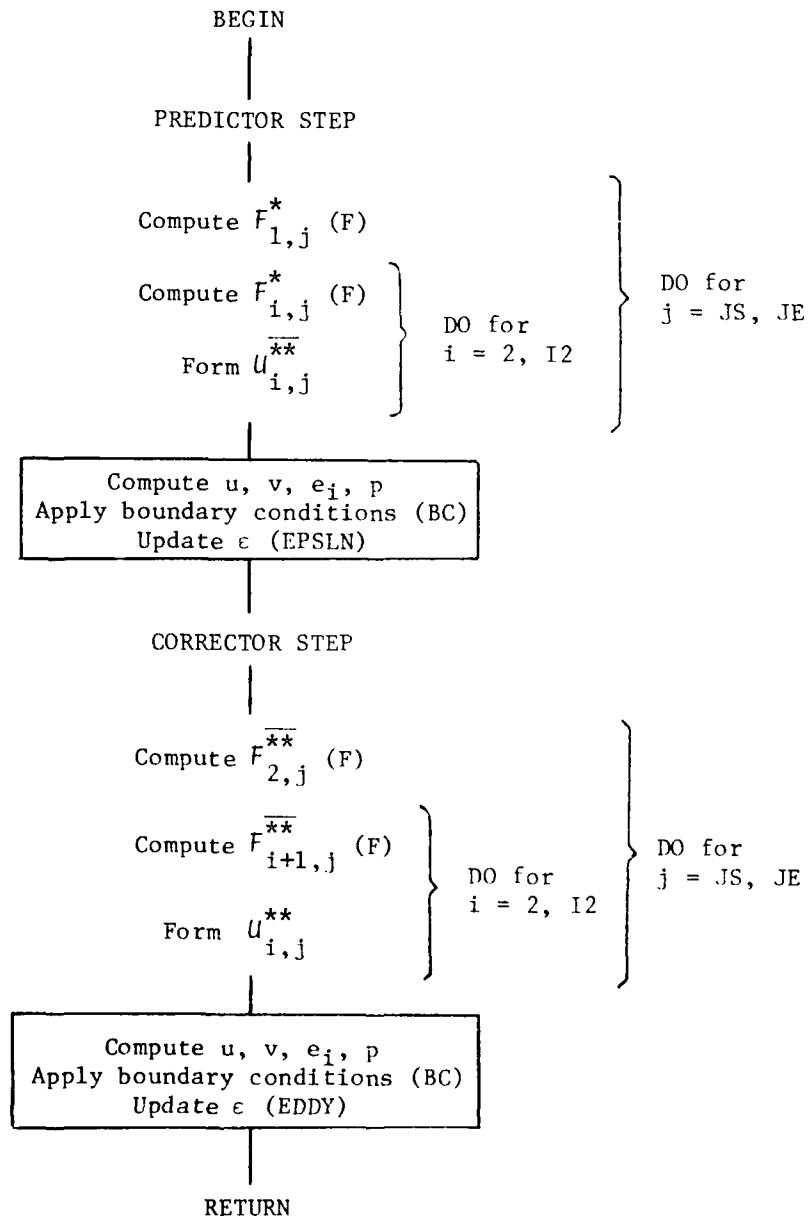






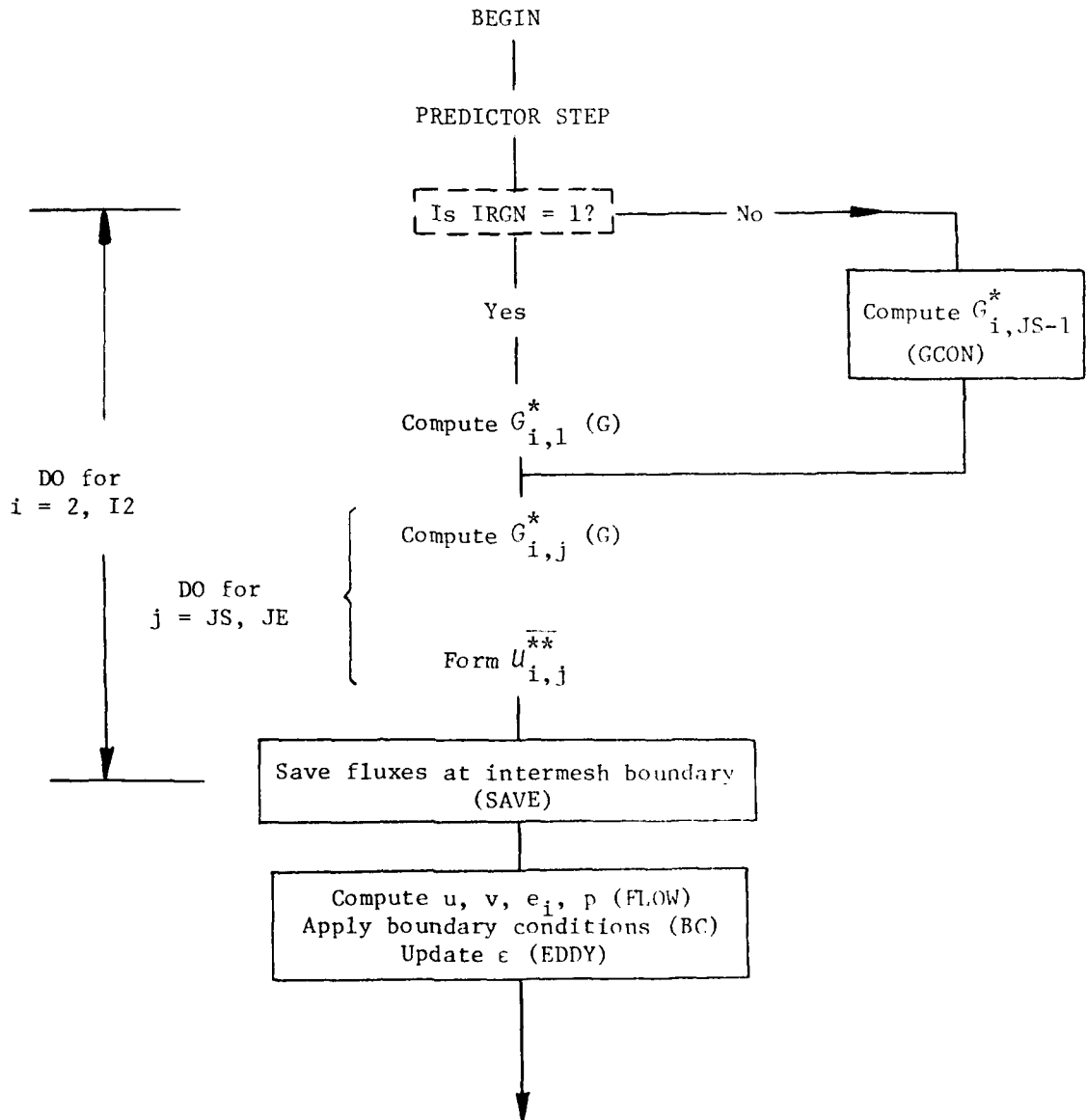
2.  $L_{\zeta}$  Operator (subroutine LZETA)

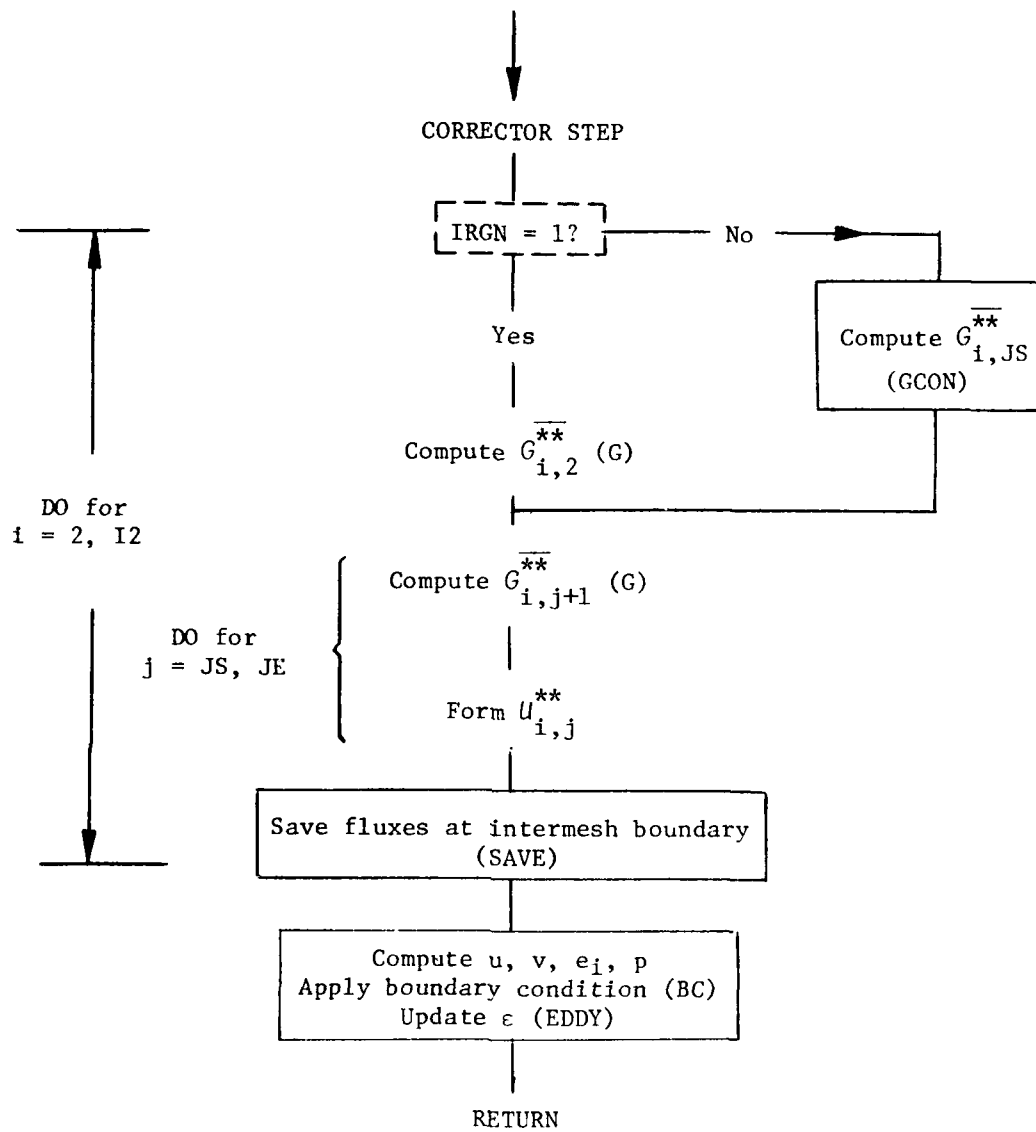
For each region, the  $L_{\zeta}$  operator is applied to a domain defined by  $2 \leq i \leq IL - 1 = I2$ ,  $JS \leq j \leq JE$ . The pertinent features are indicated below.



3.  $L_{\eta}$  Operator for Regions 1 and 2 (subroutine LETA1)

The  $L_{\eta}$  operator is applied to a domain given by  $2 \leq i \leq IL - 1 = I2$ ,  $JS \leq j \leq JE$ . The pertinent features of the  $L_{\eta}$  operator for Regions 1 and 2 are indicated below. The  $L_{\eta}$  operator for the other regions is very similar and consequently is not detailed separately.





#### D. Source Code Notation

The definition of the pertinent source code variables is given below. For any array, the index I is equivalent to the subscript i, and the index J is equivalent to the subscript j. The index K assumes values of 1 or 2, with K = 1 referring to the  $\eta = 0$  boundary layer and K = 2 referring to the  $\eta = 1$  boundary layer. The abbreviation CSL refers to the computational sublayer, and OM refers to ordinary mesh.

<u>Fortran</u>	<u>Definition</u>	<u>Range or Value</u>	<u>Reference</u>
ALPHA	$\alpha$ (pressure damping)	$0 \leq \alpha \leq 5$	(55), (56) *
BETA	$\beta$	$\beta < 0$ (transients only) $\beta = 1$ (converged solution)	II.B.5 **
CAPGAM(1), CAPGAMØ	$\Lambda$ for $\eta = 0$	Units: feet	(16)
CAPGAM(2), CAPGAM1	$\Lambda$ for $\eta = 1$	Units: feet	(16)
CF	$c_f = \tau_w / \frac{1}{2} \rho_\infty U_\infty^2$		
CFL	Courant-Friedrichs-Lewy number	$0 < CFL < 1$	(44), (45) II.B.1
CV	$c_v$ (air)	$4290 \text{ ft}^2/\text{sec}^2\text{-}^\circ\text{R}$	I.C.2
DETA	$\Delta\eta$		(21)
DT1, DT2, DT3, DT4, DT5	Quantities employed in determining proper time step in each region		
DT	$\Delta t$	Units: seconds	(37)
DUDN	$\partial u / \partial n$		(11)
DY PLUS ***	$y_m' u_* / v_w$		(61)
DYSL PLUS ***	$\Delta y_{SL} u_* N / v_w$		(14), III.A.2

\* I.e., equations (55) and (56). \*\* I.e., Section II.B.5.

\*\*\* Appear on program output.

<u>Fortran</u>	<u>Definition</u>	<u>Range or Value</u>	<u>Reference</u>
DZETA	$\Delta\zeta$		(21)
EFFIC	Measure of efficiency of code		(51)
EI(I,J)	$e_i$ at $(x_{i,j}, y_{i,j})$	Units: $\text{ft}^2/\text{sec}^2$	I.C.2
EINF	$e_\infty$	Units: $\text{ft}^2/\text{sec}^2$	I.C.2
EIINF	$e_{i\infty}$	Units: $\text{ft}^2/\text{sec}^2$	I.C.2
EPSLN(I,J)	$\epsilon_{i,j}$ in OM	Units: $\text{lb f sec}/\text{ft}^2$	(15), (17)
EPSLNI	$\epsilon_{eq_i}$	Units: $\text{lb f sec}/\text{ft}^2$	(11)
EPSLNO	$\epsilon_{eq_0}$	Units: $\text{lb f sec}/\text{ft}^2$	(12)
EPSLSL(I,J,K)	$\epsilon_{i,j}$ in CSL	Units: $\text{lb f sec}/\text{ft}^2$	(15), (17)
EREF(J)	$\epsilon_{eq}(s_0, n)$ in OM	Units: $\text{lb f sec}/\text{ft}^2$	(17)
ESLREF(J,K)	$\epsilon_{eq}(s_0, n)$ in CSL	Units: $\text{lb f sec}/\text{ft}^2$	(17)
ETAX(I,J)	$\eta_{x_{i,j}}$	Units: $\text{ft}^{-1}$	I.C.2
ETAY(I,J)	$\eta_{y_{i,j}}$	Units: $\text{ft}^{-1}$	I.C.2
FAC(I,K)	$\sqrt{ \tau_w  \rho_w / 26\mu_w}$	Units: $\text{ft}^{-1}$	
GAM(I,K)	$\Gamma$		(16)
GAMMA	$\gamma$	1.4 (air)	(10)
IDAMP1	$\begin{cases} 0: & \text{no pressure} \\ & \text{damping for } L_\zeta \\ 1: & \text{pressure} \\ & \text{damping for } L_\zeta \end{cases}$		(55), (56)
IDAMP2	Same as above for $L_\eta$		
IL	Number of points in $\zeta$ -direction	$\leq 40$	
I2	$IL - 1$		
ILE(1), ILE0	Value of $i$ at leading edge on $\eta = 0$	$1 \leq ILE0 \leq IL$	Note 1*
ILE(2), ILE1	Same as above for $\eta = 1$	$1 \leq ILE1 \leq IL$	Note 1
IOVLP	Value of $i$ in upstream region that defines restart station	$1 < IOVLP \leq IL - 5$	II.B.3

\*Notes are listed at end of this section.

<u>Fortran</u>	<u>Definition</u>	<u>Range or Value</u>	<u>Reference</u>
IPDOWN	<ul style="list-style-type: none"> <li>0: no downstream pressure applied</li> <li>1: pressure PDOWN applied at <math>\zeta = 1</math></li> </ul>		Note 5
IPRINT	Flow data printed every IPRINT steps		
IRGN	Region in split mesh	1 to 5	II.B.2
ISTART	<ul style="list-style-type: none"> <li>0: Initialize variables to uniform flow (file RSTART not used); i.e., <math>U_\infty, p_\infty</math>, etc.</li> <li>1: Continue calculation using data from file RSTART</li> <li>2: Read upstream region from file RSTART. Set <math>i = IOVLP</math> as restart station of downstream region and commence calculation</li> </ul>		
ITER	Number of time steps (if ITER = 0, code simply prints results with no integration)		
ITNE(1), ITNE $\emptyset$	Value of $i$ at end of transition region* on $\eta = 0$	$1 \leq ITNS\emptyset < ITNE\emptyset \leq IL$	Note 2
ITNE(2), ITNE1	Same as above for $\eta = 1$	$1 \leq ITNS1 < ITNE1 \leq IL$	Note 2
ITNS(1), ITNS $\emptyset$	Value of $i$ at beginning of transition region* on $\eta = 0$	See ITNE $\emptyset$ above	Note 2
ITNS(2), ITNS1	Same as above for $\eta = 1$	See ITNE1 above	Note 2
J11	Upper limit for $j$ in Region 1		II.B.2

\* Region of transition from laminar to turbulent flow.

<u>Fortran</u>	<u>Definition</u>	<u>Range or Value</u>	<u>Reference</u>
J12	Upper limit for j in Region 2		II.B.2
J13	Upper limit for j in Region 3		II.B.2
J14	Upper limit for j in Region 4		II.B.2
JL	Number of points in $\eta$ -direction	$9 \leq JL \leq 48$	
J2	JL - 1		
JMATCH(I,1)	Value of j in OM at which $\epsilon$ transfers from inner to outer expression for $\eta = 0$ boundary layer	2 to JREF $\emptyset$	(15)
JMATCH(I,2)	Same as above for $\eta = 1$ boundary layer	JREF1 to J2	(15)
JREF $\emptyset$	For all $j \leq JREF\emptyset$ , the eddy viscosity refers to the $\eta = 0$ boundary layer		Note 3
JREF1	For all $j \geq JREF1$ , the eddy viscosity refers to the $\eta = 1$ boundary layer		Note 3
JSL $\emptyset$	Number of points in CSL on $\eta = 0$	$3 \leq JSL\emptyset \leq 20$	Note 4
JSL1	Same as above for $\eta = 1$	$3 \leq JSL1 \leq 20$	Note 4
M(1), M1	$m_1$	$\geq 1$	(47)
M(2), M2	$m_2$	$\geq 1$	(47)
M(3)	$m_3$	1	(47)
M(4), M4	$m_4$	$\geq 1$	(47)
M(5), M5	$m_5$	$\geq 1$	(47)
NADV	Time step number		

<u>Fortran</u>	<u>Definition</u>	<u>Range or Value</u>	<u>Reference</u>
NI	Cumulative number of time steps		
P(I,J)	Static pressure $p_{i,j}$	Units: lbf/ft <sup>2</sup>	I.C.2
PDOWN	Static pressure at $\zeta = 1$	Units: lbf/ft <sup>2</sup>	Note 5
PINF	$p_{\infty}$	Units: lbf/ft <sup>2</sup>	
PR	$Pr$	0.72 (air)	(10)
PRTURB	$Pr_t$	0.90	(10)
QYWL(I,K)	Heat transfer at wall in CSL	0 (adiabatic wall)	
QY2(I,K)	Heat transfer normal to wall at matching point in CSL	Units: lbf/ft-sec	II.B.7
REM(1)	Max $Re_m$ in CSL on $\eta = 0$	Must be less than approximately 0.25	(65), (66)
REM(2)	Same as above for CSL on $\eta = 1$	Same	(65), (66)
RHO(I,J,L)*	$\rho_{i,j}$	Units: slugs/ft <sup>3</sup>	(3) to (6)
RHOE(I,J,L)*	$\rho e_{i,j}$	Units: lbf/ft <sup>2</sup>	(3) to (6)
RHOINF	$\rho_{\infty}$	Units: slugs/ft <sup>3</sup>	
RHOU(I,J,L)*	$\rho u_{i,j}$	Units: slugs/ft <sup>2</sup> -sec	(3) to (6)
RHOV(I,J,L)*	$\rho v_{i,j}$	Units: slugs/ft <sup>2</sup> -sec	(3) to (6)
RK1	$\kappa$	0.40	(11)
RK2	$\kappa_2$	0.0168	(12)
S(I,1)	Distance along $\eta = 0$ from leading edge	Units: feet	See S(I,1) in III.C.1
S(I,2)	Distance along $\eta = 1$ from leading edge	Units: feet	See S(I,1) in III.C.1

\*L = 1 represents value after corrector step, and L = 2 represents value after predictor step. For any analysis of converged solution, always use L = 1 level.

<u>Fortran</u>	<u>Definition</u>	<u>Range or Value</u>	<u>Reference</u>
SREF(1)	$s_0$ for $\eta = 0$ boundary layer	Units: feet	(17)
SREF(2)	Same as above for $\eta = 1$ boundary layer	Units: feet	(17)
TAUWL(I,1)	Wall shear stress on $\eta = 0$ . Positive values imply force is active in positive $\zeta$ -direction, and vice versa	ITNS0 < i < IL Units: lbf/ft <sup>2</sup>	
TAUWL(I,2)	Same as above for $\eta = 1$	ITNS1 < i < IL Units: lbf/ft <sup>2</sup>	
TAU2(I,1)	Shear stress parallel to wall in CSL on $\eta = 0$ at matching point	Same as TAUWL(I,1)	
TAU2(I,2)	Same as above for $\eta = 1$	Same as TAUWL(I,2)	
TEMP	Static temperature	Degrees Rankine	
TIME	Cumulative physical time of integration	Units: seconds	
TMAX	CP time requested on job card	Units: seconds	
TSL(I,J,K)	Static temperature in CSL	Units: Degrees Rankine	
U(I,J)	$u_{i,j}$ in OM	Units: ft/sec	(4)
UDELTA, UREFDL	$U_{ref} \delta_i^*$	Units: ft <sup>2</sup> /sec	(12)
UINF	$U_\infty$ = magnitude of freestream velocity	Units: ft/sec	
UREF, UREFER	$U_{ref}$	Units: ft/sec	(12)
USL(I,J,1)	u in CSL on $\eta = 0$	ITNS0 < i < IL Units: ft/sec	(18)
USL(I,J,2)	u in CSL on $\eta = 1$	ITNS1 < i < IL Units: ft/sec	
V(I,J)	$v_{i,j}$ in OM	Units: ft/sec	(4)
X(I,J)	$x_{i,j}$ in OM	Units: feet	



<u>Fortran</u>	<u>Definition</u>	<u>Range or Value</u>	<u>Reference</u>
XJINV(I,J)	$1/J_{i,j}$	Units: feet	(7)
XLMBDA(1), XLMBDA0	$\lambda$ on $\eta = 0$	Units: feet	(17)
XLMBDA(2), XLMBDA1	$\lambda$ on $\eta = 1$	Units: feet	(17)
XMDOT(I,1)	$\dot{m}_i$ on $\eta = 0$	Units: slugs/ft <sup>2</sup> -sec	Note 7
XMDOT(I,2)	$\dot{m}_i$ on $\eta = 1$	Units: slugs/ft <sup>2</sup> -sec	Note 7
XMINF	Freestream Mach No. $M_\infty$		
XMUSL(I,J,1)	$\mu$ in CSL on $\eta = 0$	ITNS0 < I < IL Units: lbf sec/ft <sup>2</sup> (air)	(8)
XMUSL(I,J,2)	Same as above for $\eta = 1$	ITNS1 < I < IL Units: lbf sec/ft <sup>2</sup> (air)	(8)
XN(I,J)	See XN(I,J) in III.C.4		
Y(I,J)	$y_{i,j}$ in OM	Units: feet	
ZETAX(I,J)	$\zeta_{x_{i,j}}$	Units: ft <sup>-1</sup>	I.C.2
ZETAY(I,J)	$\zeta_{y_{i,j}}$	Units: ft <sup>-1</sup>	I.C.2

Note 1: On  $\eta = 0$ , boundary conditions (53) for a no-slip wall are applied for  $i \geq ILE(1)$ . If the entire surface  $\eta = 0$  is a no-slip surface,  $ILE(1) = 1$ . If the entire surface is within the freestream, set  $ILE(1) = IL$ . Similar results hold for  $\eta = 1$ .

Note 2: If the entire boundary layer on  $\eta = 0$  is fully turbulent, set  $ITNS(1) = ITNE(1) = 1$ . If the entire boundary layer on  $\eta = 0$  is fully laminar or if there is no boundary layer, set  $ITNS(1) = IL$  and  $ITNE(1) = IL$ . Note that in mesh overlapping a restart station cannot fall within the region of transition from laminar to turbulent flow in any boundary layer. Similar results hold for  $\eta = 1$ .

Note 3: In choosing  $JREF0$  and  $JREF1$ , the following criteria must be observed:

- $1 < JREF0 < JREF < JREF1 < JL$ , where  $JREF$  is defined in Section III.C.2
- The contour  $\eta = \eta_{JREF0}$  must lie outside of the boundary layer on  $\eta = 0$  at all stations. The contour need not be close to the actual boundary layer thickness at all. For boundary layers on the ramp and cowl of roughly equal thickness at any station,  $JREF$  is chosen such that  $\eta_{JREF}$  roughly bisects the inlet height at all stations. This can be estimated using the mesh distribution on  $\zeta = 0$  and  $\zeta = 1$ .
- The contour  $\eta = \eta_{JREF1}$  must lie outside the boundary layer on  $\eta = 1$ .

- Note 4: The quantities  $JSL\emptyset$  and  $JSL1$  cannot be changed during the course of any calculation, nor during overlapping. Since the CSL calculation is very fast, it is recommended to use  $JSL\emptyset = JSL1 = 20$  in all cases.
- Note 5: The effect of a terminal shock can be achieved by specifying a desired downstream pressure  $PDOWN$  ( $lbf/ft^2$ ) and setting  $IPDOWN = 1$ . For sufficiently high downstream pressures, a terminal shock will form in the inlet throat. The necessary value of  $PDOWN$  can be approximated by a simple normal shock analysis using data at  $\zeta = 1$  (when solution is converged and  $IPDOWN = 0$ ), but the location and stability of the terminal shock will, in general, be somewhat sensitive to the value of  $PDOWN$ , as in the experimental case.
- Note 6: For all CSL variables (e.g.,  $USL(I,J,K)$ ), the index  $I$  refers to the location in the  $\zeta$ -direction in the same manner as all other variables (e.g.,  $U(I,J)$ ). The  $J$  index is defined such that  $J = 1$  is always the surface (i.e.,  $\eta = 0$  or  $\eta = 1$ ) and  $J = JSL\emptyset$  or  $JSL1$  is the matching point.
- Note 7: The array  $XMDOT(I,K)$  (i.e.,  $\dot{m}_i$ ) is the bleed mass flux (in units of slugs/ $ft^2$ -sec) at the station  $i$ . It is defined such that negative values always imply bleed (for either  $\eta = 0$  or  $\eta = 1$  surface), and positive values always imply blowing. The bleed mass flux is assumed uniform within each bleed zone and its value is given by

$$\dot{m} = \frac{\text{(Bleed flow rate in slugs/sec)}}{\text{Area in ft}^2}$$

with proper consideration for the sign as indicated above. Note that the Area above is the total surface area of the bleed zone, not the surface area of the bleed holes.

In executing the program, the values of  $\dot{m}_i$  may be changed as desired to investigate effects of different bleed distributions on the flow structure. Changes should be made gradually; e.g., by a sequence of computer runs in which  $\dot{m}_i$  is changed by 10% or so and then the flow is integrated for 10 steps, until the desired  $\dot{m}_i$  is achieved.

Note that all values of  $XMDOT(I,K)$ ,  $I = 1, IL$ , must be specified, including those positions where it is zero.

### E. File Structure

The program employs, in general, three files in addition to the conventional files INPUT and OUTPUT. The descriptions are indicated below.

<u>File</u>	<u>Description</u>	<u>Data Structure</u>
RSTART	Input file with latest results for flow variables, or converged results of upstream region in the case of overlapping	RHO, RHOV, RHOE, U, V, EI, P, EPSLN, USL, TSL, EPSLSL, XMUSL, TAUWL, TAU2, QYWL, QY2, FAC, TIME, NI, EREF, ESLREF
STORE	Output file for flow variables	Same as above
XY	Input file for coordinate transformation data	X, Y, ZETAX, ZETAY, ETAX, ETAY, XN, S

The data are written unformatted in the sequence indicated. The following indicates the size of each array, where for example RHO is dimensioned as RHO(40,48,2).

<u>Array</u>	<u>Size</u>
RHO, RHOV, RHOE, RHOE	40 x 48 x 2
U, V, EI, P, EPSLN	40 x 48
USL, TSL, EPSLSL, XMUSL	40 x 20 x 2
TAUWL, TAU2, QYWL, QY2, FAC	40 x 2
TIME, NI	1
EREF	48
ESLREF	20 x 2

For example, the sequence in which data are written on file RSTART is (consult any Fortran IV manual)

RHO(1,1,1), RHO(2,1,1), ..., RHO(40,1,1)

RHO(1,2,1), RHO(2,2,1), ..., RHO(40,2,1)

. . . . .

RHO(1,1,2), RHO(2,1,2), ..., RHO(40,1,2)

and so forth.

The utilization of the files is indicated as follows:

<u>File</u>	<u>Type</u>	<u>Utilized</u>
RSTART	Input	For ISTART = 1 or 2 only
STORE	Output	Required if ITER > 0
XY	Input	Required for every code execution

F. Sample Calculation: Upstream Inlet Region for MCAIR Case 35

In Figure 9, the general physical features of the upstream inlet region of MCAIR Case 35 are indicated. A coordinate system for this region was computed in the manner discussed in Section III.C.6, except that the mesh spacing  $\Delta x$  was taken equal to 0.125 inch and the upstream boundary at  $x = 13.93$  inch. The downstream boundary is thus  $x = 18.81$  inch. Within this region, therefore, the boundary layer bleed schedule is as follows (See Figure 9):

<u>Surface</u>	<u>Extent</u>	<u>Range in i</u>	<u><math>\dot{m}</math>(slugs/ft<sup>2</sup>-sec)</u>
Ramp	13.93 < x < 16.5	i = 1 to 21	0.
Ramp	16.5 < x < 18.8	i = 22 to 40	$-3.85 \times 10^{-3}$
Cowl	13.93 < x < 18.8	i = 1 to 40	0.

The flowfield calculation was performed by submitting a sequence of several jobs requesting 900 seconds each and having the input data indicated in Table 11. Each input line is described below.

a) Line 1

The freestream velocity  $U_{\infty}$  is 2230 ft/sec ( $UINF = 2230$ ),

TABLE 11. INPUT DATA FOR FLOWFIELD CALCULATION OF  
 UPSTREAM INLET REGION (MCAIR CASE 35 WITH  
 $\Delta x = 0.125$  INCH)

<b>Line 1</b>	UINF	PINF	XMINF	CFL	ALPHA	BETA	TMAX
(Format 7F10.8)	2230.	91.84	3.51	0.9	5.0	1.0	900.
<b>Line 2</b>	XLMBDA(1)	XLMBDA(2)	PDOWN	SREF(1)	SREF(2)		
(Format 5F10.8)	1.0	1.0	0.	999.	999.		
<b>Line 3</b>	IL	JL	ITER	ILE(1)	ILE(2)	JSLØ	JSL1
(Format 7I5)	40	48	40	1	10	20	20
<b>Line 4</b>	JREFØ	JREF1	IDAMP1	IDAMP2	ISTART	IPRINT	
(Format 6I5)	28	29	1	1	1	40	
<b>Line 5</b>	ITNS(1)	ITNS(2)	ITNE(1)	ITNE(2)	IOVLP	IPDOWN	
(Format 6I5)	1	20	1	30	1	0	
<b>Lines 6 to 11</b>	XMDOT(I,1), I = 1, ..., 40						
(Format 7F10.8)							
	0.	0.	0.	0.	0.	0.	0.
	0.	0.	0.	0.	0.	0.	0.
	0.	0.	0.	0.	0.	0.	0.
	-.00385						-.00385
	-.00385						-.00385
	-.00385						-.00385
<b>Lines 12 to 17</b>	XMDOT(I,2), I = 1,40						
(Format 7F10.8)							
	0.	0.	0.	0.	0.	0.	0.
	0.						0.
	0.						0.
	0.						0.
	0.						0.
	0.						0.

Mach number  $M_\infty$  is 3.51 ( $XMINF = 3.51$ ), and pressure  $p_\infty$  is 91.84 lbf/ft<sup>2</sup> ( $PINF = 91.84$ ). The Courant number is 0.9 ( $CFL = 0.9$ ), and the damping coefficients  $\alpha$  and  $\beta$  are taken to be 5.0 and 1.0. The requested computer time per job is 900 sec ( $TMAX = 900$ ).

b) Line 2

As discussed in Ref. 18, the eddy viscosity relaxation model was not employed in the presence of bleed. This is accomplished by setting  $SREF(1)$  and  $SREF(2)$  to any number greater than the largest value of  $S(I,1)$  and  $S(I,2)$ . In this case,  $SREF(1) = SREF(2) = 999$  is sufficient. Since  $XLMBDA(1)$  and  $XLMBDA(2)$  are thus irrelevant, they are set equal to one. A downstream pressure is not imposed (see Line 5), thus  $PDOWN$  is irrelevant and arbitrarily set equal to zero.

c) Line 3

A mesh of 40 points by 48 points is used ( $IL = 40$ ,  $JL = 48$ ). A total of 40 time steps are requested in each job ( $ITER = 40$ ). The leading edge of the ramp lies upstream of the upstream boundary, thus,  $ILE(1) = 1$ . The leading edge of the cowl lies at  $x = 15$  inch. For the mesh spacing used, this point lies between  $i = 9$  and  $i = 10$  on the upper surface, and thus  $ILE(2) = 10$ . A total of twenty points were used in each CSL ( $JSL\emptyset = JSL1 = 20$ ).

d) Line 4

In the coordinate system generated for this case, the value  $JREF = 28$  was used. Thus we choose  $JREF\emptyset = 28$  and  $JREF1 = 29$  (see Note 3 of Section IV.D.). The parameters  $IDAMP1 = IDAMP2 = 1$  indicates that pressure damping is employed due to the presence of shock waves in the flow. The parameter  $ISTART = 1$  for all runs. For the first job,

file RSTART is the same as file FLOWDN from program UPSTRM discussed in Section IV.H. For all succeeding jobs, file RSTART is the STORE file from the previous job. We choose to print the results after forty time steps (IPRINT = 40).

e) Line 5

Since the boundary layer on the  $\eta = 0$  boundary is fully turbulent at the upstream boundary, ITNS(1) = ITNE(1) = 1 (see Note 2 of Section IV.D). Using the method of Deem and Murphy<sup>14</sup>, it is estimated that the region of transition from laminar to turbulent flow on the  $\eta = 1$  surface corresponds to the range  $i = 20$  to  $i = 30$ , and thus ITNS(2) = 20 and ITNE(2) = 30. Since ISTART = 1, the value of IOVLP is irrelevant and thus IOVLP is arbitrarily set to one. A downstream pressure is not applied since the terminal shock is assumed to be downstream of the region, and thus IPDOWN = 0.

f) Lines 6 to 11

Using the bleed schedule indicated above, the bleed mass flux XMDOT(I,1),  $I = 1, \dots, 40$  on  $\eta = 0$  is entered.

g) Lines 12 to 17

Same as above for  $\eta = 1$ .

G. Sample Output: Upstream Inlet Region for MCAIR Case 35

The output from the program is illustrated in Figures 13a through 13f, where samples of each major section of output for the upstream inlet region of MCAIR Case 35 are presented sequentially. The output was generated by one of the later jobs in the job sequence. For purposes of brevity, ITER and IPRINT were changed to 10.

In Figure 13a, the values of the input parameters are indicated. They

are followed by a list of variables printed at every time step. These variables are the time step number (NADV), the total elapsed physical time (sec) of calculation for the region (TIME), the time step (DT), the values of  $m_i$  in equation (47), the values of  $j$  for the upper limit of each of the first four mesh-split regions (JI1 to JI4), the time steps in each of the five mesh-split regions (DT1 to DT5) and the parameter EFFIC discussed in equation (51). As indicated previously, the time step DT may vary substantially during program execution, although the term EFFIC remains approximately constant. At the end of the specified number of iterations, the physical time in seconds (TIME) is specified, which is important to the determination of convergence as discussed previously.

In Figure 13b, the flow variables on the ordinary mesh are given at each value of  $i$  (that is, at each station) denoted by "COLUMN 1", "COLUMN 2", etc. For brevity, only those results for  $i = 1$  and  $i = 2$  are shown. At each value of  $i$ , the corresponding value of  $x$  is indicated in feet ("X EQUALS ..."). The values of the cartesian  $y$  coordinate ( $Y$ ) are listed at each value of  $j$ , together with the values of the static temperature in  $^{\circ}R$  (TEMP), cartesian velocity components  $v$  and  $u$  ( $V,U$ ) in ft/sec, static pressure ( $P$ ) in lbf/ft<sup>2</sup> and turbulent eddy viscosity (EPSLN) in lbf-sec/ft<sup>2</sup>.

In Figure 13c, the values of  $U_{ref}$  (UREFER) and  $U_{ref} \delta_i^*$  (UDELTA) are listed at each station for the lower ( $ETA = 0$ ) and upper ( $ETA = 1$ ) boundary layers. The values of  $j$  at which the inner and outer eddy viscosity formulas are matched is also indicated (JMATCH).

In Figure 13d, the flow variables on the computational sublayer mesh adjacent to the lower boundary are given at each station. The values of the normal distance ( $XN$ ) in feet of each sublayer point are shown for each value of  $j$  from 1 to  $JSL\emptyset = 20$ , together with the values of the static

temperature (TEMP) in °R, sublayer velocity (USL) in ft/sec, turbulent eddy viscosity (EPSLN) in lbf-sec/ft<sup>2</sup> and molecular viscosity (VISCOSITY) in lbf-sec/ft<sup>2</sup>. For brevity, only those results for  $i = 1$  to 4 are shown. A similar output follows (not shown) for the flow variables on the computational sublayer mesh adjacent to the upper boundary.

In Figure 13e, the values of several useful flow variables are shown at each station on the lower and upper boundaries. These variables are  $p/p_\infty$  (P/PINF),  $\dot{m}$  (MASS BLEED) in slug/ft<sup>2</sup>-sec, and  $c_f$  (CF). Stations ahead of a leading edge have  $c_f$  equal to zero. The values of  $\dot{m}$  are identical to those specified in the input data.

Finally, in Figure 13f the values of DY PLUS and DYSL PLUS (See Section IV.D.) are listed for the lower and upper surfaces. These values assist in determining whether the mesh distribution employed was satisfactory in regards to providing sufficient flow field resolution (Section III.A.2).

#### H. Interpolating Flow Variables at Mesh Overlap Using Program UPSTRM

##### 1. Introduction

In certain instances of mesh overlapping, the heights of the two mesh systems at the restart station are not equal. This is illustrated in Figure 8, which represents a typical system of meshes employed to compute one of the MCAIR high speed inlet configurations. The flat plate portion of the ramp ahead of the inlet entrance is computed using mesh A, whose height is typically five times the boundary layer thickness of the restart station. The height of the overlapping mesh B at the restart station depends on the cowl angle, and is generally different from that of mesh A. The program UPSTRM is employed to interpolate the flow variables onto the upstream boundary.

of mesh B at the restart station. In addition, the program provides initial values for the flow variables at all other points. In this manner, a variety of different cowl angles can be considered for given freestream conditions without the need for recomputing the flow in Region A.

The program UPSTRM is employed only in the case described above. In those instances where the heights of the mesh regions at the restart station are identical (e.g., meshes B and C in Fig. 8), the program UPSTRM is not used.

The following requirements must be satisfied:

- a) The restart station is a vertical line in both the upstream and downstream meshes. In its present configuration, the program COORD insures that this requirement is satisfied.
- b) There is a boundary layer on the lower surface only in the upstream region (mesh A) as illustrated in Figure 8.
- c) The height of the first row of ordinary mesh points above the lower surface at the restart station is the same in the upstream and downstream meshes. This requirement must be met in defining the  $\zeta = 0$  boundary of the downstream mesh using program BNDRY. All other ordinary points may be distributed as desired on this boundary, with care taken to provide adequate resolution as discussed in Section III.A.

The following table provides information on the resources required to execute program UPSTRM on the CYBER 175.

TABLE 12. RESOURCES REQUIRED FOR EXECUTION OF PROGRAM UPSTRM

<u>Resource</u>	<u>Details</u>
Computer Time	< 5 sec (typical)
Input/Output Time	< 5 sec (typical)
Core Memory	< 150,000 words (octal)
Files Required	INPUT, OUPUT, FLOWUP, FLOWDN, MESHUP, MESHDN (See Section IV.H.5)

## 2. Description of Input Variables

The input to program UPSTRM consists of two cards. The definition and format of the input data are indicated in the required order in Table 13.

TABLE 13. INPUT DATA FOR PROGRAM UPSTRM

Line 1:	JSLOLD, JLOLD, IL, JL, JSLØ, JSL1, JREFØ, IOVLP
---------	---

(Format 8I5)

<u>Fortran</u>	<u>Definition</u>	<u>Range or Value</u>
JSLOLD	Number of points in CSL on $\eta = 0$ in upstream mesh	3; JSLOLD $\leq$ 20
JLOLD	Number of points in $\eta$ -direction in upstream mesh	9; JLOLD $\leq$ 40
IL	Number of points in $\zeta$ -direction in downstream mesh	0-40
JL	Number of points in $\eta$ -direction in downstream mesh	9; JL $\leq$ 40
JSLØ	Number of points in CSL on $\eta = 0$ on downstream mesh	3; JSLØ $\leq$ 20
JSL1	Number of points in CSL on $\eta = 1$ on downstream mesh	3; JSL1 $\leq$ 20
JREFØ	Value of JREFØ in downstream mesh	See Section IV. D
IOVLP	Value of i in upstream region that defines restart station	See Section IV. B

TABLE 13. CONT'D

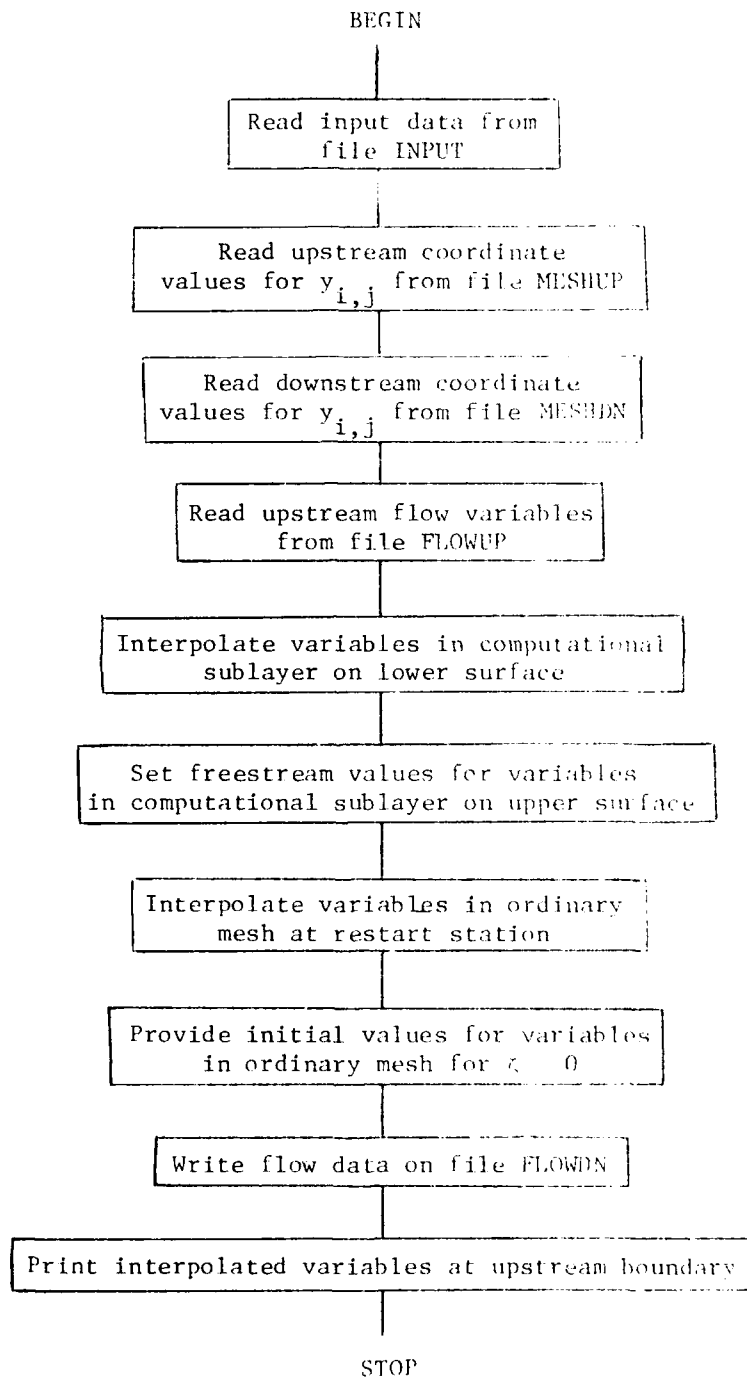
Line 2:	UINF, VINF, EIINF, PINF, EPSINF, DELTA
---------	--

(Format 6F10.4)

<u>Fortran</u>	<u>Definition</u>	<u>Range or Value</u>
UINF	$U_{\infty}$	Units: ft/sec
VINF	$V_{\infty}$ (vertical velocity at edge of boundary layer at restart station)	Units: ft/sec
EIINF	$e_{i_{\infty}} = c_v T_{\infty}$	Units: ft <sup>2</sup> /sec <sup>2</sup>
PINF	$P_{\infty}$	Units: lbf/ft <sup>2</sup>
EPSINF	$\epsilon$ at edge of boundary layer at restart station	Units: lbf-sec/ft <sup>2</sup>
DELTA	Boundary layer thickness at restart station	Units: ft

3. Flow Chart: Program UPSTRM

The pertinent features of the program UPSTRM are indicated below.



#### 4. Source Code Notation

The definition of the pertinent source code variables is given below. The labeling conventions for the subscripts I, J and K are the same as in Section IV.D.

<u>Fortran</u>	<u>Definition</u>	<u>Range or Value</u>
DELTA	Boundary layer thickness at restart station	Units: feet
EI(I,J)	$e_i$ at $(x_{i,j}, y_{i,j})$	Units: $\text{ft}^2/\text{sec}^2$
EIINF	$e_{i_\infty} = c_v T_\infty$	Units: $\text{ft}^2/\text{sec}^2$
EPSINF	$\epsilon$ at edge of boundary layer	Units: $\text{lbf-sec}/\text{ft}^2$
EPSLN(I,J)	$\epsilon_{i,j}$ in OM	Units: $\text{lbf-sec}/\text{ft}^2$
EPSLSL(I,J,K)	$\epsilon_{i,j}$ in CSL	Units: $\text{lbf-sec}/\text{ft}^2$
EREF(J)	$\epsilon_{eq}(s_o, n)$ in OM	Units: $\text{lbf-sec}/\text{ft}^2$
ESLREF(J,K)	$\epsilon_{eq}(s_o, n)$ in CSL	Units: $\text{lbf-sec}/\text{ft}^2$
FAC(I,K)	$\sqrt{ \tau_w  \rho_w / 26 \mu_w}$	Units: $\text{ft}^{-1}$
IL	Number of points in $\zeta$ -direction in downstream mesh	$\leq 40$
IOVLP	Value of $i$ in upstream region that defines restart station	See IV.D.
JL	Number of points in $\eta$ -direction in downstream mesh	$9 \leq JL \leq 48$
JLOLD	Number of points in $\eta$ -direction in upstream mesh	$9 \leq JL \leq 48$
JSLOLD	Number of points in CSL on $\eta = 0$ in upstream mesh	$3 \leq JSLOLD \leq 20$
JSLØ	Number of points in CSL on $\eta = 0$ in downstream mesh (need not be same as JSLOLD)	$3 \leq JSLØ \leq 20$
JSL1	Number of points in CSL on $\eta = 1$ in downstream mesh	$3 \leq JSL1 \leq 20$

<u>Fortran</u>	<u>Definition</u>	<u>Range or Value</u>
JREFØ	Value of JREFØ in downstream mesh	See IV.D
P(I,J)	$P_{i,j}$	Units: $\text{lb}/\text{ft}^2$
PINF	$P_\infty$	Units: $\text{lb}/\text{ft}^2$
QYWL(I,K)	Heat transfer at wall in CSL	0 (adiabatic wall)
QY2(I,K)	Heat transfer normal to wall at matching point	Units: $\text{lb}/\text{ft}\text{-sec}$
RHO(I,J,L)	$\rho_{i,j}$	See IV.D
RHOE(I,J,L)	$\rho e_{i,j}$	See IV.D
RHOU(I,J,L)	$\rho u_{i,j}$	See IV.D
RHOV(I,J,L)	$\rho v_{i,j}$	See IV.D
TAUWL(I,K)	Wall shear stress	See IV.D
TAU2(I,K)	Shear stress at matching point	See IV.D
TSL(I,J,K)	Static temperature in CSL	See IV.D
U(I,J)	$u_{i,j}$ in OM	See IV.D
USL(I,J,K)	$u$ in CSL	See IV.D
UINF	$U_\infty$	Units: $\text{ft}/\text{sec}$
V(I,J)	$v_{i,j}$ in OM	Units: $\text{ft}/\text{sec}$
VINF	$v_\infty$	Units: $\text{ft}/\text{sec}$
XMUSL(I,J,K)	$u$ in CSL	See IV.D
YUP(I,J)	$y_{i,j}$ in upstream mesh	Units: feet
YDOWN(I,J)	$y_{i,j}$ in downstream mesh	Units: feet
YSLUP(J)	Mesh point distribution in CSL at restart station	Units: feet

## 5. File Structure

The program employs four files, in addition to the conventional files INPUT and OUTPUT. The descriptions are indicated below. For further information see Section IV.E.

<u>File</u>	<u>Description</u>	<u>Data Structure</u>
FLOWUP	Input file of flow variables in upstream region	See file RSTART
FLOWDN	Output file of flow variables in downstream region	Same as FLOWUP
MESHUP	Input file of coordinate transformation data for upstream region	See file XY in Section IV.D
MESHDN	Input file of coordinate transformation data for downstream region	Same as FLOWDN

All four files are required for each execution of the program.

## 6. Output

The printed output consists of (1) the interpolated flow variables  $u$ ,  $v$ ,  $e_1$ ,  $p$  and  $\epsilon$  on the ordinary mesh of the downstream region at the restart station, and (2) the interpolated flow variables  $T$ ,  $u$ ,  $\epsilon$  and  $\mu$  on the computational sublayer mesh ( $\eta = 0$  boundary) of the downstream region at the restart station. The format is similar to that employed by the Navier-Stokes code (see Figures 13b and 13d). It should be noted that the messages "RM ERROR 0142 on LFN MESHUP" and "RM ERROR 0142 ON LFN MESHDN" may appear in the dayfile. These messages are of no significance, and may be ignored.

#### REFERENCES

1. Thompson, J. F., Thames, F. C., and Mastin, C. W., "Automatic Numerical Generation of Body-Fitted Curvilinear Coordinate System for Field Containing Any Number of Arbitrary Two-Dimensional Bodies," J. Comp. Physics, 15, 1974, 299-319.
2. Rubesin, M. W., and Rose, W. C., "The Turbulent Mean-Flow, Reynolds-Stress, and Heat-Flux Equations in Mass Averaged Dependent Variables," NASA TMX-62248, March 1973.
3. Lapidus, A., "A Detached Shock Calculation by Second-Order Finite Differences," J. Comp. Physics, 2, 1967, 154-177.
4. Steger, J. L., "Implicit Finite-Difference Simulation of Flow about Arbitrary Two-Dimensional Geometries," AIAA J., 16, 1978, 679-686.
5. Shang, J. S., "Computation of Hypersonic Turbulent Boundary Layers with Heat Transfer," AIAA Paper 73-699, AIAA 6th Fluid and Plasma Dynamics Conference, 1973; also, AIAA J., 12, 1974, 883 (Synoptic).
6. Cebeci, T., Smith, A. M. O., and Mosinskis, G., "Calculations of Compressible Adiabatic Turbulent Boundary Layers," AIAA J., 8, 1970, 1974-1982.
7. Cebeci, T., "Calculations of Compressible Turbulent Boundary Layers with Heat and Mass Transfer," AIAA J., 9, 1971, 1091-1097.
8. Cebeci, T., and Smith, A. M. O., Analysis of Turbulent Boundary Layers, Academic Press, 1974.
9. Harris, J. E., "Numerical Solution of the Equations for Compressible Laminar, Transitional and Turbulent Boundary Layers and Comparison with Experimental Data," NASA TR T-368, 1971.
10. Shang, J. S., and Hankey, W. L., Jr., "Numerical Solution for Supersonic Turbulent Flow over a Compression Ramp," AIAA J., 13, 1975, 1368-1374.
11. Coakley, T. J., and Bergman, M. Y., "Effects of Turbulence Model Selection on the Prediction of Complex Aerodynamic Flows," AIAA Paper 79-0070, AIAA 17th Aerospace Sciences Meeting, 1979.
12. Viegas, J. R., and Horstman, C. C., "Comparison of Multiequation Turbulence Models for Several Shock Separated Boundary Layer Interaction Flows," AIAA Paper 78-1165, AIAA 11th Fluid and Plasma Dynamics Conference, 1978.
13. Horstman, C. C., et al., "Reynolds Number Effects on Shock-Wave Turbulent Boundary Layer Interactions," AIAA J., 15, 1977, 1172-1178.
14. Hopkins, E. J., Jillic, D. W., and Sorensen, V. L., "Charts for Estimating Boundary layer Transition on Flat Plates," NASA TN D-5846, June 1970.

15. Deissler, R. G., "Evolution of a Moderately Short Turbulent Boundary Layer in a Severe Pressure Gradient," J. Fluid Mech., 64, 1974.
16. Shang, J. S., Hankey, W. L., Jr., and Law, C. H., "Numerical Simulation of Shock Wave-Turbulent Boundary Layer Interaction," AIAA J., 14, 1976, 1451-1457.
17. Wilcox, D. C., "Numerical Study of Separated Turbulent Flows," ARL TR 74-0133, November 1974.
18. Knight, D. D., "Calculations of High Speed Inlet Flows Using the Navier-Stokes Equations. Vol. I: Description of Results," AFFDL-TR-79-3138.
19. Isaacson, E., and Keller, H., Analysis of Numerical Methods, John Wiley and Sons, Inc., 1966.
20. Mac Cormack, R. W., "Numerical Solution of the Interaction of a Shock Wave with a Laminar Boundary Layer," Lecture Notes in Physics, 8, 1971, 151-163.
21. MacCormack, R. W., and Baldwin, B. S., "A Numerical Method for Solving the Navier-Stokes Equations with Application to Shock-Boundary Layer Interactions," AIAA Paper 75-1, AIAA 13th Aerospace Sciences Meeting, 1975.
22. MacCormack, R. W., and Baldwin, B. S., "Numerical Solution of the Interaction of a Strong Shock Wave with a Hypersonic Turbulent Boundary Layer," AIAA Paper 74-558, AIAA 7th Fluid and Plasma Dynamics Conference, 1974.
23. Deiwert, G. S., "Numerical Simulation of High Reynolds Number Transonic Flows," AIAA J., 13, 1975, 1354-1359.
24. Hung, C. M., and MacCormack, R. W., "Numerical Solutions of Supersonic and Hypersonic Laminar Compression Corner Flows," AIAA J., 14, 1976, 475-481.
25. Knight, D. D., and Hankey, W. L., Jr., "Numerical Simulation of Non-chemically Reacting Radial Supersonic Diffusion Laser," AIAA Paper 76-60, AIAA 14th Aerospace Sciences Meeting, 1976.
26. Knight, D. D., "Numerical Simulation of Realistic High Speed Inlets Using the Navier-Stokes Equations," AIAA J., 15, 1977, 1583-1589.
27. Shang, J. S., Hankey, W. L., Jr., and Petty, J. S., "Three-Dimensional Supersonic Interacting Turbulent Flow along a Corner," AIAA Paper 78-1210, AIAA 11th Fluid and Plasma Dynamics Conference, 1978.
28. Rakich, J. V., Vigneron, Y. C., and Tannehill, J. C., "Navier-Stokes Calculations for Laminar and Turbulent Hypersonic Flow over Indented Noretips," AIAA Paper 78-260, AIAA 16th Aerospace Sciences Meeting, 1978.

29. Shang, J. S., Buning, P. G., Hankey, W. L., Jr., and Wirth, M. C., "The Performance of a Vectorized 3-D Navier-Stokes Code on the Cray-1 Computer," AIAA Paper 79-1448, AIAA 4th Computational Fluid Dynamics Conference, 1979.
30. Hankey, W. L., Jr., and Shang, J. S., "The Numerical Solution to Pressure Oscillations in an Open Cavity," AIAA Paper 79-0136, AIAA 17th Aerospace Sciences Meeting, 1979.
31. Kutler, P., Chakravarthy, S. R., and Lombard, C. P., "Supersonic Flow over Ablated Nosedtips Using an Unsteady Implicit Numerical Procedure," AIAA Paper 78-213, AIAA 16th Aerospace Sciences Meeting, 1978.
32. McRae, D. S., "A Numerical Study of Supersonic Viscous Cone Flow at High Angles of Attack," AIAA Paper 76-97, AIAA 14th Aerospace Sciences Meeting, 1976.
33. Carter, T. D., and Spong, E. D., "High Speed Inlet Investigation. Vol. I: Description of Program and Results. Vol. II: Data Summary," AFFDL-TR-77-105, November 1977.
34. Roache, P., Computational Fluid Dynamics, Hermosa Publishers, Albuquerque, N. M., 1972.
35. Rose, W. C., "Practical Aspects of Using Navier-Stokes Codes for Predicting Separated Flows," AIAA Paper 76-96, AIAA 14th Aerospace Sciences Meeting, 1976.
36. Horstman, C. C., and Hung, C. M., "Computation of Three-Dimensional Turbulent Separated Flows at Supersonic Speeds," AIAA Paper 79-0002, AIAA 17th Aerospace Sciences Meeting, 1979.
37. Baldwin, B., and Lomax, H., "Thin Layer Approximation and Algebraic Model for Separated Turbulent Flows," AIAA Paper 78-257, AIAA 16th Aerospace Sciences Meeting, 1978.
38. Schlichting, H., Boundary Layer Theory, Seventh Edition, McGraw-Hill Co., 1979.

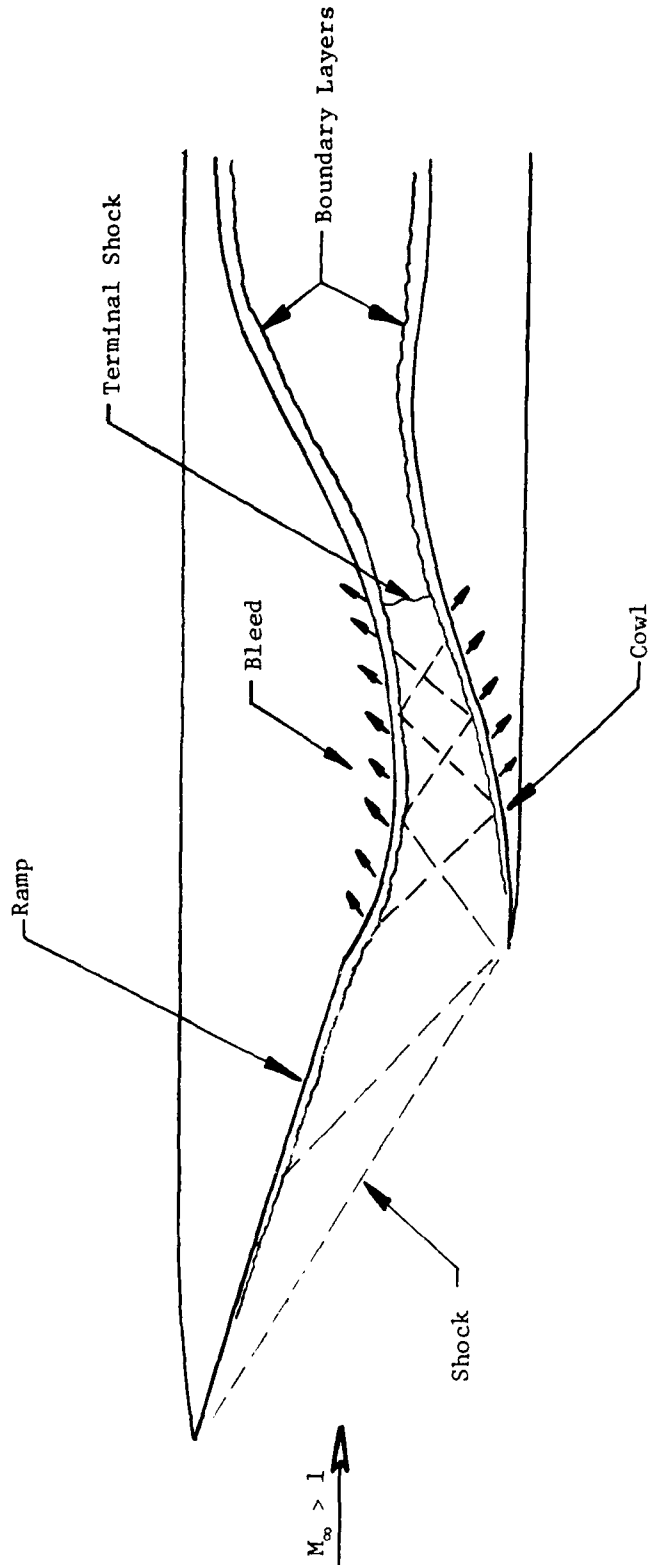


Figure 1. Characteristics of Mixed Compression High Speed Inlet (from Ref. 33)

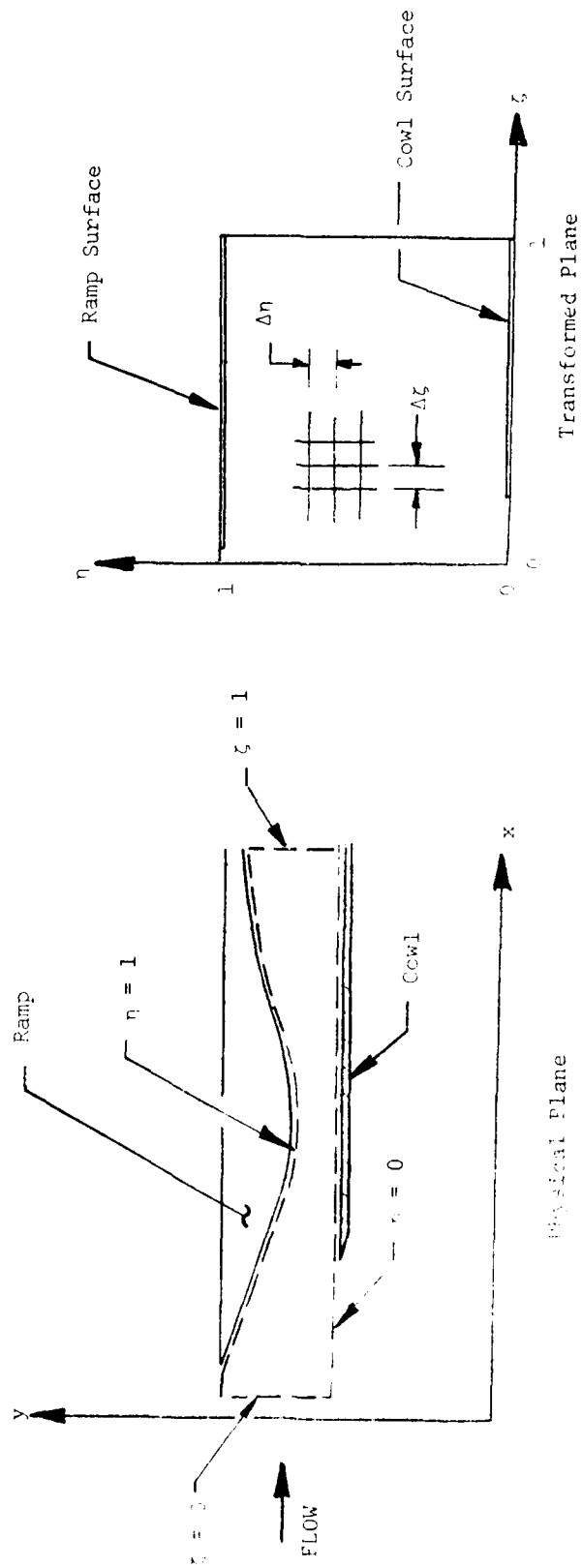


Figure 2. Coordinate Transformation

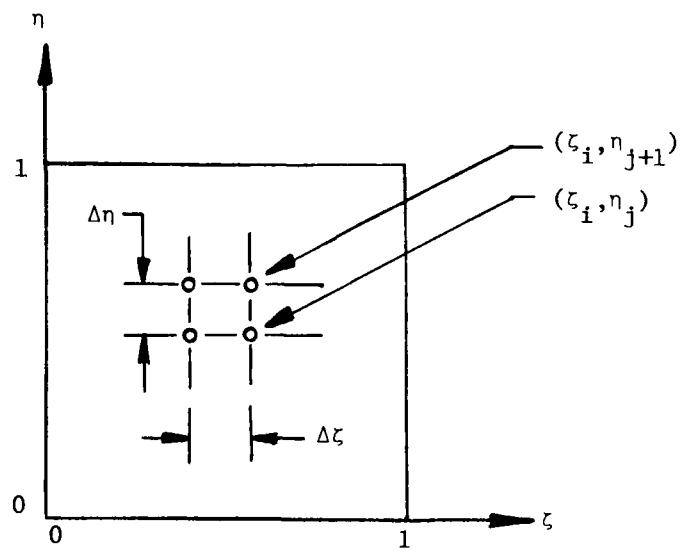
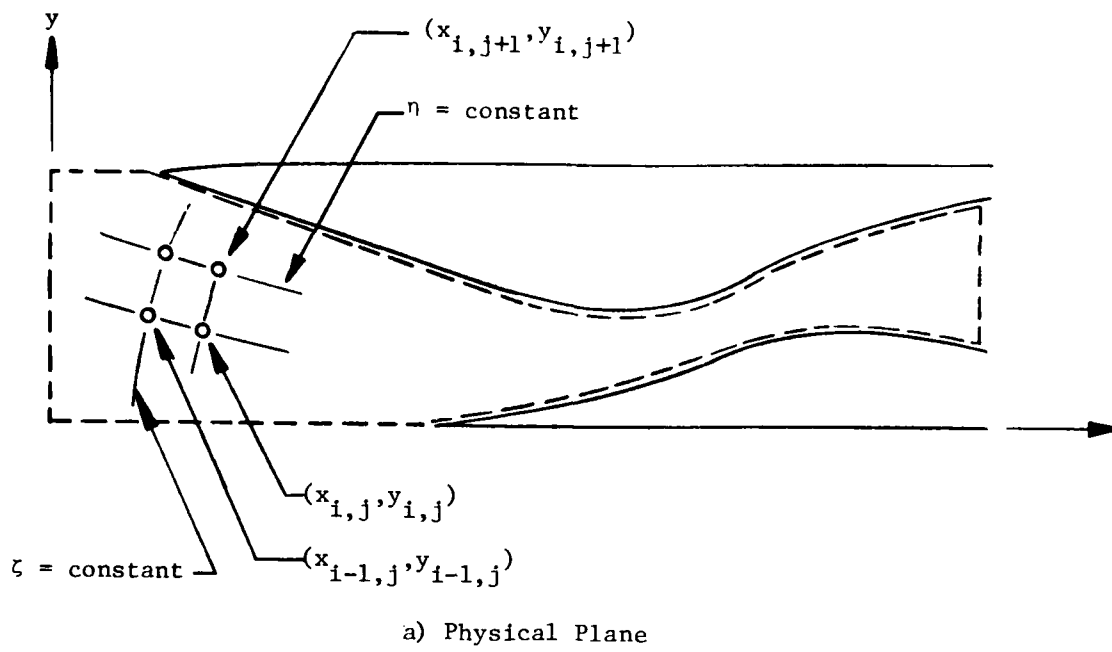


Figure 3. Details of Mesh Distribution

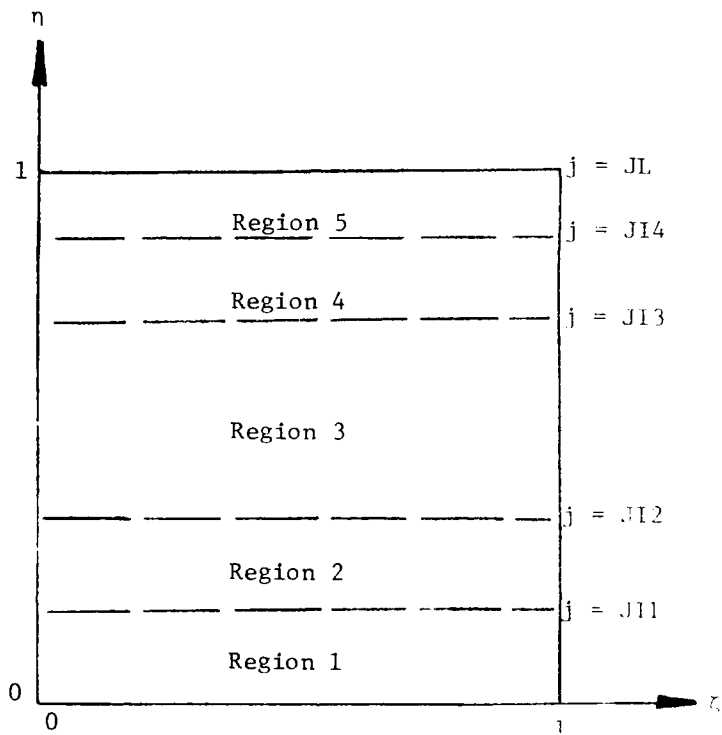
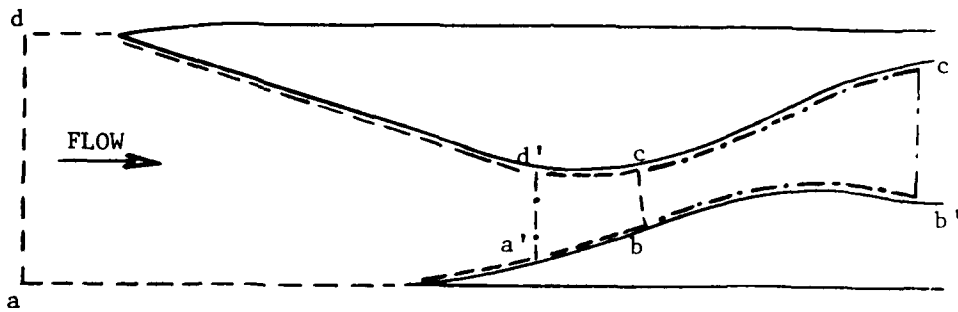


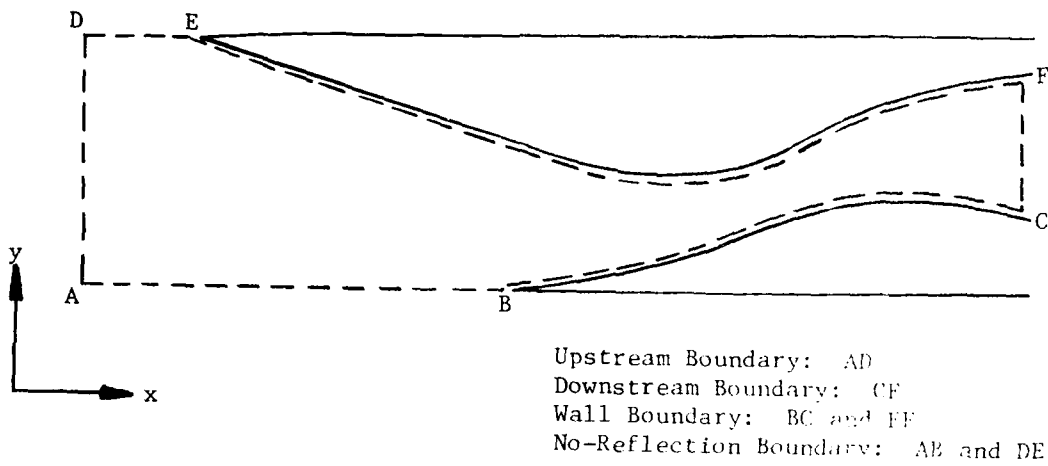
Figure 4. Mesh Splitting



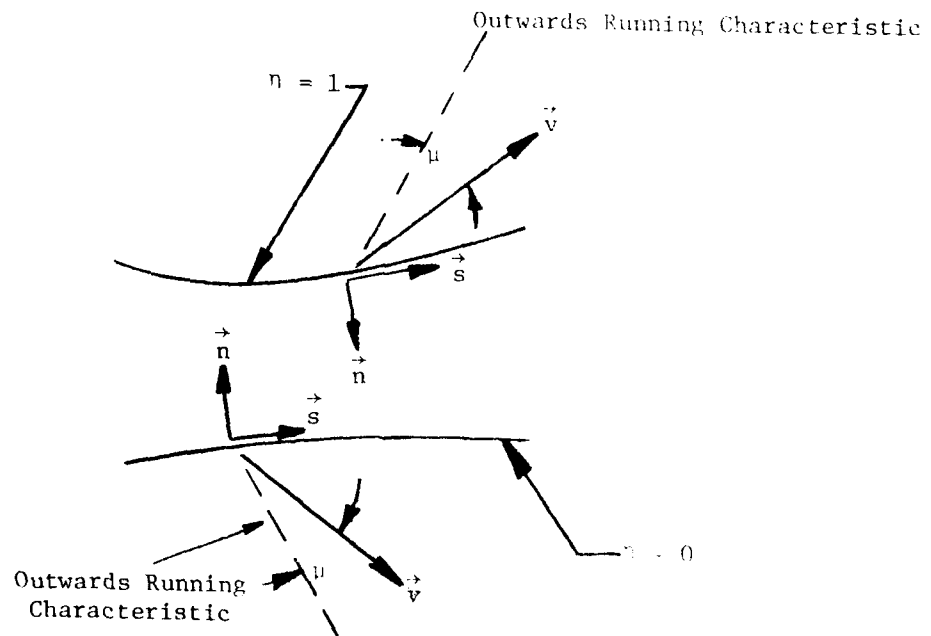
Region A: abcd

Region B: a'b'c'd'

Figure 5. Mesh Overlapping

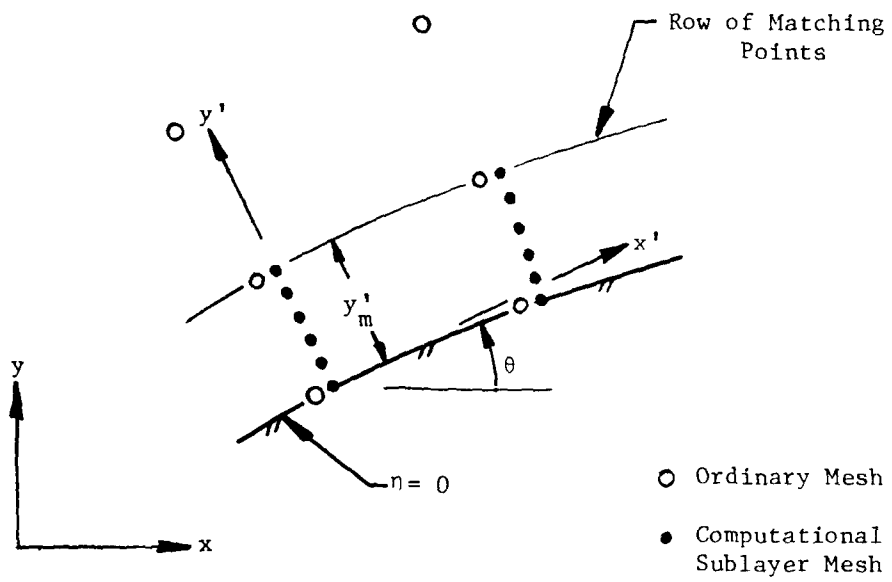


a) Types of Boundary Conditions

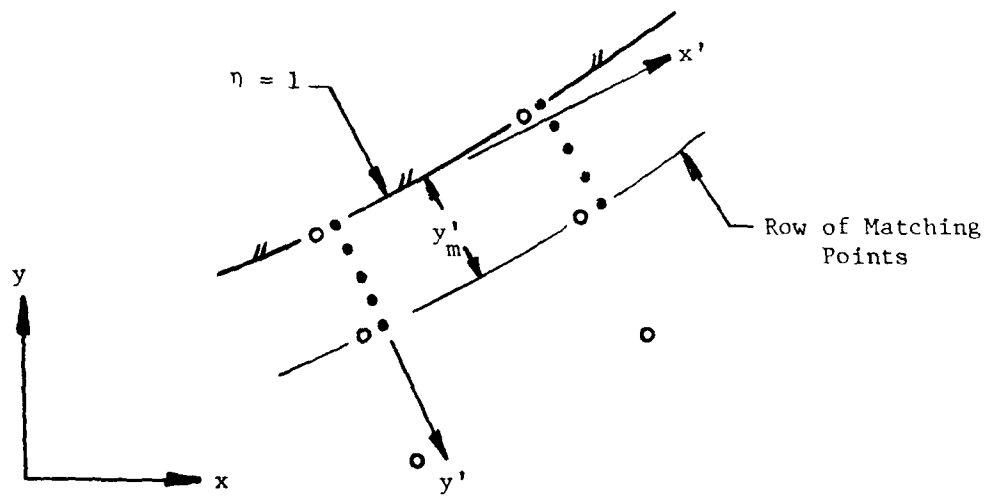


b) Orientation of Unit Vectors and Outwards Running Characteristics

Figure 6. Boundary Conditions



a) Computational Sublayer on  $\eta = 0$



b) Computational Sublayer on  $\eta = 1$

Figure 7. Computational Sublayer Geometry

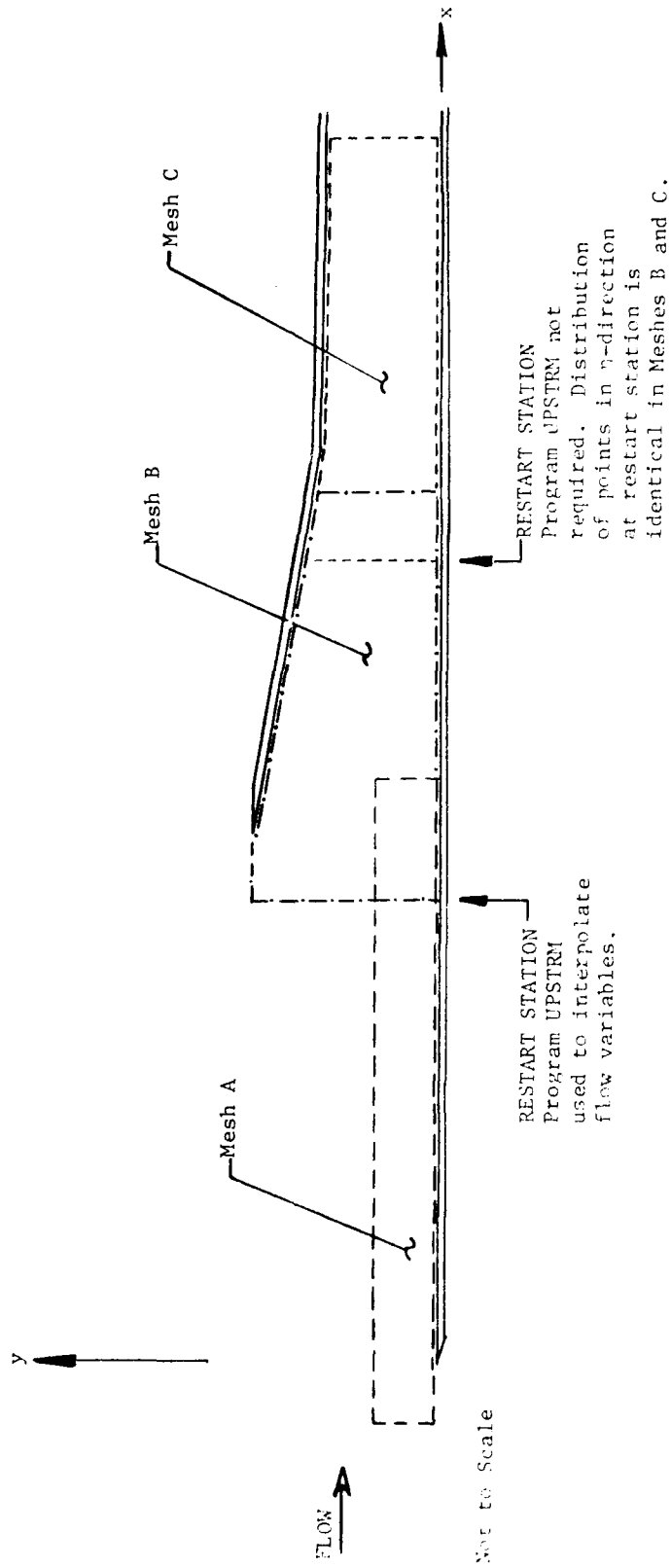
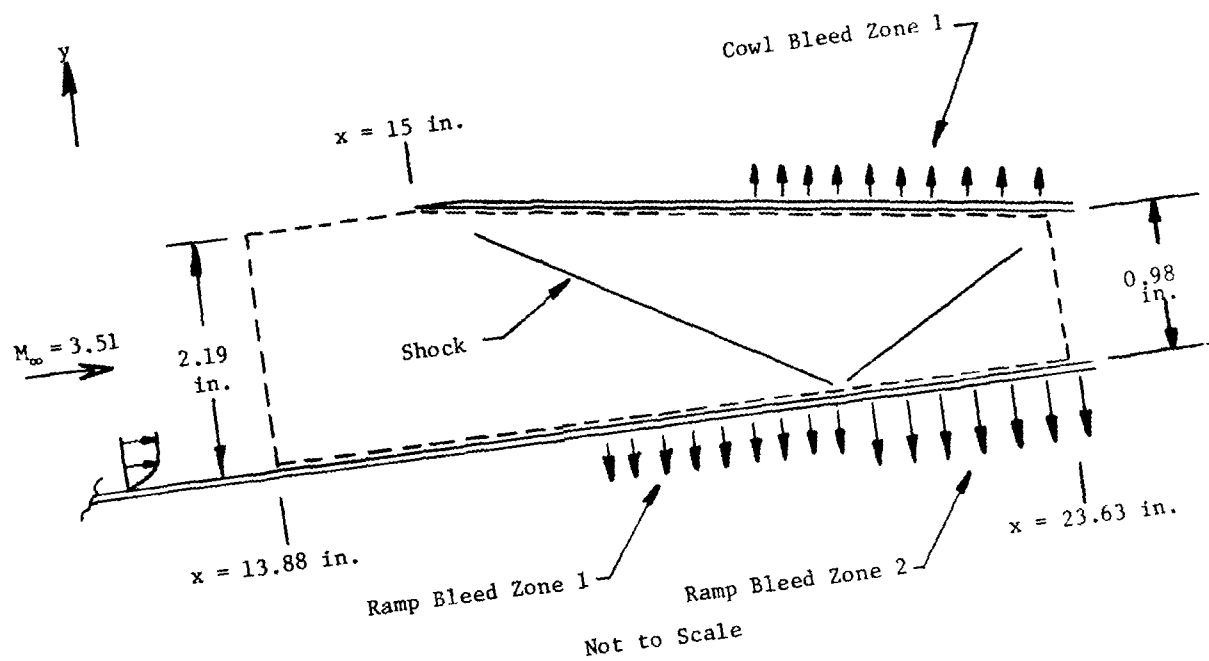


Figure 8. Mesh Overlapping Employed for MCAIR Inlet



Experimental Boundary Layer Thickness

Ramp:  $\delta = 0.25$  in. at  $x = 19.2$  in.  
 $\delta = 0.20$  in. at  $x = 24$  in.  
 Cowl:  $\delta = 0.10$  in. at  $x = 25$  in.

Boundary Layer Bleed Schedule

Surface	Extent (in.)	$\dot{m}$ (slugs/ft <sup>2</sup> -sec)
Ramp	$16.5 \leq x < 20.5$	$-3.85 \times 10^{-3}$
	$20.5 \leq x \leq 25$	$-8.18 \times 10^{-3}$
Cowl	$19.5 \leq x \leq 23.1$	$-2.88 \times 10^{-3}$

Experimental Surface Pressures in Region

Surface	Extent (in.)	$p/p_\infty$ (approx.)
Surface	$x < 20$	1
Ramp	$x > 20$	5
Cowl	$x > 15$	2

Figure 9. Upstream Region of MCAIR Inlet--Case 35

DYO (FEET)    DYL (FEET)    R1 (FEET)    YJ (FEET)    JL  
 0.500000E-03    0.500000E-03    0.132642E 03    0.0    48

\*\*\*\* MESH DISTRIBUTION FOR J0 = 18 AND J1 = 28 \*\*\*\*  
 WITH C1 = 0.289008E 01 AND C2 = 0.287725E 01

J	YY(J) (FEET)	YY(J)-YY(J-1) (FEET)	YY(J) (INCHES)	YY(J)-YY(J-1) (INCHES)
1	0.0	0.0	0.0	0.0
2	0.499999E-03	0.499999E-03	0.599999E-02	0.599999E-02
3	0.109267E-02	0.592674E-03	0.131121E-01	0.711209E-02
4	0.179520E-02	0.702530E-03	0.215424E-01	0.843036E-02
5	0.262795E-02	0.832731E-03	0.315353E-01	0.999289E-02
6	0.361504E-02	0.987098E-03	0.433805E-01	0.118452E-01
7	0.478509E-02	0.117304E-02	0.574210E-01	0.140405E-01
8	0.617202E-02	0.138693E-02	0.740042E-01	0.166432E-01
9	0.781602E-02	0.164400E-02	0.937922E-01	0.197280E-01
10	0.976473E-02	0.194871E-02	0.117177E 00	0.233846E-01
11	0.120746E-01	0.230992E-02	0.144896E 00	0.277190E-01
12	0.148127E-01	0.273604E-02	0.177752E 00	0.328504E-01
13	0.180583E-01	0.324558E-02	0.216599E 00	0.389470E-01
14	0.219054E-01	0.384713E-02	0.262965E 00	0.461658E-01
15	0.264656E-01	0.456020E-02	0.317383E 00	0.547228E-01
16	0.318711E-01	0.540546E-02	0.382453E 00	0.648655E-01
17	0.382785E-01	0.640740E-02	0.459342E 00	0.768887E-01
18	0.458735E-01	0.759500E-02	0.550462E 00	0.911399E-01
19	0.541325E-01	0.825900E-02	0.649590E 00	0.991080E-01
20	0.623915E-01	0.825904E-02	0.748698E 00	0.991085E-01
21	0.706505E-01	0.825900E-02	0.847806E 00	0.991080E-01
22	0.789095E-01	0.825900E-02	0.946914E 00	0.991080E-01
23	0.871586E-01	0.825906E-02	0.104602E 01	0.991087E-01
24	0.954276E-01	0.825900E-02	0.114513E 01	0.991080E-01
25	0.103687E 00	0.825905E-02	0.124424E 01	0.991087E-01
26	0.111946E 00	0.825900E-02	0.134335E 01	0.991080E-01
27	0.120205E 00	0.825906E-02	0.144246E 01	0.991087E-01
28	0.128464E 00	0.825900E-02	0.154156E 01	0.991080E-01
29	0.136156E 00	0.769246E-02	0.153387E 01	0.923095E-01
30	0.142816E 00	0.566155E-02	0.171361E 01	0.799398E-01
31	0.148527E 00	0.576913E-02	0.178304E 01	0.692296E-01
32	0.153585E 00	0.499600E-02	0.184299E 01	0.599520E-01
33	0.157910E 00	0.432604E-02	0.189451E 01	0.519197E-01
34	0.161656E 00	0.374693E-02	0.193988E 01	0.449631E-01
35	0.164901E 00	0.324466E-02	0.197882E 01	0.389378E-01
36	0.167711E 00	0.281006E-02	0.201254E 01	0.3337207E-01
37	0.170145E 00	0.243348E-02	0.204174E 01	0.292017E-01
38	0.172252E 00	0.210744E-02	0.206703E 01	0.252893E-01
39	0.174077E 00	0.182309E-02	0.208893E 01	0.219011E-01
40	0.175658E 00	0.158348E-02	0.210769E 01	0.189657E-01
41	0.177027E 00	0.136876E-02	0.212432E 01	0.164251E-01
42	0.178212E 00	0.118536E-02	0.213854E 01	0.142242E-01
43	0.179238E 00	0.102651E-02	0.215086E 01	0.123181E-01
44	0.180127E 00	0.888944E-03	0.216153E 01	0.106673E-01
45	0.180857E 00	0.769854E-03	0.217077E 01	0.923824E-02
46	0.181564E 00	0.666678E-03	0.217877E 01	0.800014E-02
47	0.182141E 00	0.577390E-03	0.218570E 01	0.692868E-02
48	0.182642E 00	0.500619E-03	0.219170E 01	0.600743E-02

Figure 10. Sample Output: Program BNDRY

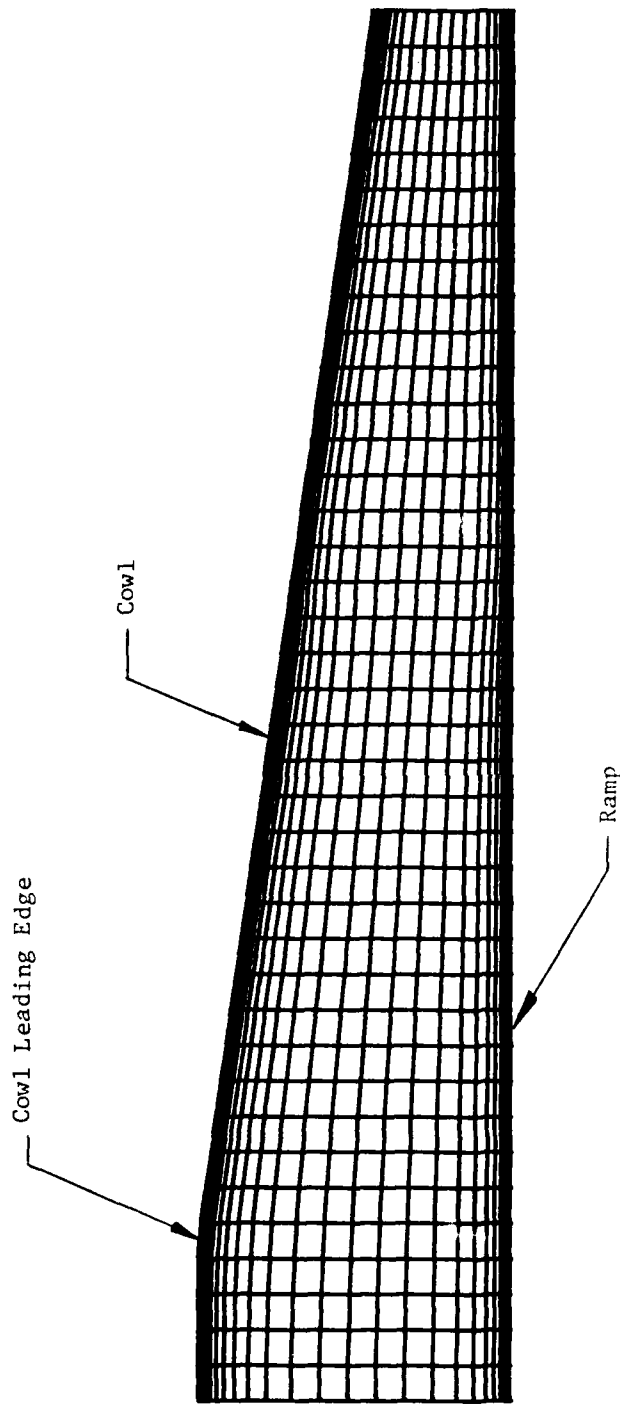


Figure 11a. Coordinate Transformation for MCAIR Inlet (Upstream)--Case 35

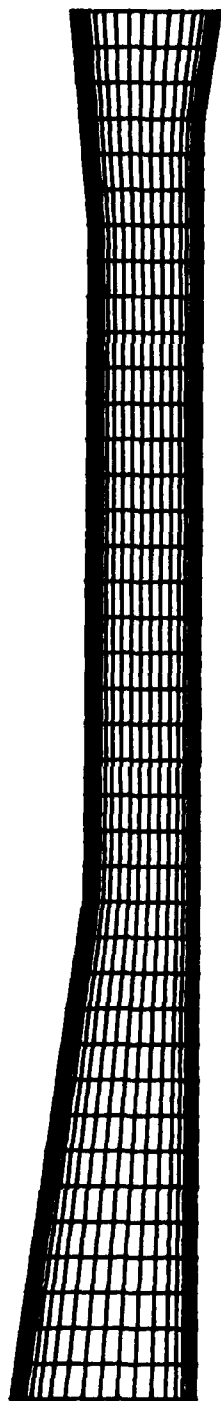


Figure 11b. Coordinate Transformation for MCAIR Inlet (Downstream)--Case 35



\*\*\* COORDINATES \*\*\*  
 THE FOLLOWING ARE THE VALUES OF X(I,J),Y(I,J) IN FELT AT EACH  
 VALUE OF ETA FOR I EQUAL 1 TO M  
 CONVERGENCE ACHIEVED IN 380 ITERATIONS

ETA = 0.0	J = 1	J = 2	J = 3	J = 4	J = 5
U.1156E 01.00.0	(U.1177E 01.00.0	(U.1198E 01.00.0	(U.1219E 01.00.0	(U.1240E 01.00.0	(U.1260E 01.00.0
U.1260E 01.00.0	(U.1302E 01.00.0	(U.1323E 01.00.0	(U.1344E 01.00.0	(U.1364E 01.00.0	(U.1384E 01.00.0
U.1489E 01.00.0	(U.1510E 01.00.0	(U.1531E 01.00.0	(U.1552E 01.00.0	(U.1572E 01.00.0	(U.1592E 01.00.0
U.1731E 01.00.0	(U.1752E 01.00.0	(U.1773E 01.00.0	(U.1794E 01.00.0	(U.1814E 01.00.0	(U.1834E 01.00.0
U.1885E 01.00.0	(U.1906E 01.00.0	(U.1927E 01.00.0	(U.1948E 01.00.0	(U.1969E 01.00.0	(U.1990E 01.00.0
LTA = 0.021277	(U.1177E 01.00.4959E-03)	(U.1198E 01.00.4934E-03)	(U.1219E 01.00.4908E-03)	(U.1240E 01.00.4881E-03)	(U.1260E 01.00.4856E-03)
U.1260E 01.00.4875E-03	(U.1302E 01.00.4907E-03)	(U.1323E 01.00.4919E-03)	(U.1344E 01.00.4926E-03)	(U.1364E 01.00.4932E-03)	(U.1384E 01.00.4937E-03)
U.1489E 01.00.4930E-03	(U.1510E 01.00.4934E-03)	(U.1531E 01.00.4931E-03)	(U.1552E 01.00.4928E-03)	(U.1572E 01.00.4925E-03)	(U.1592E 01.00.4922E-03)
U.1731E 01.00.4913E-03	(U.1752E 01.00.4908E-03)	(U.1773E 01.00.4905E-03)	(U.1794E 01.00.4902E-03)	(U.1814E 01.00.4899E-03)	(U.1834E 01.00.4896E-03)
U.1885E 01.00.4878E-03	(U.1906E 01.00.4873E-03)	(U.1927E 01.00.4868E-03)	(U.1948E 01.00.4863E-03)	(U.1969E 01.00.4858E-03)	(U.1990E 01.00.4853E-03)
LTA = 0.042553	(U.1177E 01.00.1084E-02)	(U.1198E 01.00.1079E-02)	(U.1219E 01.00.1073E-02)	(U.1240E 01.00.1067E-02)	(U.1260E 01.00.1061E-02)
U.1260E 01.00.1065E-02	(U.1302E 01.00.1074E-02)	(U.1323E 01.00.1071E-02)	(U.1344E 01.00.1067E-02)	(U.1364E 01.00.1063E-02)	(U.1384E 01.00.1059E-02)
U.1489E 01.00.1074E-02	(U.1510E 01.00.1068E-02)	(U.1531E 01.00.1065E-02)	(U.1552E 01.00.1061E-02)	(U.1572E 01.00.1057E-02)	(U.1592E 01.00.1053E-02)
U.1731E 01.00.1053E-02	(U.1752E 01.00.1048E-02)	(U.1773E 01.00.1045E-02)	(U.1794E 01.00.1041E-02)	(U.1814E 01.00.1037E-02)	(U.1834E 01.00.1033E-02)
U.1885E 01.00.1034E-02	(U.1906E 01.00.1029E-02)	(U.1927E 01.00.1024E-02)	(U.1948E 01.00.1019E-02)	(U.1969E 01.00.1014E-02)	(U.1990E 01.00.1009E-02)
LTA = 0.063830	(U.1177E 01.00.1753E-02)	(U.1198E 01.00.1751E-02)	(U.1219E 01.00.1748E-02)	(U.1240E 01.00.1745E-02)	(U.1260E 01.00.1742E-02)
U.1260E 01.00.1752E-02	(U.1302E 01.00.1753E-02)	(U.1323E 01.00.1752E-02)	(U.1344E 01.00.1751E-02)	(U.1364E 01.00.1750E-02)	(U.1384E 01.00.1749E-02)
U.1489E 01.00.1749E-02	(U.1510E 01.00.1748E-02)	(U.1531E 01.00.1747E-02)	(U.1552E 01.00.1746E-02)	(U.1572E 01.00.1745E-02)	(U.1592E 01.00.1744E-02)
U.1731E 01.00.1744E-02	(U.1752E 01.00.1743E-02)	(U.1773E 01.00.1742E-02)	(U.1794E 01.00.1741E-02)	(U.1814E 01.00.1740E-02)	(U.1834E 01.00.1739E-02)
U.1885E 01.00.1739E-02	(U.1906E 01.00.1738E-02)	(U.1927E 01.00.1737E-02)	(U.1948E 01.00.1736E-02)	(U.1969E 01.00.1735E-02)	(U.1990E 01.00.1734E-02)
LTA = 0.085106	(U.1177E 01.00.2628E-02)	(U.1198E 01.00.2626E-02)	(U.1219E 01.00.2624E-02)	(U.1240E 01.00.2622E-02)	(U.1260E 01.00.2620E-02)
U.1260E 01.00.2627E-02	(U.1302E 01.00.2628E-02)	(U.1323E 01.00.2627E-02)	(U.1344E 01.00.2626E-02)	(U.1364E 01.00.2625E-02)	(U.1384E 01.00.2624E-02)
U.1489E 01.00.2624E-02	(U.1510E 01.00.2623E-02)	(U.1531E 01.00.2622E-02)	(U.1552E 01.00.2621E-02)	(U.1572E 01.00.2620E-02)	(U.1592E 01.00.2619E-02)
U.1731E 01.00.2619E-02	(U.1752E 01.00.2618E-02)	(U.1773E 01.00.2617E-02)	(U.1794E 01.00.2616E-02)	(U.1814E 01.00.2615E-02)	(U.1834E 01.00.2614E-02)
U.1885E 01.00.2614E-02	(U.1906E 01.00.2613E-02)	(U.1927E 01.00.2612E-02)	(U.1948E 01.00.2611E-02)	(U.1969E 01.00.2610E-02)	(U.1990E 01.00.2609E-02)

Figure 12b. Sample Output: Program COORD





```

*** DISTANCE ALONG LUNER BOUNDARY (ETA=0.) FOR I EQUAL I TO M ***
0.11203 01 0.11771 01 0.11979 01 0.12187 01 0.12390 01 0.12604 01 0.12812 01 0.13021 01 0.13229 01 0.13437 01 0.13640 01
0.13856 01 0.14064 01 0.14271 01 0.14479 01 0.14687 01 0.14896 01 0.15104 01 0.15312 01 0.15521 01 0.15729 01 0.15937 01
0.16146 01 0.16352 01 0.16562 01 0.16771 01 0.16979 01 0.17187 01 0.17396 01 0.17604 01 0.17812 01 0.18021 01 0.18229 01
0.18437 01 0.18646 01 0.18854 01 0.19062 01 0.19271 01 0.19479 01 0.19687 01

*** DISTANCE ALONG UPPER ECUNDARY (ETA=1.) FOR I EQUAL I TO M ***
-0.93133 01 -0.72300 01 -0.51467 01 -0.30634 01 -0.09803 02 0.11090 01 0.32126 01 0.53163 01 0.74199 01 0.95236 01 1.16271 01
0.13731 00 0.15935 00 0.17939 00 0.20042 00 0.22145 00 0.24249 00 0.26353 00 0.28456 00 0.30560 00 0.32664 00 0.34767 00
0.36871 00 0.38975 00 0.41078 00 0.43182 00 0.45286 00 0.47389 00 0.49493 00 0.51597 00 0.53700 00 0.55804 00 0.57908 00
0.60011 00 0.62113 00 0.64216 00 0.66320 00 0.68423 00 0.70526 00 0.72630 00

```

Figure 12e. Sample Output: Program COORD





E T A = 0					E T A = 1				
I	JREFER	UDELTA		JMATCH	JREFER	UDELTA		JMATCH	
2	0.223E	04	0.599E	01					
3	0.223E	04	0.604E	01					
4	0.223E	04	0.609E	01					
5	0.223E	04	0.614E	01					
6	0.223E	04	0.619E	01					
7	0.223E	04	0.623E	01					
8	0.223E	04	0.629E	01					
9	0.223E	04	0.634E	01					
10	0.223E	04	0.639E	01					
11	0.223E	04	0.644E	01					
12	0.223E	04	0.648E	01					
13	0.223E	04	0.652E	01					
14	0.223E	04	0.653E	01					
15	0.223E	04	0.652E	01					
16	0.223E	04	0.649E	01					
17	0.223E	04	0.640E	01					
18	0.223E	04	0.643E	01					
19	0.223E	04	0.648E	01					
20	0.223E	04	0.649E	01					
21	0.223E	04	0.660E	01					
22	0.223E	04	0.618E	01	0.219E	04	0.395E	01	46
23	0.223E	04	0.585E	01	0.218E	04	0.349E	01	46
24	0.223E	04	0.553E	01	0.217E	04	0.285E	01	46
25	0.223E	04	0.529E	01	0.215E	04	0.222E	01	46
26	0.223E	04	0.505E	01	0.214E	04	0.191E	01	46
27	0.223E	04	0.483E	01	0.213E	04	0.166E	01	46
28	0.223E	04	0.463E	01	0.213E	04	0.144E	01	46
29	0.223E	04	0.447E	01	0.213E	04	0.138E	01	46
30	0.223E	04	0.445E	01	0.213E	04	0.139E	01	46
31	0.224E	04	0.435E	01	0.213E	04	0.178E	01	46
32	0.224E	04	0.435E	01	0.212E	04	0.180E	01	46
33	0.224E	04	0.430E	01	0.212E	04	0.182E	01	46
34	0.224E	04	0.422E	01	0.212E	04	0.184E	01	46
35	0.224E	04	0.417E	01	0.212E	04	0.189E	01	46
36	0.224E	04	0.410E	01	0.212E	04	0.192E	01	46
37	0.224E	04	0.403E	01	0.212E	04	0.197E	01	46
38	0.224E	04	0.398E	01	0.212E	04	0.197E	01	46
39	0.223E	04	0.380E	01	0.212E	04	0.206E	01	46

Figure 13c. Sample Output: Program INLET

\*\*\*\* VISCOS SUBLAYER JN ETA = 0

J	COLUMN XN	TEMP	USL	X EQUALS 0.1162E 01	EPSLN	VISCOSITY	CJ-UAN	Z	USL	X EQUALS 0.1172E 01	EPSLN	VISCOSITY
1	0.0	0.5307E 03	0.0	0.0	0.0	0.3805E-06	0.5314E 03	0.0	0.0	0.0	0.0	0.3804E-06
2	0.2632E-04	0.52297E 03	0.4743E 02	0.3132E-04	0.3132E-04	0.3805E-06	0.5314E 03	0.0	0.450E 02	0.0	0.3243E-10	0.3807E-06
3	0.5263E-04	0.52297E 03	0.1749E 03	0.3264E-06	0.3264E-06	0.3805E-06	0.52297E 03	0.0	0.1749E 03	0.0	0.5112E-09	0.3807E-06
4	0.7893E-04	0.52297E 03	0.2614E 03	0.4510E-08	0.4510E-08	0.3805E-06	0.52297E 03	0.0	0.2574E 03	0.0	0.2415E-04	0.3807E-06
5	0.1053E-03	0.52297E 03	0.3496E 03	0.4839E-08	0.4839E-08	0.3805E-06	0.52297E 03	0.0	0.3496E 03	0.0	0.7284E-04	0.3807E-06
6	0.1310E-03	0.52297E 03	0.4326E 03	0.5443E-07	0.5443E-07	0.3805E-06	0.52297E 03	0.0	0.4274E 03	0.0	0.1746E-07	0.3807E-06
7	0.1579E-03	0.52297E 03	0.5144E 03	0.5988E-07	0.5988E-07	0.3805E-06	0.52297E 03	0.0	0.5092E 03	0.0	0.3510E-07	0.3807E-06
8	0.1845E-03	0.52297E 03	0.5931E 03	0.6711E-07	0.6711E-07	0.3805E-06	0.52297E 03	0.0	0.5874E 03	0.0	0.6069E-07	0.3807E-06
9	0.2109E-03	0.52297E 03	0.6679E 03	0.7615E-06	0.7615E-06	0.3805E-06	0.52297E 03	0.0	0.6819E 03	0.0	0.9495E-07	0.3807E-06
10	0.2382E-03	0.4913E 03	0.7301E 03	0.1465E-06	0.1465E-06	0.3805E-06	0.4913E 03	0.0	0.7242E 03	0.0	0.1379E-06	0.3807E-06
11	0.2652E-03	0.4852E 03	0.7911E 03	0.1996E-06	0.1996E-06	0.3805E-06	0.4852E 03	0.0	0.7911E 03	0.0	0.1970E-06	0.3807E-06
12	0.2925E-03	0.4792E 03	0.8539E 03	0.2596E-06	0.2596E-06	0.3805E-06	0.4792E 03	0.0	0.8407E 03	0.0	0.2477E-06	0.3807E-06
13	0.3198E-03	0.4731E 03	0.9083E 03	0.3281E-06	0.3281E-06	0.3805E-06	0.4731E 03	0.0	0.8804E 03	0.0	0.3132E-06	0.3807E-06
14	0.3471E-03	0.4673E 03	0.9552E 03	0.4009E-06	0.4009E-06	0.3805E-06	0.4673E 03	0.0	0.9084E 03	0.0	0.3850E-06	0.3807E-06
15	0.3744E-03	0.4614E 03	0.9952E 03	0.4823E-06	0.4823E-06	0.3805E-06	0.4614E 03	0.0	0.9473E 03	0.0	0.4627E-06	0.3807E-06
16	0.4017E-03	0.4554E 03	0.1038E 04	0.5655E-06	0.5655E-06	0.3805E-06	0.4554E 03	0.0	0.1038E 04	0.0	0.5457E-06	0.3807E-06
17	0.4290E-03	0.4494E 03	0.1106E 04	0.6549E-06	0.6549E-06	0.3805E-06	0.4494E 03	0.0	0.1064E 04	0.0	0.6339E-06	0.3807E-06
18	0.4563E-03	0.4434E 03	0.1134E 04	0.7591E-06	0.7591E-06	0.3805E-06	0.4434E 03	0.0	0.1059E 04	0.0	0.7272E-06	0.3807E-06
19	0.4836E-03	0.4374E 03	0.1162E 04	0.8627E-06	0.8627E-06	0.3805E-06	0.4374E 03	0.0	0.1126E 04	0.0	0.8212E-06	0.3807E-06
20	0.5109E-03	0.4314E 03	0.1190E 04	0.1016E-05	0.1016E-05	0.3805E-06	0.4314E 03	0.0	0.1152E 04	0.0	0.9245E-06	0.3807E-06

J	COLUMN XN	TEMP	USL	X EQUALS 0.1162E 01	EPSLN	VISCOSITY	CJ-UAN	Z	USL	X EQUALS 0.1193E 01	EPSLN	VISCOSITY
1	0.0	0.5312E 03	0.0	0.0	0.0	0.2808E-06	0.5311E 03	0.0	0.0	0.0	0.0	0.2808E-06
2	0.2609E-04	0.52309E 03	0.5271E 02	0.3267E-10	0.3267E-10	0.2808E-06	0.5311E 03	0.0	0.8575E 02	0.0	0.3241E-10	0.2808E-06
3	0.5239E-04	0.52294E 03	0.1719E 03	0.3306E-06	0.3306E-06	0.2808E-06	0.52294E 03	0.0	0.1719E 03	0.0	0.5047E-09	0.2808E-06
4	0.7868E-04	0.52272E 03	0.2571E 03	0.4502E-08	0.4502E-08	0.2808E-06	0.52272E 03	0.0	0.2571E 03	0.0	0.2483E-08	0.2808E-06
5	0.1048E-03	0.52241E 03	0.3432E 03	0.4746E-08	0.4746E-08	0.2808E-06	0.52241E 03	0.0	0.3432E 03	0.0	0.7289E-08	0.2808E-06
6	0.1305E-03	0.52222E 03	0.4274E 03	0.5274E-07	0.5274E-07	0.2808E-06	0.52222E 03	0.0	0.4266E 03	0.0	0.1774E-07	0.2808E-06
7	0.1562E-03	0.52103E 03	0.5072E 03	0.5902E-07	0.5902E-07	0.2808E-06	0.52103E 03	0.0	0.5084E 03	0.0	0.3478E-07	0.2808E-06
8	0.1827E-03	0.5094E 03	0.5810E 03	0.6544E-07	0.6544E-07	0.2808E-06	0.5094E 03	0.0	0.6001E 03	0.0	0.5991E-07	0.2808E-06
9	0.2092E-03	0.4978E 03	0.6549E 03	0.7293E-06	0.7293E-06	0.2808E-06	0.4978E 03	0.0	0.6601E 03	0.0	0.9495E-07	0.2808E-06
10	0.2357E-03	0.4862E 03	0.7197E 03	0.1374E-06	0.1374E-06	0.2808E-06	0.4862E 03	0.0	0.7283E 03	0.0	0.1306E-06	0.2808E-06
11	0.2622E-03	0.4746E 03	0.7807E 03	0.1868E-06	0.1868E-06	0.2808E-06	0.4746E 03	0.0	0.7909E 03	0.0	0.1773E-06	0.2808E-06
12	0.2887E-03	0.4630E 03	0.8357E 03	0.2411E-06	0.2411E-06	0.2808E-06	0.4630E 03	0.0	0.8497E 03	0.0	0.2355E-06	0.2808E-06
13	0.3152E-03	0.4514E 03	0.8937E 03	0.3041E-06	0.3041E-06	0.2808E-06	0.4514E 03	0.0	0.8957E 03	0.0	0.3105E-06	0.2808E-06
14	0.3417E-03	0.4400E 03	0.9476E 03	0.3691E-06	0.3691E-06	0.2808E-06	0.4400E 03	0.0	0.9467E 03	0.0	0.3819E-06	0.2808E-06
15	0.3682E-03	0.4284E 03	0.9976E 03	0.4391E-06	0.4391E-06	0.2808E-06	0.4284E 03	0.0	0.9894E 03	0.0	0.4570E-06	0.2808E-06
16	0.3947E-03	0.4168E 03	0.1044E 04	0.5151E-06	0.5151E-06	0.2808E-06	0.4168E 03	0.0	0.1028E 04	0.0	0.5424E-06	0.2808E-06
17	0.4212E-03	0.4052E 03	0.1074E 04	0.5991E-06	0.5991E-06	0.2808E-06	0.4052E 03	0.0	0.1063E 04	0.0	0.6339E-06	0.2808E-06
18	0.4477E-03	0.3936E 03	0.1104E 04	0.6827E-06	0.6827E-06	0.2808E-06	0.3936E 03	0.0	0.1063E 04	0.0	0.7250E-06	0.2808E-06
19	0.4742E-03	0.3820E 03	0.1134E 04	0.7691E-06	0.7691E-06	0.2808E-06	0.3820E 03	0.0	0.1059E 04	0.0	0.8174E-06	0.2808E-06
20	0.5007E-03	0.3704E 03	0.1162E 04	0.8627E-06	0.8627E-06	0.2808E-06	0.3704E 03	0.0	0.1152E 04	0.0	0.9179E-06	0.2808E-06

Figure 14. Sample Output: Program INLET

I	X(I,1) FEET	PZPINF	E T A = 0 SLG/F (**2*S	MASS BLEED	CF	X(I,JL) FEET	E T A = 1 PZPINF	SLG/F (**2*S	MASS BLEED	CF
1	0.11722	01	0.10302	01	0.0	0.15792	01	0.99508	00	0.0
2	0.11722	01	0.10302	01	0.0	0.15832	01	0.99508	00	0.0
3	0.11932	01	0.10302	01	0.0	0.15832	01	0.99508	00	0.0
4	0.11932	01	0.10302	01	0.0	0.15832	01	0.99508	00	0.0
5	0.12032	01	0.10302	01	0.0	0.15832	01	0.99508	00	0.0
6	0.12142	01	0.10302	01	0.0	0.15832	01	0.99508	00	0.0
7	0.12242	01	0.10302	01	0.0	0.15832	01	0.99508	00	0.0
8	0.12342	01	0.10302	01	0.0	0.15832	01	0.99508	00	0.0
9	0.12452	01	0.10302	01	0.0	0.15832	01	0.99508	00	0.0
10	0.12552	01	0.10302	01	0.0	0.15832	01	0.99508	00	0.0
11	0.12662	01	0.10302	01	0.0	0.15832	01	0.99508	00	0.0
12	0.12762	01	0.10302	01	0.0	0.15832	01	0.99508	00	0.0
13	0.12862	01	0.10302	01	0.0	0.15832	01	0.99508	00	0.0
14	0.12972	01	0.10302	01	0.0	0.15832	01	0.99508	00	0.0
15	0.13072	01	0.10302	01	0.0	0.15832	01	0.99508	00	0.0
16	0.13182	01	0.10302	01	0.0	0.15832	01	0.99508	00	0.0
17	0.13282	01	0.10302	01	0.0	0.15832	01	0.99508	00	0.0
18	0.13392	01	0.10302	01	0.0	0.15832	01	0.99508	00	0.0
19	0.13492	01	0.10302	01	0.0	0.15832	01	0.99508	00	0.0
20	0.13592	01	0.10302	01	0.0	0.15832	01	0.99508	00	0.0
21	0.13702	01	0.10302	01	0.0	0.15832	01	0.99508	00	0.0
22	0.13802	01	0.10302	01	0.0	0.15832	01	0.99508	00	0.0
23	0.13912	01	0.10302	01	0.0	0.15832	01	0.99508	00	0.0
24	0.14012	01	0.10302	01	0.0	0.15832	01	0.99508	00	0.0
25	0.14112	01	0.10302	01	0.0	0.15832	01	0.99508	00	0.0
26	0.14212	01	0.10302	01	0.0	0.15832	01	0.99508	00	0.0
27	0.14312	01	0.10302	01	0.0	0.15832	01	0.99508	00	0.0
28	0.14412	01	0.10302	01	0.0	0.15832	01	0.99508	00	0.0
29	0.14512	01	0.10302	01	0.0	0.15832	01	0.99508	00	0.0
30	0.14612	01	0.10302	01	0.0	0.15832	01	0.99508	00	0.0
31	0.14712	01	0.10302	01	0.0	0.15832	01	0.99508	00	0.0
32	0.14812	01	0.10302	01	0.0	0.15832	01	0.99508	00	0.0
33	0.14912	01	0.10302	01	0.0	0.15832	01	0.99508	00	0.0
34	0.15012	01	0.10302	01	0.0	0.15832	01	0.99508	00	0.0
35	0.15112	01	0.10302	01	0.0	0.15832	01	0.99508	00	0.0
36	0.15212	01	0.10302	01	0.0	0.15832	01	0.99508	00	0.0
37	0.15312	01	0.10302	01	0.0	0.15832	01	0.99508	00	0.0
38	0.15412	01	0.10302	01	0.0	0.15832	01	0.99508	00	0.0
39	0.15512	01	0.10302	01	0.0	0.15832	01	0.99508	00	0.0

Figure 13e. Sample Output: Program INLET

```

      E T A = 0
I  D Y S L P L U S      D Y P L U S
2  0.7824E 00      0.1487E 02
3  0.7815E 00      0.1485E 02
4  0.7800E 00      0.1482E 02
5  0.7781E 00      0.1478E 02
6  0.7758E 00      0.1474E 02
7  0.7734E 00      0.1469E 02
8  0.7710E 00      0.1465E 02
9  0.7687E 00      0.1461E 02
10 0.7682E 00      0.1460E 02
11 0.7687E 00      0.1459E 02
12 0.7699E 00      0.1463E 02
13 0.7704E 00      0.1464E 02
14 0.7717E 00      0.1466E 02
15 0.7718E 00      0.1466E 02
16 0.7732E 00      0.1469E 02
17 0.7724E 00      0.1465E 02
18 0.7747E 00      0.1472E 02
19 0.7708E 00      0.1465E 02
20 0.7791E 00      0.1480E 02
21 0.7878E 00      0.1497E 02
22 0.4852E 00      0.2639E 02
23 0.4976E 00      0.2722E 02
24 0.5177E 00      0.2773E 02
25 0.5342E 00      0.2814E 02
26 0.5474E 00      0.2847E 02
27 0.5582E 00      0.2867E 02
28 0.5670E 00      0.2894E 02
29 0.5748E 00      0.2913E 02
30 0.5810E 00      0.2928E 02
31 0.5871E 00      0.2942E 02
32 0.5920E 00      0.2954E 02
33 0.5981E 00      0.2968E 02
34 0.6026E 00      0.2979E 02
35 0.6085E 00      0.2994E 02
36 0.6106E 00      0.3000E 02
37 0.6159E 00      0.3017E 02
38 0.6163E 00      0.3012E 02
39 0.6250E 00      0.3034E 02
40 0.6276E 00      0.3047E 02
      E T A = 1
I  D Y S L P L U S      D Y P L U S
21 0.1198E 01      0.2276E 02
22 0.1366E 01      0.2595E 02
23 0.1542E 01      0.2930E 02
24 0.1661E 01      0.3155E 02
25 0.1716E 01      0.3264E 02
26 0.1738E 01      0.3301E 02
27 0.1726E 01      0.3279E 02
28 0.1713E 01      0.3255E 02
29 0.1703E 01      0.3235E 02
30 0.1698E 01      0.3226E 02
31 0.1699E 01      0.3227E 02
32 0.1701E 01      0.3232E 02
33 0.1699E 01      0.3226E 02
34 0.1688E 01      0.3207E 02
35 0.1671E 01      0.3175E 02
36 0.1658E 01      0.3150E 02
37 0.1645E 01      0.3126E 02
38 0.1641E 01      0.3117E 02
39 0.1618E 01      0.3075E 02
40 0.1612E 01      0.3064E 02
MAX VALUE OF BLEED REYNOLDS NO. ON ETA= 0 IS 0.1837E 00
MAX VALUE OF BLEED REYNOLDS NO. ON ETA= 1 IS 0.0

```

Figure 13f. Sample Output: Program INLET